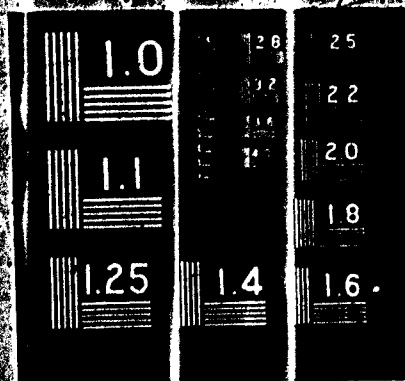


1 OF 2

ADD

621897



**BEST
AVAILABLE COPY**

MISSING PAGE
NUMBERS ARE BLANK
AND WERE NOT
FILMED



Office of Naval Research
Contract Nonr-1866(10)
NR - 017 - 308

Advanced Research Projects Agency
Contract SD-88

THE EFFECT OF PRESSURE AND TEMPERATURE
ON THE EFFECTIVE MASS AND ENERGY GAP OF GaAs

by

Walter M. DeMeis

August, 1965

The research reported in this document was made possible through support extended the Division of Engineering and Applied Physics, Harvard University, by the Office of Naval Research, under Contract Nonr-1866(10) and the Advanced Research Projects Agency under Contract SD-88. Reproduction in whole or in part is permitted for any purpose of the United States Government.

Technical Report No. HP-15

Technical Report No. ARPA-16

Gordon McKay Laboratory

Division of Engineering and Applied Physics

Harvard University

Cambridge, Massachusetts

ACKNOWLEDGMENT

I would like to express my appreciation to Professor William Paul for suggesting this research topic and serving as my thesis advisor at Harvard. I am grateful to him for instruction (at times painful but always beneficial) in the methods and attitudes of rigorous scientific inquiry and explanation. Finally, I am indebted to Professor Paul for suggesting corrections (in great detail) to this manuscript.

The apparatus of this investigation was constructed with the help of Albert Manning and the aid and advice (in great detail) of James Inglis. David MacLeod developed polishing techniques and prepared the optical surfaces used in this work. I wish to thank these skillful men for their essential contribution to this thesis.

I would also like to gratefully acknowledge the loan of apparatus by and stimulating discussions (in great detail) with Vidyut Prakash.

Lastly, I appreciate the financial assistance given me by Harvard University, the Office of Naval Research, and the Advanced Research Projects Agency.

TABLE OF CONTENTS

	Page
ACKNOWLEDGMENT	iii
TABLE OF CONTENTS	v
LIST OF FIGURES	vii
ABSTRACT	ix
CHAPTER 1 THEORY	1-1
A. INTRODUCTION	1-1
B. BAND THEORY	1-2
a. Zero Temperature	1-2
b. Finite Temperature	1-4
C. THEORY OF FARADAY ROTATION	1-11
a. Semiclassical Theory	1-11
b. Quantum Mechanical Theory	1-14
BIBLIOGRAPHY	1-18
CHAPTER 2 EQUIPMENT	2-1
A. INTRODUCTION	2-1
B. OPTICAL EQUIPMENT	2-3
a. Sources	2-3
b. Spectrometer and Mirrors	2-3
c. Polarizers	2-4
d. Detectors	2-6
C. OTHER EQUIPMENT	2-7
a. Magnet and Power Supply	2-7
b. Pressure Equipment	2-8
c. Cryostat, Sample Holders, and Positioning Mechanism	2-13
BIBLIOGRAPHY	2-15

	Page
CHAPTER 3 RESULTS	3-1
A. SAMPLES AND LIST OF EXPERIMENTS	3-1
B. PRESSURE DEPENDENCE OF THE ABSORPTION EDGE IN GaAs	3-3
C. REFRACTIVE INDEX IN GaAs	3-10
D. FARADAY ROTATION MEASUREMENTS IN GaAs	3-16
a. Experimental Method	3-16
b. Experimental Procedure	3-21
c. Experimental Difficulties	3-25
d. Infra-red Faraday Rotation Results	3-31
BIBLIOGRAPHY	3-43
CHAPTER 4 CONCLUSIONS	4-1
A. FORBIDDEN ENERGY GAP IN GaAs	4-1
a. Pressure Dependence	4-1
b. Temperature Dependence	4-8
B. EFFECTIVE MASS IN GaAs	4-10
a. Room Conditions	4-10
b. Pressure Dependence	4-13
c. Temperature Dependence	4-15
C. SUMMARY	4-17
BIBLIOGRAPHY	4-20

LIST OF FIGURES

	Page
FIG. 2-1 PLAN OF THE EXPERIMENTAL SYSTEM	2-2
FIG. 2-2 LIGHT INTENSITY TRANSMITTED THROUGH POLARIZER AND ANALYZER VERSUS TIME	2-5
FIG. 2-3 SCHEMATIC DIAGRAM OF PRESSURE SYSTEM	2-9
FIG. 2-4 PRESSURE GENERATING CYLINDER	2-10
FIG. 3-1 EFFECT OF PRESSURE ON THE OPTICAL TRANSMISSION OF GaAs 11	3-5
FIG. 3-2 ENERGY OF CONSTANT TRANSMISSION VERSUS PRESSURE FOR GaAs 11	3-6
FIG. 3-3 EFFECT OF PRESSURE ON THE OPTICAL TRANSMISSION OF GaAs 11a	3-7
FIG. 3-4 ENERGY OF CONSTANT TRANSMISSION VERSUS PRESSURE FOR GaAs 11a	3-8
FIG. 3-5 REFRACTIVE INDEX OF GaAs VERSUS LIGHT ENERGY	3-12
FIG. 3-6 (a) REFRACTIVE INDEX OF GaAs AT 1.00 eV VERSUS TEMPERATURE (b) REFRACTIVE INDEX OF GaAs AT 1.39 eV VERSUS PRESSURE	3-14
FIG. 3-7 (a) % TEMPERATURE COEFFICIENT OF n VERSUS LIGHT ENERGY (b) % PRESSURE COEFFICIENT OF n VERSUS LIGHT ENERGY	3-15
FIG. 3-8 SCHEMATIC DIAGRAM OF FARADAY ROTATION MEASUREMENT	3-18
FIG. 3-9 RECORDER TRACE SHOWING MEASUREMENT OF ANGLE OF FARADAY ROTATION	3-22
FIG. 3-10 MAGNETIC FIELD DEPENDENCE OF FARADAY ROTATION	3-24
FIG. 3-11 ANOMALOUS ROTATION IN GaAs NEAR THE 4.25μ CO ₂ ABSORPTION BAND	3-27

	Page
FIG. 3-12 THE EFFECT OF INTERBAND ROTATION AND MULTIPLE REFLECTION ON FREE CARRIER VERDET COEFFICIENT	3-28
FIG. 3-13 V FOR GaAs 12cw AND 19aw AS A FUNCTION OF λ^2 FOR ROOM CONDITIONS	3-32
FIG. 3-14 V FOR GaAs 18aw, 24aw, AND 11bw AS A FUNCTION OF λ^2 FOR ROOM CONDITIONS	3-33
FIG. 3-15 TEMPERATURE DEPENDENCE OF INTERBAND V	3-35
FIG. 3-16 TEMPERATURE DEPENDENCE OF V FOR GaAs 18aw	3-36
FIG. 3-17 TEMPERATURE DEPENDENCE OF V FOR GaAs 19aw	3-37
FIG. 3-18 TEMPERATURE DEPENDENCE OF V FOR GaAs 12cw	3-38
FIG. 3-19 PRESSURE DEPENDENCE OF INTERBAND V	3-39
FIG. 3-20 PRESSURE DEPENDENCE OF V FOR GaAs 18aw	3-40
FIG. 3-21 PRESSURE DEPENDENCE OF V FOR GaAs 19aw	3-41
FIG. 3-22 PRESSURE DEPENDENCE OF V FOR GaAs 12cw	3-42
FIG. 4-1 ENERGY SEPARATIONS IN GaAs VERSUS TEMPERATURE	4-9
FIG. 4-2 EFFECTIVE MASS OF N-TYPE GaAs AS A FUNCTION OF CARRIER CONCENTRATION	4-11
FIG. 4-3 PERCENT INCREASE OF m_{op}^* VERSUS PRESSURE FOR 3 N-TYPE GaAs SAMPLES	4-14
FIG. 4-4 PERCENT DECREASE OF m_{op}^* VERSUS TEMPERATURE FOR 3 N-TYPE GaAs SAMPLES	4-16

ABSTRACT

This report describes the results of an investigation of the effect of pressure and temperature on the energy gap and electron effective mass of GaAs. For this material, the applicability of the zero temperature Kane $k \cdot p$ theory at finite temperature was quantitatively tested by measuring the Faraday rotation as a function of pressure and temperature.

The quantitative comparison of experimentally determined masses with theory required three subsidiary measurements: (1) the pressure change of energy gap of GaAs was found to be $dE_g/dP = (1.17 \pm .03) \cdot 10^{-5}$ eV/bar; (2) the long wavelength pressure change of refractive index of GaAs was found to be $(1/n)(dn/dP) = -(7.0 \pm 0.5) \cdot 10^{-7}$ (1/bar); and (3) the long wavelength temperature change of refractive index of GaAs was confirmed to be $(1/n)(dn/dT) = (4.5 \pm 0.5) \cdot 10^{-5}$ (1/°K).

In the process of determining effective mass, a number of possible experimental errors in measuring Faraday rotation were delineated. Careful consideration of these errors led to an effective mass at the bottom of the GaAs Γ_{1c} conduction band of $m_0^* = (.064 \pm .002)m$ for room temperature and atmospheric pressure.

The results of measurements on three n-type samples of GaAs as a function of temperature and pressure show that the data were fitted best by using the Kane $k \cdot p$ theory at finite temperature

with an energy gap corrected from 0°K by accounting only for lattice expansion, rather than the experimentally determined optical energy gap which may be considered to have an implicit temperature dependence due to lattice expansion and an explicit temperature dependence.

If a suggestion by James is correct, the optical energy gap should be considered a free energy gap composed of the forbidden energy gap and an explicitly temperature dependent electron-phonon interaction. In this context, this investigation demonstrated that the most appropriate GaAs energy gap for the Kane $k \cdot p$ theory is the forbidden energy gap corrected for lattice expansion, and that effective mass in GaAs is very little affected, if at all, by electron-phonon interaction.

CHAPTER 1

THEORY

A. INTRODUCTION

The purpose of this investigation is to compare the experimentally determined temperature and pressure dependences of carrier effective mass in semiconductors with the predictions of semiconductor band theory. In particular, this work investigates (1) whether the relation between masses and energy gaps, given by the $k \cdot p$ method for zero temperature, is strictly applicable at finite temperatures, (2) the relation between effective mass, forbidden energy gap, and optical energy gap, and (3) the effect of electron-phonon interactions on effective mass.

The method chosen for this determination was the measurement of free carrier Faraday rotation, which is inversely proportional to the square of effective mass, independent of scattering time for light of high enough frequency, and capable of being measured at magnetic fields low enough to avoid magnetic quantization effects.

The material chosen was n-Type GaAs, which is known to have a Γ_1 conduction band minimum, a direct energy gap large enough to permit the observation of free carrier effects in isolation at relatively short wavelengths, and yet an effective mass small enough to be readily observed by Faraday rotation.

Chapter 1 contains the relevant band theory and the theory of Faraday rotation. The experimental equipment is discussed in Chapter 2. Chapter 3 includes the detailed method of measuring Faraday rotation and the raw experimental results. Finally, the implications of the results and conclusions are presented in Chapter 4.

B. BAND THEORY

a. Zero Temperature

The assumptions of semiconductor band theory at absolute zero can be summarized [1-1] as:

- (1) the properties of a crystal are derivable by separating it into a rigid perfect lattice of ion cores (nuclei plus closed electron shells) and the valence electrons;
- (2) the wave function of the valence electrons is separable into a product of single electron wave functions (1 electron approximation);
- (3) the lattice of ion cores is periodic, implying Bloch's theorem that the 1 electron wave function may be separated into a plane wave and a lattice periodic function; and
- (4) the coulomb interaction between electrons can be accounted for by assuming each electron moves in a self-consistent Hartree-Fock field produced by all the other electrons.

With these assumptions, the valence electrons can be shown to have the dynamical properties of free electrons with an effective

mass different from the free electron mass. In particular, Kane [1-2] has used a semi-empirical $\underline{k} \cdot \underline{p}$ perturbation approach to calculate band parameters for InSb by neglecting electron interaction. He begins by assuming the solution of the Schrodinger equation

$$\left[\frac{\underline{p}^2}{2m} + V \right] U_i = E_i U_i, \quad (1-1)$$

where U_i are the 1-electron basis wave functions with energy E_i , V is the effective potential for the electrons, and \underline{p} is the crystal momentum of a valence electron at a symmetry point in \underline{k} -space. At a small distance \underline{k} away from the symmetry point, (\underline{p}) in Eq. (1-1) becomes $(\underline{p} + \hbar \underline{k})$ and Eq. (1-1) becomes (neglecting terms of order \underline{k}^2)

$$\left[\frac{\underline{p}^2}{2m} + V + \frac{\hbar}{m} \underline{k} \cdot \underline{p} \right] U_i = E_i U_i. \quad (1-2)$$

The third term in the left-hand side bracket is the simple $\underline{k} \cdot \underline{p}$ interaction. Kane [1-3] uses a more complete formulation including spin-orbit interaction and treats exactly the interaction of valence bands and conduction band by diagonalizing an 8×8 matrix.

The results of Kane may be applied to GaAs, and the energy $E(\underline{k})$ versus reciprocal lattice vector \underline{k} for the Γ_1 conduction band minimum [1-5] can be shown to be (to order \underline{k}^2)

$$E(\underline{k}) = \frac{\hbar^2 \underline{k}^2}{2m} + \frac{E_g}{2} \left[\left(1 + \frac{4 \underline{k}^2 p^2}{3 E_g^2} \left(\frac{2}{E_g} + \frac{1}{E_g + \Delta} \right) \right)^{\frac{1}{2}} - 1 \right], \quad (1-3)$$

where m is the free electron mass, E_g the energy separation and P [1-2] the momentum matrix element between Γ_{lc} and Γ_{15v} states [1-3], and Δ is the \underline{k} -independent spin-orbit splitting of the Γ_{15v} band.

An electron effective mass m^* can then be defined by equating

$$E(\underline{k}) = \frac{\hbar^2 \underline{k}^2}{2m^*}, \quad (1-4)$$

and obtaining

$$\frac{1}{m^*} = \frac{1}{m} \left[1 + \frac{E_g m}{\hbar^2 \underline{k}^2} \left(1 + \frac{4 \underline{k}^2 P^2}{3 E_g} \left(\frac{2}{E_g} + \frac{1}{E_g + \Delta} \right) \right)^{\frac{1}{2}} - 1 \right]. \quad (1-5)$$

The effective mass at the bottom of the Γ_{lc} band is then m_o^* given by

$$\frac{1}{m_o^*} = \frac{1}{m} \left[1 + \frac{2m P^2}{3 \hbar^2} \left(\frac{2}{E_g} + \frac{1}{E_g + \Delta} \right) \right]. \quad (1-6)$$

Equation (1-6) can be simplified by defining an energy equivalent to the square of momentum matrix element as

$$E_p = \frac{2m P^2}{\hbar^2}, \quad (1-7)$$

so that Eq. (1-6) becomes

$$\frac{1}{m_o^*} = \frac{1}{m} \left[1 + \frac{E_p}{3} \left(\frac{2}{E_g} + \frac{1}{E_g + \Delta} \right) \right]. \quad (1-8)$$

b. Finite Temperature

At finite temperature T the lattice of ion cores is no longer perfect and the electron and lattice systems can no longer be considered uncoupled. In short, assumption (1) of the preceding

section no longer holds rigorously. However, the adiabatic approximation still allows the properties of a crystal to be derived by separating it into a system of valence electrons whose motion closely follows a distinct system of slightly displaced lattice ion cores. The interaction between the systems, termed the electron-phonon interaction, is then treated as a perturbation.

This situation has been examined from the viewpoint of statistical mechanics by James [1-4] and Brooks [1-5]. The discussion which follows is taken from James [1-4]. and assumes constant volume.

For a crystal in which the adiabatic approximation holds (i.e., weak electron-phonon interaction) the energy of the coupled crystal E_{ij} is defined as

$$E_{ij} = E_i + U_j + I_{ij} , \quad (1.9)$$

where E_i is the energy of the uncoupled valence electrons in the i th state, U_j is the energy of the uncoupled lattice in the j th state, and I_{ij} is the change in energy of the i,j quantum state due to electron-phonon interaction.

The partition function $Z(T)$ for the coupled crystal is

$$Z(T) = \sum_i \sum_j \exp[-E_{ij}/kT] = \exp[-F(T)/kT] , \quad (1.10)$$

where $F(T)$ is the free energy of the crystal. The partition function $Z_L(T)$ and free energy $F_L(T)$ of the decoupled lattice are

$$Z_L(T) = \sum_j \exp[-U_j/kT] = \exp[-F_L(T)/kT] . \quad (1-11)$$

Then the partition function $Z_i(T)$ and free energy $F_i(T)$ for the crystal in a particular electronic state i are

$$Z_i(T) = \sum_j \exp[-E_{ij}/kT] = \exp[-F_i(T)/kT] . \quad (1-12)$$

Using Eqs. (1-9), (1-11), and (1-12), it can be shown that

$$F_i(T) = E_i + F_L(T) + \Delta F_i(T) \quad (1-13)$$

where $\Delta F_i(T)$ is the change in the free energy of the i th electronic state due to the electron-phonon coupling. James [1-4] shows that

$$\Delta F_i(T) \approx \frac{\sum_j I_{ij} \exp[-U_j/kT]}{\sum_j \exp[-U_j/kT]} \approx I_{i\langle j \rangle} . \quad (1-14)$$

That is, $\Delta F_i(T)$ is the electron-phonon interaction averaged over the lattice states.

The internal energy, $E_i(T)$, of the crystal in the i th electronic state is found by averaging E_{ij} over all j states weighted with the appropriate Boltzmann factor:

$$E_i(T) = E_{i\langle j \rangle}(T) = \sum_j \frac{E_{ij} \exp[-E_{ij}/kT]}{Z_i(T)} . \quad (1-15)$$

$E_i(T)$ can be written as

$$E_i(T) = E_i + E_L(T) + \Delta E_i(T) , \quad (1-16)$$

where $E_L(T)$ is the internal energy of the lattice alone and $\Delta E_i(T)$ is the change in the average internal energy of the crystal due to electron-phonon interaction when the electronic system is in its i th state. James [1-4] shows that $\Delta E_i(T)$ consists of 2 parts: the average value of the electron-phonon coupling energy and the change in the average vibrational energy of the lattice due to the fact that electron-phonon coupling changes the relative weights of the states.

For a pure semiconductor in the 1-electron approximation,

$$E_i = n_i E_g + \sum_{\tau=1}^{n_i} (\epsilon_{\tau}^{(i)} + \eta_{\tau}^{(i)}) , \quad (1-17)$$

where E_g is the forbidden energy gap at 0°K , n_i is the number of electrons in the conduction band and of holes in the valence band in the i th electronic state, $\epsilon_{\tau}^{(i)}$ is the energy of the τ th excited electron and $\eta_{\tau}^{(i)}$ the energy of the τ th hole, each measured from the appropriate edge of the gap. Clearly E_i is zero at 0°K when the valence band is completely filled and the conduction band entirely empty, and this may be considered the zero of energy.

By substituting Eq. (1-17) into Eq. (1-16) and if it can be assumed that $\Delta E_i(T)$ is proportional to n_i , the number of excited particles, and independent of any particular set of occupied states, then

$$E_i(T) = n_i E_g(T) + \sum_{\tau} [\epsilon_{\tau}^{(i)} + \eta_{\tau}^{(i)}] + E_L(T) , \quad (1-18)$$

where

$$E_g(T) = E_g + \Delta E_g(T) , \quad (1-19)$$

and

$$\Delta E_g(T) = \Delta E_i(T)/n_i . \quad (1-20)$$

In this context $\Delta E_g(T)$ represents the minimum additional energy (other than the forbidden energy gap E_g) needed to create an electron-hole pair while the lattice is in thermal equilibrium. That is, $E_g(T)$ is the thermal forbidden energy gap since it is the minimum energy needed to excite an electron-hole pair (E_g), supply the average electron-phonon coupling energy, and supply the change in the average lattice vibrational energy.

From Gibbs-Helmholtz relations, James [1-4] shows that $\Delta F_i(T)$ implies a minimum change $\Delta F_g(T)$ in a free energy gap $F_g(T)$ as

$$\Delta F_g(T) = \Delta F_i(T)/n_i \quad (1-21)$$

and

$$F_g(T) = E_g + \Delta F_g(T) . \quad (1-22)$$

Thus $F_g(t)$ is the energy needed to excite an electron-hole pair (E_g) and supply the minimum change in the free energy of the crystal ith electronic state due to the electron-phonon coupling.

Equation (1-13) becomes

$$F_i(T) = \eta_i F_g(T) + \sum_{\tau} [\epsilon_{\tau}^{(i)} + \eta_{\tau}^{(i)}] + F_L(T) \quad (1-23)$$

so $F_g(T)$ is the minimum free energy change on creation of an electron-hole pair.

James has speculated that the change in the optical energy gap with temperature should be interpreted as a change in the free energy gap of Eq. (1-22). To determine if this is plausible, it is useful to point out the physical meaning of the thermal and free energy gaps. $E_g(T)$ may be written as

$$E_g(T) = E_g + [I_{i\langle j \rangle} + J_{i\langle j \rangle}]/n_i \quad (1-24)$$

where $J_{i\langle j \rangle}$ represents the change in the average vibrational energy of the lattice due to state weight change by electron-phonon coupling. Similarly the free energy gap of Eq. (1-22) may be written

$$F_g(T) = E_g + \Delta F_i(T)/n_i \simeq E_g + I_{i\langle j \rangle}/n_i \quad (1-25)$$

It can be seen that the difference between the free energy gap and the thermal energy gap is just $J_{i\langle j \rangle}/n_i$. Thus it is physically plausible to assign $F_g(T)$ to the optical energy gap since optical excitation of an electron-hole pair does not change the average lattice vibrational energy ($J_{i\langle j \rangle} = 0$) but does include the change in the electronic state energy due to electron-phonon coupling. That is, in an optical excitation, the excitation energy includes the energy to cross the forbidden energy gap plus the energy of the electron-phonon coupling appropriate to the excited electronic distribution. The lattice ion cores remain fixed and do not adjust to the new electronic state. However, the thermal excitation energy includes the energies mentioned in the optical excitation together with the

change in average vibrational energy as the ion cores adjust to thermal equilibrium with the new electronic state produced by the excitation.

The primary purpose of this investigation is to determine if the $k \cdot p$ theory of Eqs. (1-3) through (1-8) is adequate to describe the temperature and pressure dependences of effective mass at finite temperature. However, the experimental results must be fitted to the theory by choice of parameters m_0^* and some E_g . The above discussion defines 3 different E_g 's at constant volume:

- (1) the forbidden energy gap at zero temperature, E_g ,
- (2) the thermal energy gap, $E_g(T) = E_g + \Delta E_g(T)$,
- (3) the optical energy gap, $F_g(T) = E_g + \Delta F_g(T)$.

These gaps will be considered in Chapter 4 in fitting the theory to results which were not obtained at constant volume. In particular, as the temperature increases from 0°K , there will be lattice expansion which implicitly affects the energy gaps. This has been accounted for in Chapter 4 by using known values of lattice thermal expansion, lattice compressibility, and energy gap pressure coefficient to calculate a forbidden energy gap E_{gT} , with explicit temperature dependence, which replaces the constant E_g . Any implicit effect of the lattice expansion on the electron-phonon interaction is then concealed in the increase in free energy with

temperature, $\Delta F_g(T)$. Within this context, then, the applicability of the various energy gaps and the possibilities of electron-phonon effects on effective mass are considered.

C. THEORY OF FARADAY ROTATION

a. Semi-Classical Theory

Since classical theory does not include interband transitions and other quantum mechanical effects of semiconductor theory, the following conditions must be specified in order for a semi-classical approach to quasi-free carrier Faraday rotation to be valid:

$$(1) \omega < \omega_g = E_g/\hbar ;$$

$$(2) \omega \gg \tau^{-1}; \omega \gg \omega_c = eH/m^*c; \text{ and } \omega \gg \omega_p^2 = 4\pi N e^2/\epsilon m^*$$

where ω is the frequency of light of velocity c , E_g is the band gap of the material, H is the magnetic field, m^* the carrier effective mass, N the carrier concentration, and ϵ the dielectric constant of the material.

These assumptions insure that interband effects are negligible and that a semi-classical wave packet approach is valid. That is, the quasi-free electrons obey classical equations of motion with some effective mass and their interaction with light may be adequately described by Maxwell's equations.

Faraday rotation consists of the rotation of the plane of linearly polarized electro-magnetic radiation propagating in a material parallel to a static magnetic field. Plane polarized

light may be resolved into two oppositely rotating circularly polarized components and the rotation results from a differential dispersion of one component with respect to the other. This dispersion arises only from moving electrons or currents. Thus there can be no contributions to Faraday rotation from electrons in a filled band of a semiconductor. Only the quasi-free electrons produce Faraday rotation.

Thus the propagation of radiation in the material will be governed by a semi-classical wave equation for quasi-free electrons. The two circularly polarized components of linear polarization are governed by separate propagation constants whose different refractive indices imply the differential dispersion which causes Faraday rotation.

It can easily be shown that; if n_+ and n_- are respectively the refractive indices of the right and left-hand circularly polarized components, the angle of Faraday rotation θ_F is given by

$$\theta_F = \frac{\omega d}{2c} (n_+ - n_-) , \quad (1-26)$$

where ω is the frequency of the polarized light and d is the material thickness in the direction of propagation.

Stephen and Lidiard [1-6] have shown that $n_+ - n_-$, in terms of the low magnetic field conductivity tensor components of Abeles and Meiboom [1-7], can be written as

$$n_+ - n_- = -\frac{4\pi}{\omega \epsilon^{1/2}} \sigma_{xyz} H_z, \quad (1-27)$$

where σ_{xyz} is a conductivity tensor component and H_z is the static magnetic field along the direction of light propagation.

The general expression for σ_{xyz} for a single energy surface $\mathcal{E}(\underline{k})$ having cubic symmetry can be shown to be [1-9]

$$\sigma_{xyz} = \frac{e^3}{4\pi^3 \hbar^4 c \omega^2} \int \frac{df_o}{d\mathcal{E}} \frac{\partial \mathcal{E}}{\partial k_x} \left[\frac{\partial \mathcal{E}}{\partial k_y} \frac{\partial \mathcal{E}}{\partial k_x \partial k_y} - \frac{\partial \mathcal{E}}{\partial k_x} \frac{\partial^2 \mathcal{E}}{\partial k_y^2} \right] d\underline{k}, \quad (1-28)$$

where f_o is the Fermi distribution function. Combining Eqs. (1-26), (1-27), and (1-28), the semi-classical Faraday rotation is

$$\theta_F = \frac{e^3 dH}{2\pi^2 \hbar^4 c^2 n \omega^2} \int \frac{df_o}{d\mathcal{E}} \frac{\partial \mathcal{E}}{\partial k_x} \left[\frac{\partial \mathcal{E}}{\partial k_y} \frac{\partial^2 \mathcal{E}}{\partial k_x \partial k_y} - \frac{\partial \mathcal{E}}{\partial k_x} \frac{\partial^2 \mathcal{E}}{\partial k_y^2} \right] d\underline{k}, \quad (1-29)$$

whereas the classical Faraday rotation is

$$\theta_F = \frac{2\pi e^3 dHN}{nc^2 \omega^2 m^2} = \frac{e^3 dHN \lambda^2}{2\pi nc^4 m^2}. \quad (1-30)$$

Equations (1-29) and (1-30) may be equated if θ_F is considered to be determined by an optical effective mass, m_{op}^* , given by

$$\frac{1}{(m_{op}^*)^2} = \frac{1}{4\pi^3 \hbar^4 N} \int \frac{df_o}{d\mathcal{E}} \frac{\partial \mathcal{E}}{\partial k_x} \left[\frac{\partial \mathcal{E}}{\partial k_y} \frac{\partial^2 \mathcal{E}}{\partial k_x \partial k_y} - \frac{\partial \mathcal{E}}{\partial k_x} \frac{\partial^2 \mathcal{E}}{\partial k_y^2} \right] d\underline{k} \quad (1-31)$$

in place of the free electron mass m .

Thus by using Eq. (1-30), slopes of θ_F versus λ^2 are obtained which are inversely proportional to the square of the optical effective mass defined in Eq. (1-31).

Finally by using $k \cdot p$ theory as applicable to GaAs in Eqs. (1-3) through (1-8), Eq. (1-31) may be evaluated in terms of the band parameters m_o^* , E_g , and Δ . It can be shown that

$$N = \frac{1}{4\pi^3} \int f_o d\mathbf{k} = \frac{\sqrt{2}(kT)^{3/2} (m_o^*)^{3/2} \Gamma(3/2)}{\pi^2 \hbar^3} \left[\mathfrak{F}_{1/2} + \frac{5kT}{6} \left(1 - \frac{m_o^*}{m} \right)^2 \left(\frac{2}{E_g} + \frac{1}{E_g + \Delta} \right) \frac{\Gamma(3/2)}{\Gamma(3/2)} \mathfrak{F}_{3/2} \right], \quad (1-32)$$

and

$$\frac{1}{m_{op}^*} = \frac{1}{m_o^*} \left[1 - \frac{5kT}{3} \left(\frac{2}{E_g} + \frac{1}{E_g + \Delta} \right) \left(1 - \frac{m_o^*}{m} \right)^2 \frac{\mathfrak{F}_{3/2}}{\mathfrak{F}_{1/2}} \right], \quad (1-33)$$

where k is Boltzmann's constant and $\mathfrak{F}_{3/2}$, $\mathfrak{F}_{1/2}$ are Fermi integrals defined by Blakemore [1-8].

b. Quantum Mechanical Theory

Roch [1-9] has derived a quantum mechanical theory of Faraday rotation which gives the form of θ predicted by the semi-classical theory of Eqs. (1-26) and (1-27) in the high frequency limit of $\omega_g \gg \omega \gg e\hbar/m^*c$. This provides assurance that the semi-classical theory is adequate to describe the free carrier measurements at long wavelengths.

A quantum mechanical theory of interband Faraday rotation θ_{IB} which is slightly easier to apply to the present investigation has been developed by Boswarva, Howard, and Lidiard [1-10]. They find

that, in the one electron approximation in spectral regions where absorption is small, θ_{IB} is given by

$$\theta_{IB} = \frac{\pi e^2}{nc\hbar} \sum_n^o \sum_{n'}^u \left[\left(\frac{|v_{n'n}(+)|^2 - |v_{n'n}(-)|^2}{\omega_{n'n}^2 - \omega^2} \right) \frac{\omega^2}{\omega_{n'n}^2} \right], \quad (1-34)$$

where the sum over n is over all occupied electron states, the sum over n' is over all unoccupied states, and $\hbar\omega_{n'n}$ is the energy of the $n - n'$ transition. The velocity operator matrix elements are $|v_{n'n}(\pm)|$ for right (+) and left (-) circular polarized components of light.

This investigation is concerned with interband effects only to the extent that they affect measurement of free carrier Faraday rotation θ_F in GaAs. It will be seen in Chapter 3 that in the wavelength range 3 to 5μ it is necessary to correct for interband rotation arising from the transitions across the energy gap to obtain accurate θ_F . This has been done by measuring θ_{IB} in an n-type low carrier density sample and subtracting the result from the measured θ_F for higher carrier density samples. This is not strictly correct, since the carriers in the more highly doped samples exclude some of the possible transitions in Eq. (1-34) by occupying conduction band states. However, it is expected that the effect will be small since the energies involved in the measurements ($\hbar\omega < .4$ eV) are considerably smaller than the transition energies ($\hbar\omega_{n'n} \approx 1.5$ eV). Thus the effect on θ_{IB} (near ω) of excluding a

few transitions, from a set which all have high and nearly equal energies compared to $\hbar\omega$, should be small. Indeed Roth [1-11] has calculated the effect of free carriers on interband rotation and found that, for $N = 8 \cdot 10^{18} \text{ cm}^{-3}$, θ_{IB} in GaAs at 3μ is changed by at most 10%. For lower carrier concentrations the effect is even smaller. For a sample with $N = 3.4 \cdot 10^{18}$, $V = \theta/dH$ at 3μ for quasi-free carriers was found to be $4 \cdot 10^{-4}$ radians/(cm. gauss). $V_{IB} = \theta_{IB}/dH$ at 3μ was found to be $1 \cdot 10^{-5}$ radians/(cm. gauss). Thus 10% of V_{IB} at 3μ is $1 \cdot 10^{-6}$ radians/(cm. gauss) which is negligible compared to $4 \cdot 10^{-4}$ radians/(cm. gauss).

A second possible effect of interband rotation may arise from the additional absorption from 3 to 5μ in GaAs first reported by Spitzer and Whelan [1-12]. However, it is possible to make an order of magnitude estimate of any θ_{IB} arising from the transitions responsible for the additional absorption. Boswarva, Howard, and Lidiard [1-10] have shown that direct allowed transitions give the largest θ_{IB} effect. The form of θ_{IB} for direct allowed transitions can be written as

$$\frac{\theta_{IB}}{dH} = \frac{\mathcal{K}(g_{eff})\beta}{nz\hbar} \left[\frac{1}{(\omega + \frac{1}{\tau})(\omega_{n'n} - \omega - \frac{1}{\tau})^{1/2}} - \frac{1}{(\omega + \frac{1}{\tau})(\omega_{n'n} + \omega + \frac{1}{\tau})^{1/2}} \right] + \frac{1}{\omega_{n'n}^{3/2}}, \quad (1-35)$$

where τ is a damping time, β is a Bohr magneton, g_{eff} is an effective g factor for the transition, and \mathcal{K} may be written

$$\mathcal{K} = \frac{\alpha n \omega}{4(\omega + \frac{1}{\tau} - \omega_{n'n})^{1/2}}. \quad (1-36)$$

In Eq. (1-36), α is the absorption coefficient. The maximum χ may be estimated from α measured by Spitzer and Whelan [1-12] on a sample with $N = 5.4 \cdot 10^{18} \text{ cm}^{-3}$. This carrier concentration is larger than any used in this investigation. χ can be found as

$$\frac{\chi}{n} \approx 3.0 \cdot 10^8. \quad (1-37)$$

Estimating $\frac{1}{\tau}$ to be about 10^{14} sec^{-1} , it can be shown that

$$\frac{\theta_{IB}}{dH} \approx 2 \cdot 10^{-7} \frac{\text{radians}}{\text{cm. gauss}}, \quad (1-38)$$

which is about 50 times smaller than θ_{IB} arising from the forbidden energy gap, and hence is completely negligible.

CHAPTER 1 BIBLIOGRAPHY

- [1-1] See, for example, J. M. Ziman, Electrons and Phonons, chapter II, Clarendon Press, Oxford, 1960.
- [1-2] E. O. Kane, J. Phys. Chem. Solids, 1, p. 249, 1957.
- [1-3] Group Theory notation of R. H. Parmenter, Phys. Rev., 100, p. 573, 1955.
- [1-4] H. M. James, Photoconductivity Conference, pp. 204-212, Wiley and Sons, New York, 1956.
- [1-5] H. Brooks, Advances in Electronics and Electron Physics, Volume VII, pp. 117-127, Academic Press Inc., New York, 1955.
- [1-6] M. J. Stephen and A. B. Lidiard, J. Phys. Chem. Solids, 9, p. 43, 1958.
- [1-7] B. Abeles and S. Meiboom, Phys. Rev., 95, p. 31, 1954.
- [1-8] J. S. Blakemore, Semiconductor Statistics, Appendix B, Pergamon Press, New York, 1962.
- [1-9] L. M. Roth, Phys. Rev., 133, A542, 1964.
- [1-10] I. M. Boswarva, R. E. Howard, and A. B. Lidiard, Proc. Roy. Soc. A, 269, p. 125, 1962.
- [1-11] L. M. Roth, Bull. Am. Phys. Soc., II, 10, 1965, and private communication, 1965.
- [1-12] W. G. Spitzer and J. M. Whelan, Phys. Rev., 114, p. 59, 1959.

CHAPTER 2

EQUIPMENT

A. INTRODUCTION

All measurements were conducted in a constant temperature, controlled 40% humidity room. A scaled plan of the experimental system is shown in Figure 2-1. Light from a source was mechanically chopped at 13 cps and made monochromatic by a Perkin-Elmer[†] model 12C single-beam spectrometer modified to allow the beam from the exit slit to emerge from the case. The divergent beam was turned 90° and made convergent by the mirror system $M_1 - M_2 - M_3$. For the Faraday rotation measurements the light then passed through a polarizer held in the 2 inch axial hole of the magnet. After being focused at the center of the magnet gap (sample area), the beam passed through an analyzer held in the opposite axial magnet hole by a rotatable mount. The light was then focused by the mirror M_4 on the detector. The resultant AC signal then passed through a Perkin-Elmer[†] preamplifier and model 107 amplifier in which the signal was phase detected and rectified. The DC signal was then recorded by a Leeds and Northrup[‡] type G recorder.

For the measurements of the pressure shift of the GaAs absorption edge, the polarizer, analyzer, rotatable mount, detector and mirror M_4 were removed and a photomultiplier housing and tube described by Zallen [2-1] were placed to intercept the beam as it emerged from the axial magnet hole.

[†] Perkin-Elmer Corporation, Norwalk, Connecticut.

[‡] Leeds and Northrup Company, Philadelphia, Pennsylvania.

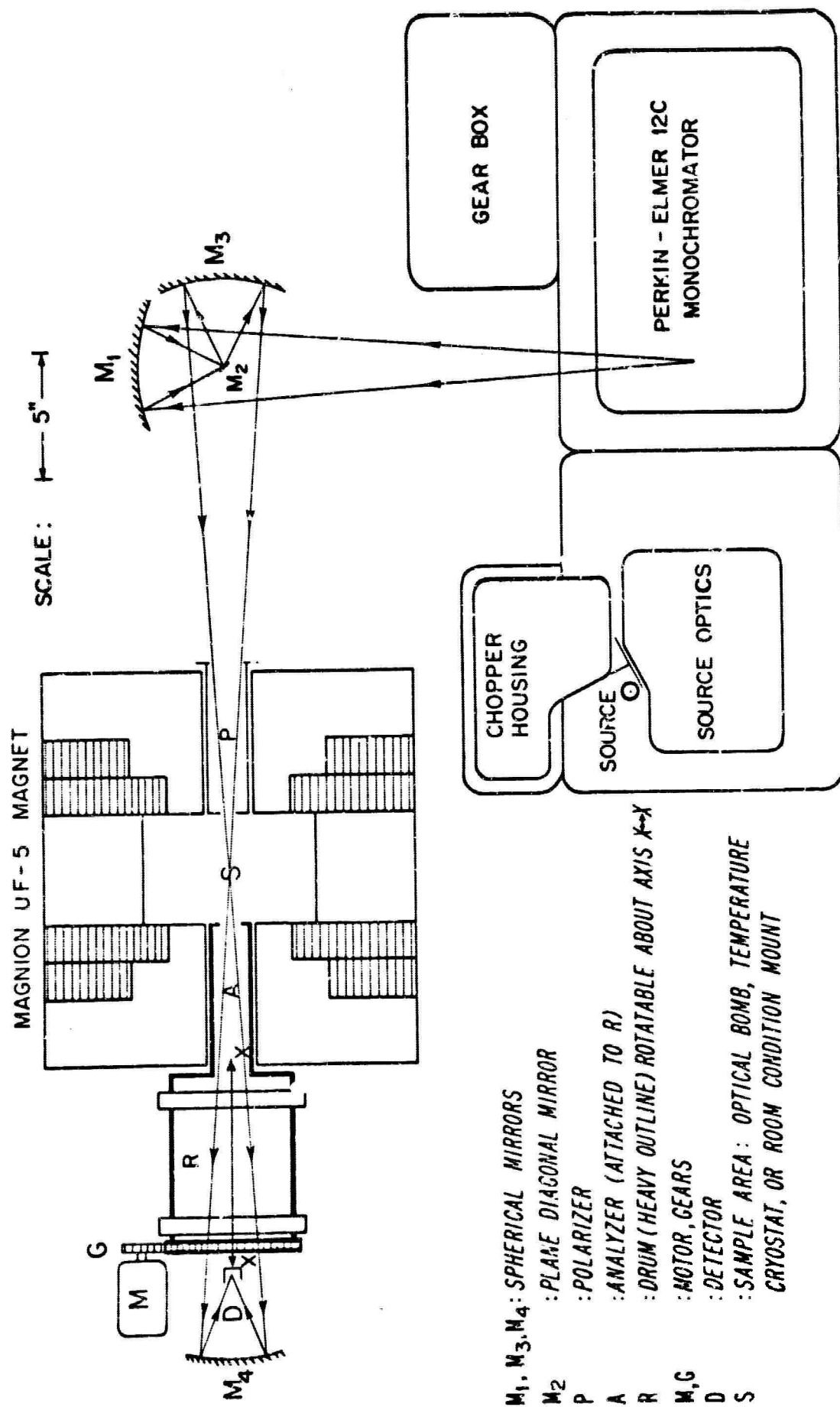


FIG. 2-1 PLAN OF THE EXPERIMENTAL SYSTEM

The measurements of pressure and temperature shifts of the refractive index were done using the same spectrometer but with an optical path and pressure system described by Prakash [2-2].

B. OPTICAL EQUIPMENT

a. Sources

Since the pressure and temperature experiments of this investigation lasted on the order of 10 hours, it was desirable that the radiation source be as stable as possible. The source supply was a .5 kva ballasted regulating 120 volt transformer which was in turn supplied by a 1.5 kva regulating transformer. A Nernst glower tested in the infra-red had a 15 minute stability of .8% and a 2 hour stability of 1-2%. A 200 watt globar under the same conditions gave only 1/2 to 2/3 of the light intensity of the Nernst glower. However, the globar had a 15 minute stability of .4% and a 10 hour stability of < 1% and was the source used in the infra-red for wavelengths > 2.5 μ .

For wavelengths between .7 and 2.5 μ a GE[†] 18A-T10 SR3 tungsten lamp connected to a 6.3 volt stepdown transformer was powered by the above supply and gave more light than the globar with the same stability.

b. Spectrometer and Mirrors

The model 12C spectrometer was used with the following prisms for the best combination of transmission and resolving power in the

[†]General Electric Co., Lamp Department, Cleveland, Ohio.

given wavelength λ regions: KBr, $18\mu < \lambda < 8\mu$; NaCl, $13\mu < \lambda < 5\mu$; CaF_2 , $8\mu < \lambda < 2.5\mu$; DF glass, $2.5\mu < \lambda < 0.7\mu$.

The KBr, NaCl, and CaF_2 prisms were calibrated using absorption bands of CO_2 , H_2O , NH_3 , and HBr vapors [2-3]. The DF glass prism was calibrated using Argon and Mercury spectrum tubes [2-4]. The errors of all calibrations are estimated as $< 1\%$.

All mirrors throughout the system were uncoated front-surface aluminized pyrex. The effect of differing mirror reflectivities on polarized light modes is discussed in section 3.D.

c. Polarizers

The polarizers used were constructed of rolled AgCl^\dagger in a "zero-displacement" design due to Makas and Shurcliff [2-5]. Transmission was constant from 2 to 18μ and the degree of polarization [2-6] obtained in the light beam was 94%. The six AgCl plates each of the polarizer and analyzer were placed at an angle to the light beam of 64° in non-magnetic collimating tubes that fitted snugly inside the 2-inch axial magnet holes. The analyzer was attached to a large non-magnetic rotatable drum mount geared to an electric motor. A typical trace recorded while the analyzer was slowly rotated is shown in Figure 2-2. It can be seen that the transmitted intensity obeys the relation:

$$I_T = I_m + I_M \cos^2(\omega_A s) \quad (2-1)$$

where I_T is the transmitted intensity, I_m is the intensity at a

[†] Harshaw Chemical Co., Cleveland, Ohio.

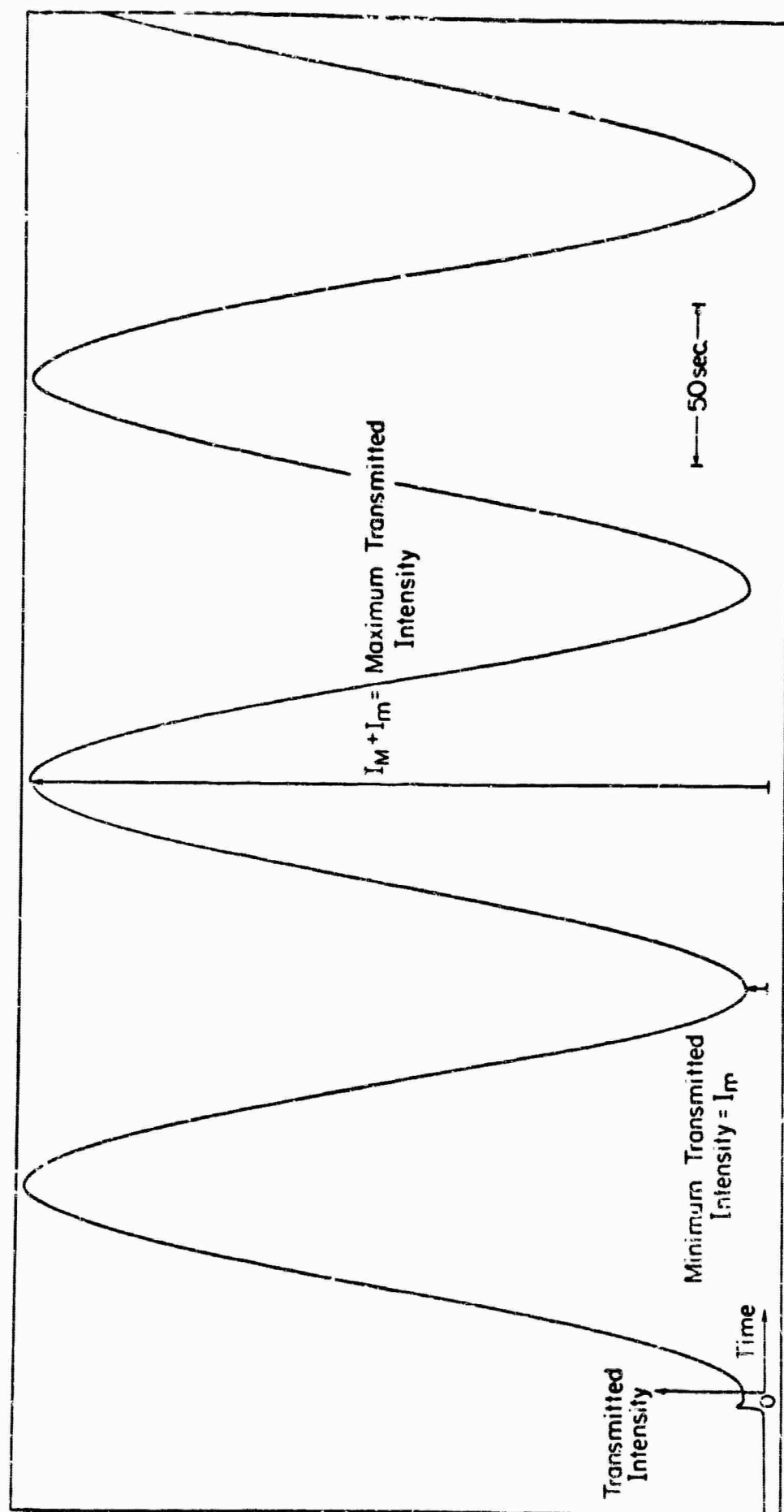


FIG. 2-2 LIGHT INTENSITY TRANSMITTED THROUGH POLARIZER AND ANALYZER VERSUS TIME

minimum, $I_M + I_m$ is the intensity at a maximum, ω_A is the angular frequency of rotation of the analyzer, and s is the time.

d. Detectors

It will be shown in section 3.D that Faraday rotation measurements using wavelength dependent sources demand a certain minimum resolution. The best detectors in the 1 to 5μ region are cooled PbS photoconductive cells and cooled InSb photovoltaic diodes. Unfortunately in the experimental system shown in Figure 2-1 a stray magnetic field of the order of 20 gauss existed in the detector area and altered the response of these detectors when the magnet was turned on. Magnetic shielding of μ metal partially enclosing the area was unable to eliminate this effect and the detector for the Faraday rotation experiments was limited to a Reeder[†] RP-5W thermocouple with KBr window which was unaffected by magnetic field. To our knowledge, this is the best available commercial thermocouple compatible with a Perkin-Elmer spectrometer. Determinations in section 3.D demonstrate that the experimental system using this detector attains the critical minimum resolution for accurate Faraday rotation measurements.

For the absorption edge pressure shifts and the refractive index experiments, an RCA[‡] 7102 photomultiplier tube in a housing powered by a Beva^{*} model 302B-5 .1% regulated supply. The tube was cooled by dry ice and used in the wavelength region .7 to 1.3μ . For refractive

[†] Charles M. Reeder and Co., Inc., Detroit, Michigan

[‡] Radio Corporation of America, Electron Tube Division, Harrison, New Jersey.

^{*} Beva Electronics Inc., Trenton, New Jersey.

index measurements from 1.0 to 2.5μ , an ECA[†] PbS photoconductive cell cooled by dry ice was used as a detector. For wavelengths from 2.5 to 4.2μ in the refractive index determinations, a TI[‡] model M-2000 InSb photovoltaic diode cooled by liquid N₂ was used.

C. OTHER EQUIPMENT

a. Magnet and Power Supply

The magnet shown in scale in Figure 2-1 was a Magnion^{*} model UF-5 electromagnet with a 2 ohm impedance. The 5 inch pole pieces and the supporting X-frame were pierced by 2 inch axial holes. The gap could be varied by using spacers and was fixed at a separation of $4\frac{1}{2}$ inches to admit the optical bomb.

The .01% regulated DC power supply for the magnet was a Harvey Wells (division of Magnion^{*}) model HS 1050 with an output impedance of 2 ohms and a modification to produce $7\frac{1}{2}$ kilowatts at 115 volts for the peak current of 65 amperes. This supply was further modified by McElroy [2-7] to include devices to warn of magnet cooling water stoppage and excess magnet temperature and a field reversal switch.

The magnet's field was probed using a Rawson^{††} type 722 rotating coil gaussmeter, and was found to be linear with power supply current and homogeneous to 1% over the central cubic inch. The field

[†] Electronics Corporation of America, Cambridge, Massachusetts

[‡] Texas Instruments Inc., Materials and Sensors Department, Dallas, Texas.

^{*} Magnion Inc., Burlington, Massachusetts.

^{††} Rawson Electric Instrument Co., Cambridge, Massachusetts.

showed no hysteresis on reversal. At peak current, the magnetic field stability was $> 1\%$ while the field at the center of the gap was 5.35 kilogauss with an error of 1% . This field was used for all Faraday rotation measurements except tests of magnetic field dependence.

b. Pressure Equipment

The pressure system was a conventional gas apparatus such as the one described by Holland [2-8]. A schematic diagram is shown in Figure 2-3. The pressure fluid chosen was He gas for reasons detailed below. The system is operated by letting gas at 2000 psi into the Harwood[†] double-acting intensifier whose operation has been described by Feinleib [2-9]. The intensifier compresses the gas through the bypass into the pressure cylinder and optical bomb to 2 kilobars. The hand oil pump is then used to pressurize the oil press which drives a piston into the pressure generating cylinder. A piston head seal [2-10] at the end of this piston moves past the bypass isolating the optical bomb and pressure cylinder and compressing the He gas to 10 kilobars.

The pressure generating cylinder is shown in scale in Figure 2-4. It has been tested to a nominal (counting friction) 12.5 kilobars. The gauge plug had one standard coned electrical terminal shown in Figure 4-5 of reference [2-8] and mounted a Manganin gauge coil.

[†] Harwood Engineering Co., Inc., Walpole, Massachusetts.

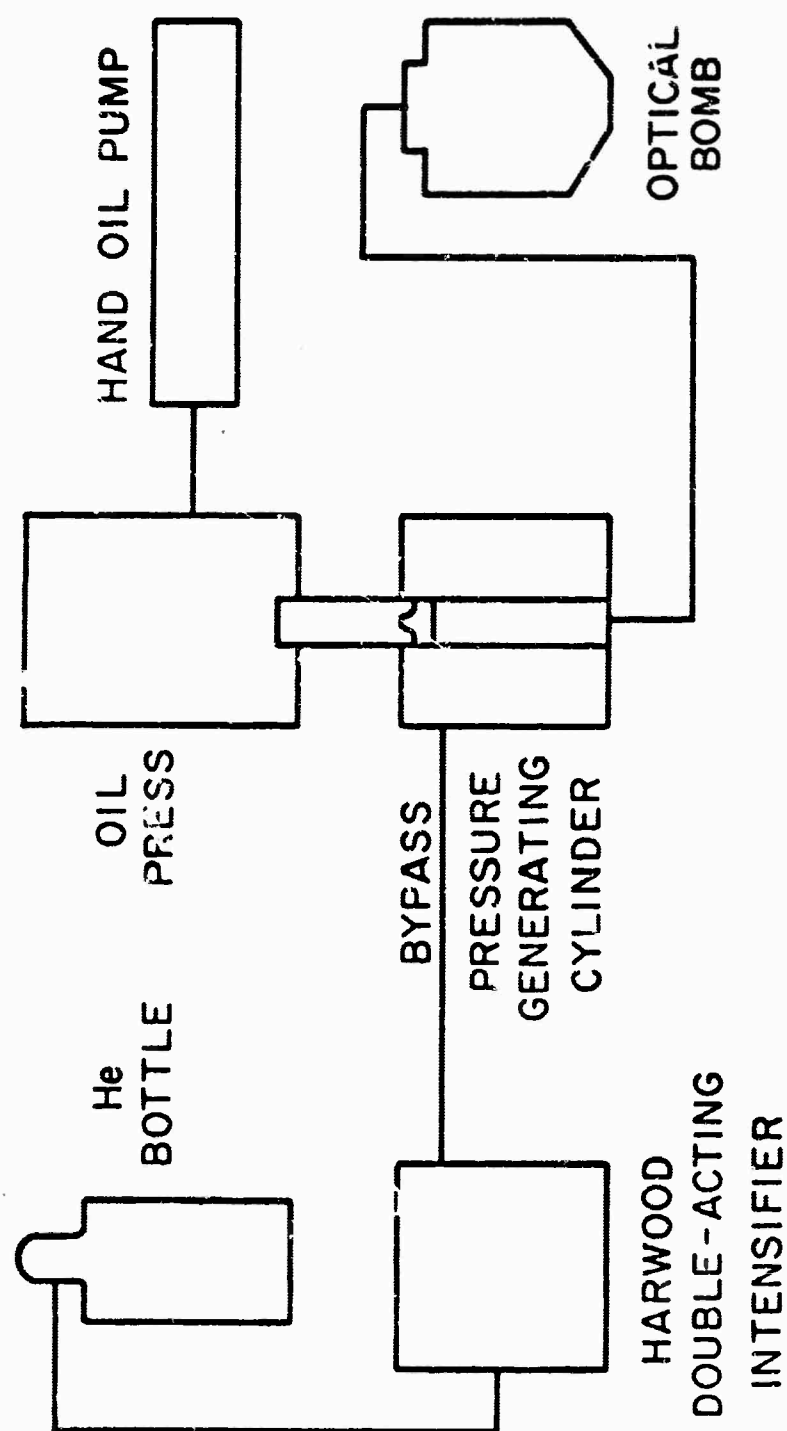


FIG. 2-3 SCHEMATIC DIAGRAM OF PRESSURE SYSTEM

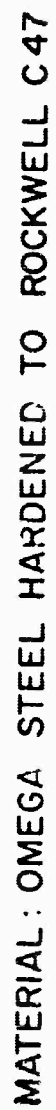


FIG. 2-4 PRESSURE GENERATING CYLINDER

The pressure was determined by measuring the change of resistance of the gauge coil by means of a bridge circuit [2-11]. The coil was calibrated by observing the pressure (7566.2 bars) [2-12] at 0°C when the resistance changed in a freezing Hg capillary on a terminal plug mounted in the optical bomb. The calibration was assumed linear [2-13]. The determination was made twice during the period of the investigation and the calibration repeated to 1% which is about the experimental error in the determination. A sudden change of 2% in the 1 bar resistance of the coil which occurred between the two determinations thus had no observable effect on the calibration. Similarly, an explosive decompression which left the 1 bar resistance of the coil unchanged was assumed to have not changed the calibration. This assumption is supported by the fact that nominal pressures, after subtracting a constant frictional effect, agreed to $\pm 3\%$ with the coil both before and after the explosion, and indeed throughout the entire investigation. Consequently the error in measuring pressure is estimated to be the error of the calibration or $\pm 1\%$.

The non-magnetic optical bomb was made from a design by Langer and Warschauer [2-14] using Westinghouse[†] W545 stainless steel having a magnetic permeability at 26°C of 1.0039. The bomb was hardened to the maximum for the material, Rockwell (R) C 39. It was tested to a nominal 12 kilobars and showed signs of stretching. The maximum

[†]Westinghouse Electric Corporation, Materials Manufacturing Division, Blairsville, Pennsylvania.

pressure since applied has been 10.3 kilobars. The optical plugs, cones, push pieces, t-pieces, and spacers were made of non-magnetic BeCu hardened to RC 38 which is about that material's maximum hardness. Unsupported portions of the push pieces have a tendency to stretch non-elastically under a pressure to a limit of about .001 inches for 10 pressure cycles after which they must be remachined. The optical windows [2-15] were C-axis sapphires for reasons explained in section 3.D.

The liquids pentane, CS_2 , and Freon 11 and 12 were considered for use as pressure fluids, but rejected because of their many absorption bands in the range 1 to 5μ . Nitrogen gas was rejected for the same reason when experiment showed the formation of an absorption band near 4μ as pressure was applied. While N_2 is a symmetric molecule and hence has no infra-red absorption, an impurity molecule under high pressure couples with the N_2 molecule to produce a change in dipole moment and consequent absorption bands.

A similar experiment on Helium gas showed that no such bands appeared up to 10 kilobars. The total transmission through two sapphire windows and He gas changed by only 2% in 10 kilobars indicating that He was the most suitable fluid for absolute transmission measurements.

c. Cryostat, Sample Holders, and Positioning Mechanism

The cryostat used for temperature measurements has been described by Cardona [2-16]. A modification was made in the cold finger to allow the coolant to circulate around the sample holding block.

For Faraday rotation measurements, the sample holders were $5/8$ inch diameter brass disks $1/16$ inch thick which had central apertures slightly smaller than the sample dimensions. When the holders were placed in optical bomb, cryostat, or room-condition mount, radiation could pass only through sample and aperture. The samples were of the order of .1 cm. thick. They were attached to the holders by an upright edge using a tiny drop of GE 7301 adhesive cement which was sufficient to hold them firmly against the sample holders while prohibiting strain as temperature and pressure were changed. Temperature measurements with a thermocouple soldered to a sample and another attached to its sample holder while in the cryostat showed that the sample assumed the same temperature as the holder. Thereafter, all temperature measurements were made with a calibrated copper-constantin thermocouple attached to the sample holder.

For the absorption edge and refractive index measurements a sample holder described by Zallen [2-17] was used without the sapphire plates.

The positioning mechanism consisted of a Palmgren[†] No. 82 rotary table mounted vertically below the magnet. A heavy 2 inch Al column attached to the table extended up into the sample area to support optical bomb, cryostat, and room-condition mount. These instruments could then be positioned to .001 inches perpendicularly to the light beam by vertical and horizontal adjustment micrometers which were a great aid in optical alignment. The mechanism is massive enough to be quite stable and was unaffected by magnetic field.

[†] Chicago Tool and Engineering Co., Chicago, Illinois.

CHAPTER 2 - BIBLIOGRAPHY

- [2-1] R. Zallen, Technical Report No. HP-12, Fig. 2-6, Gordon McKay Laboratory of Applied Science, Harvard University, 1964 (unpublished).
- [2-2] V. Prakash, Technical Report No. HP-13, Fig. 2-1, Gordon McKay Laboratory of Applied Science, Harvard University, 1965 (unpublished).
- [2-3] Instruction Manual, 3A, pp. 51-52, Perkin-Elmer Corporation, Norwalk, Connecticut, 1956 (unpublished).
- [2-4] S. Zwerdling and J. P. Theriault, *Spectrochimica Acta*, 17, p. 819, 1961.
- [2-5] A. S. Makas and W. A. Shurcliff, *J. Opt. Soc. Amer.*, 45, p. 998, 1955.
- [2-6] W. A. Shurcliff, Polarized Light, p. 11, Harvard University Press, Cambridge, Massachusetts, 1962.
- [2-7] P. T. McElroy, Gordon McKay Laboratory of Applied Science, Harvard University (to be published).
- [2-8] M. G. Holland, Technical Report No. HP-4, Gordon McKay Laboratory of Applied Science, Harvard University, 1958 (unpublished).
- [2-9] J. Feinleib, Technical Report No. HP-11, p. III-2, Gordon McKay Laboratory of Applied Science, Harvard University, 1963 (unpublished).
- [2-10] P. W. Bridgman, The Physics of High Pressure, p. 39, G. Bell and Sons, Ltd., London, 1949.
- [2-11] D. M. Warschauer and W. Paul, *Rev. Sci. Instr.*, 29, p. 675, 1958.
- [2-12] D. N. Newhall, L. H. Abbott and R. A. Dunn, in High-Pressure Measurement, ed. by A. A. Gardini and E.C. Lloyd, Butterworth Inc., Washington, 1963.
- [2-13] See reference [2-10], but p. 73.

- [2-14] D. Langer and D. M. Warschauer, Rev. Sci. Instr., 32,
p. 32, 1961.
- [2-15] See reference [2-1], but Fig. 2-2.
- [2-16] M. Cardona, Technical Report No. HP-5, Fig. 6-2, Gordon
McKay Laboratory of Applied Science, Harvard University,
1959 (unpublished).
- [2-17] See reference [2-1], but Fig. 2-4.

CHAPTER 3

RESULTS

A. SAMPLES AND LIST OF EXPERIMENTS

The single crystal GaAs optical samples and the experiments in which they were used in this investigation are characterized in Table 3-1.

The carrier concentrations N result from doping with Sn and Te impurity atoms. At the present time there exist no simple relations for the effect of impurities on the conduction band energy levels predicted using the $k \cdot p$ theory of Chapter 1. The point of view of this investigation has been to assume that each sample contains N quasi-free electrons distributed according to Eq. (1-32) over a conduction band unaffected by impurities. This is tantamount to assuming that, in replacing a host atom, each impurity atom contributes a quasi-free electron and an electron energy level identical to the state which would arise from the replaced host atom. Under this assumption, no deionization can take place and N remains constant as a function of temperature and pressure.

The available experimental evidence indicates that the assumption of constant N is not unreasonable for samples 18aw, 19aw, and 12cw. Several investigators (3-23) have shown there is no deionization in GaAs down to 70 K. for similar samples. In general, for these values of N , donor impurity states in GaAs are considered to have merged into the conduction band. Finally, the consistency of the final results with the

assumption of constant N for several different N indicate the assumption is likely to be valid.

The carrier concentrations were determined at 295 K. by measuring the Hall constant R of parallelepiped samples whose dimensions were approximately $.13 \times .13 \times 1.3 \text{ cm}^3$ and which were adjacent in the ingot to the optical samples. Hall voltages were measured at a magnetic field of 5.85 kilogauss where R is independent of field (3-24).

A five probe technique was used which, with reversal of field and current, allows subtraction of magneto-resistive and voltage drop effects. Voltages were measured on a Leeds and Northrup[†] type K-3 potentiometer. The voltage probes were $> .27 \text{ cm}$ distant from the current leads so that shorting effects reduced the Hall voltage by $< 1\%$ [3-1]. All contacts were tested to be ohmic and the current was chosen so that power dissipation in the sample was < 1 microwatt. The estimated error in measuring the Hall constant R was $\pm 5\%$.

R was taken as determined by

$$R = \frac{1}{Nec} , \quad (3-1)$$

[†] Leeds and Northrup Company, Philadelphia, Pennsylvania.

TABLE 3-1 SAMPLES AND EXPERIMENTS

Sample	N^{\dagger} (cm.^{-3})	d^{\ddagger} (cm.)	$\mu^{\dagger\dagger}$ ($\text{cm}^2/\text{volt. sec}$)
11	$< 1.5 \cdot 10^{15}$	$1.53 \cdot 10^{-3}$	> 6000
11a	$< 1.5 \cdot 10^{15}$	$2.54 \cdot 10^{-3}$	> 6000
11bw ^{††}	$< 1.5 \cdot 10^{15}$	$3.61 \cdot 10^{-1}$	> 6000
24aw ^{††}	$3.2 \cdot 10^{16}$	$2.55 \cdot 10^{-1}$	6150
18aw ^{††}	$1.3 \cdot 10^{17}$	$3.81 \cdot 10^{-2}$	2400
19aw ^{††}	$7.3 \cdot 10^{17}$	$4.29 \cdot 10^{-2}$	2680
12cw ^{††}	$3.4 \cdot 10^{18}$	$1.01 \cdot 10^{-2}$	2500

Experiment	Samples	Runs
Transmission vs. Pressure	11, 11a	2
Refractive Index vs. Pressure	11	3
Refractive Index vs. Temperature	11	2
Faraday Rotation vs. Wavelength	11bw, 24aw, 18aw 19aw, 12cw	5
Faraday Rotation vs. Pressure	11bw, 28aw, 19aw, 12cw	4
Faraday Rotation vs. Temperature	11bw, 18aw, 19aw, 12cw	4

[†]N : n-type carrier concentration

[‡]d : thickness

^{††} μ : Hall mobility

^{††}w : 1° wedged sample

where e is the electron charge in esu. Ehrenreich [3-2] has shown the most likely scattering in GaAs is a mixture of polar and ionized impurity scattering. He uses a Hall coefficient scattering factor of 1. It cannot be less but might be greater. To account for this possibility, the error in N was estimated to be $\pm 15\%$, -5% .

The Hall mobility μ was determined using the measured resistivity ρ in the relation

$$\mu = \frac{1}{\rho N e \cdot 3 \cdot 10^2} \quad +5\% - 15\% . \quad (3-2)$$

Optical sample thicknesses $d > 10^{-2}$ cm. were measured to $\pm 2 \cdot 10^{-4}$ cm. by using a micrometer comparator and precision gage blocks. Samples with thicknesses $< 10^{-2}$ cm. were measured using a fringe technique described in section 3.C. Those samples with a suffix w in Table 3-1 were wedged 1° (see 3:D) and their thicknesses were averaged. The samples were polished on both sides using a method described by Zallen [3-3].

3. PRESSURE DEPENDENCE OF THE ABSORPTION EDGE IN GaAs

The **ratio** of light intensity I transmitted through a medium to the incident light intensity I_0 is defined as the **optical transmission** t . For a dielectric medium of index of refraction $\bar{n} = (n + ik)$, under the condition that $n \gg k$, t is given by [3-4]

$$t = \frac{(1 - R)^2}{(e^{\alpha d/2} - R e^{-\alpha d/2})^2 + 4R \sin^2 \varphi} \quad (3-3)$$

$$R = \frac{(n - 1)^2}{(n + 1)^2} \quad \alpha = \frac{4\pi k}{\lambda} \quad \varphi = \frac{2\pi n d}{\lambda} \quad (3-4)$$

where λ is the wavelength of normally incident monochromatic light.

For αd large enough, Eq. (3-3), averaged over the band width $\Delta\lambda$, becomes [3-5]

$$t_{av.} = (1 - R)^2 e^{-\alpha d} \quad (3-5)$$

In this investigation, under conditions such that Eq. (3-5) is valid, optical transmission to $I/I_0 = 10^{-3}$ as a function of pressure P to 10 kilobars has been measured for two samples of GaAs near the fundamental absorption edge at 295°K.

Figure 3-1 shows the effect of pressure on the transmission of GaAs 11. The experiment was performed with the system used for refractive index measurements [2-2]. Spectral slit width was .004 eV. Figure 3-2 is taken from Fig. 3-1 and displays the effect of pressure on the energy of constant transmission $h\nu_t$ for various values of $t < 10^{-2}$.

For Fig. 3-3, equivalent to Fig. 3-1 for GaAs 11a, the experimental system of Fig. 2-1 was used as described in Chapter 2 for transmission measurements. Spectral slit width was .002 eV. Figure 3-4 is taken from Fig. 3-3 exactly as Fig. 3-2 is taken from Fig. 3-1.

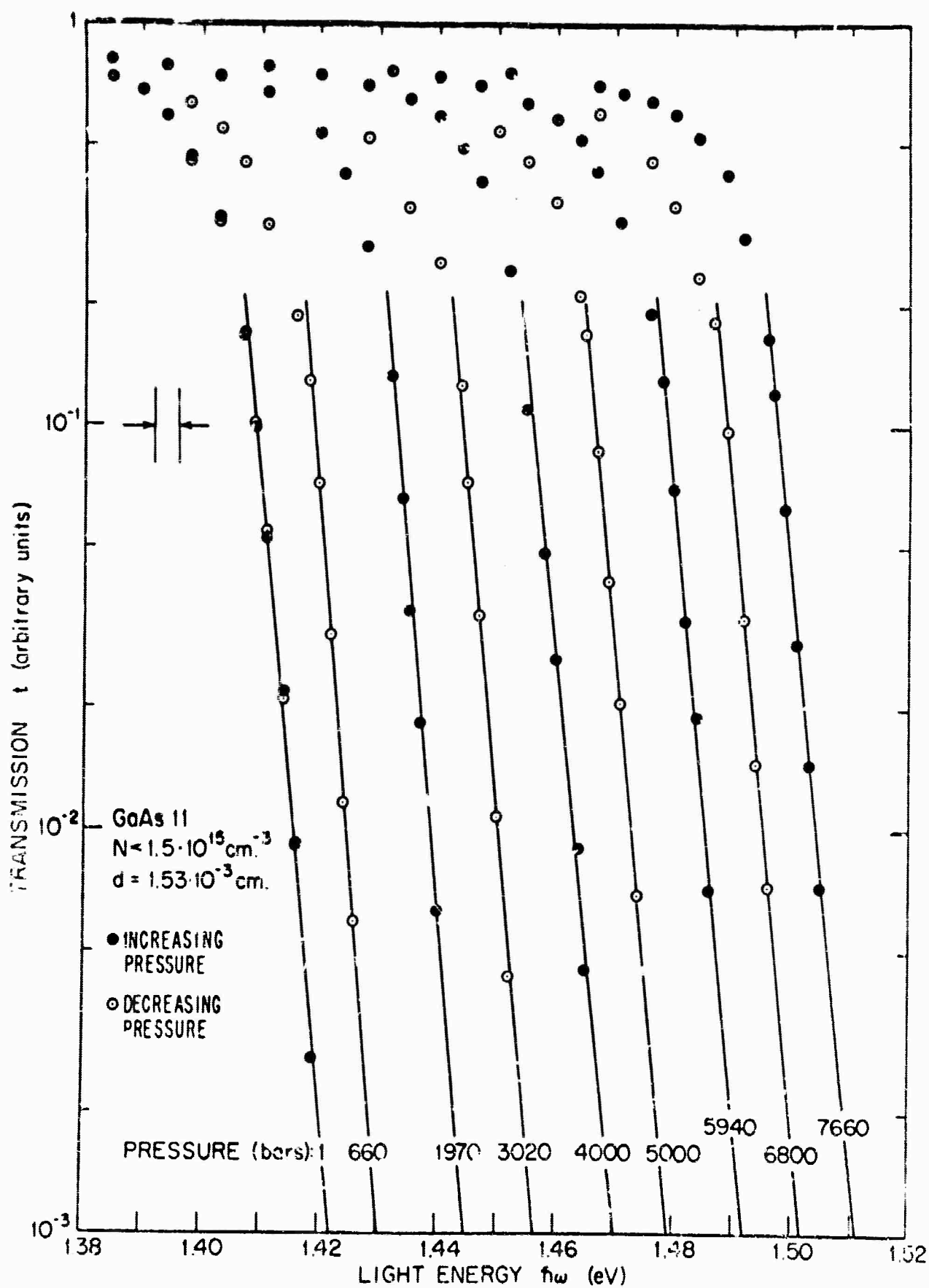


FIG. 3-1 EFFECT OF PRESSURE ON THE OPTICAL TRANSMISSION OF GaAs II

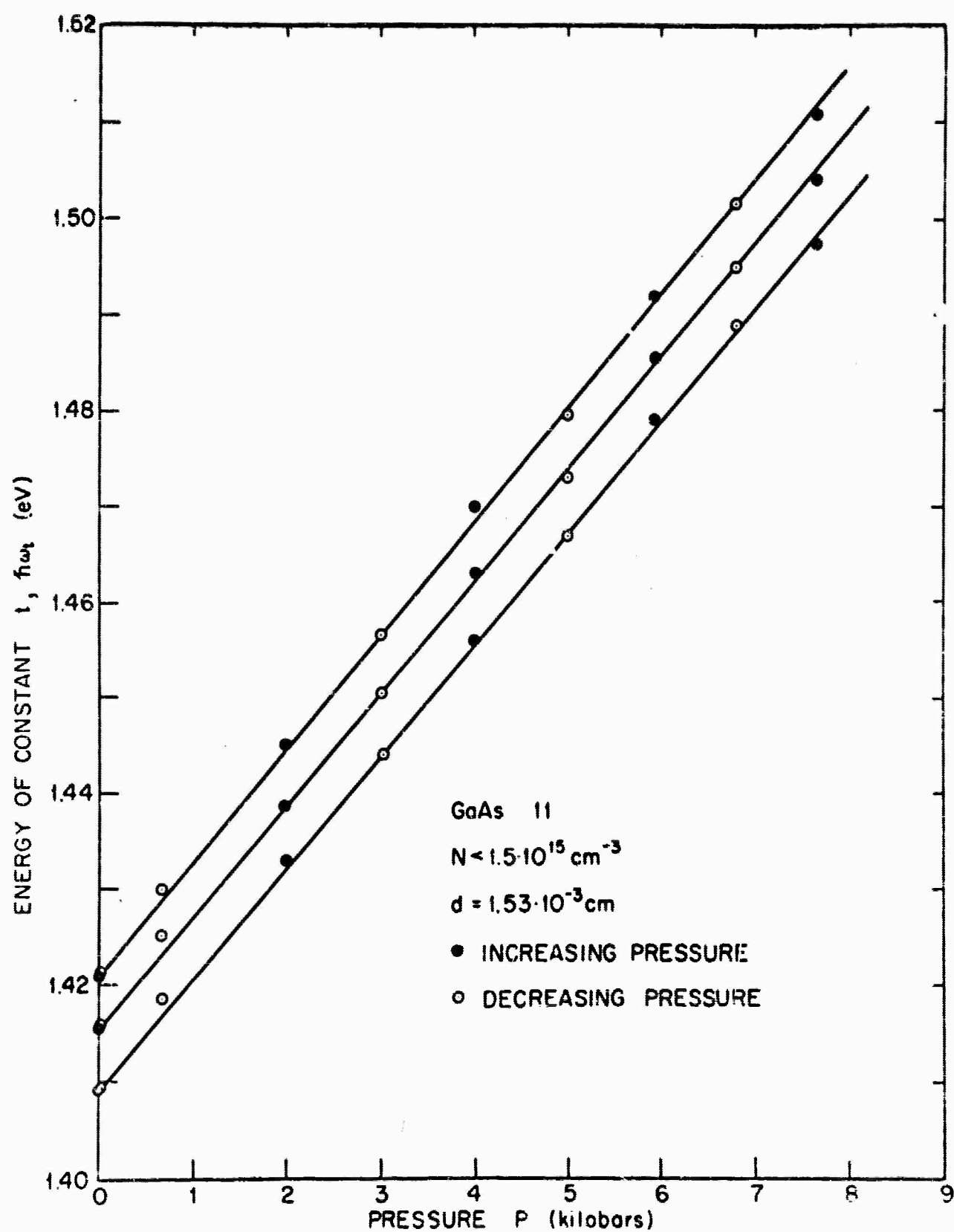


FIG. 3-2 ENERGY OF CONSTANT TRANSMISSION VERSUS PRESSURE FOR GaAs II.

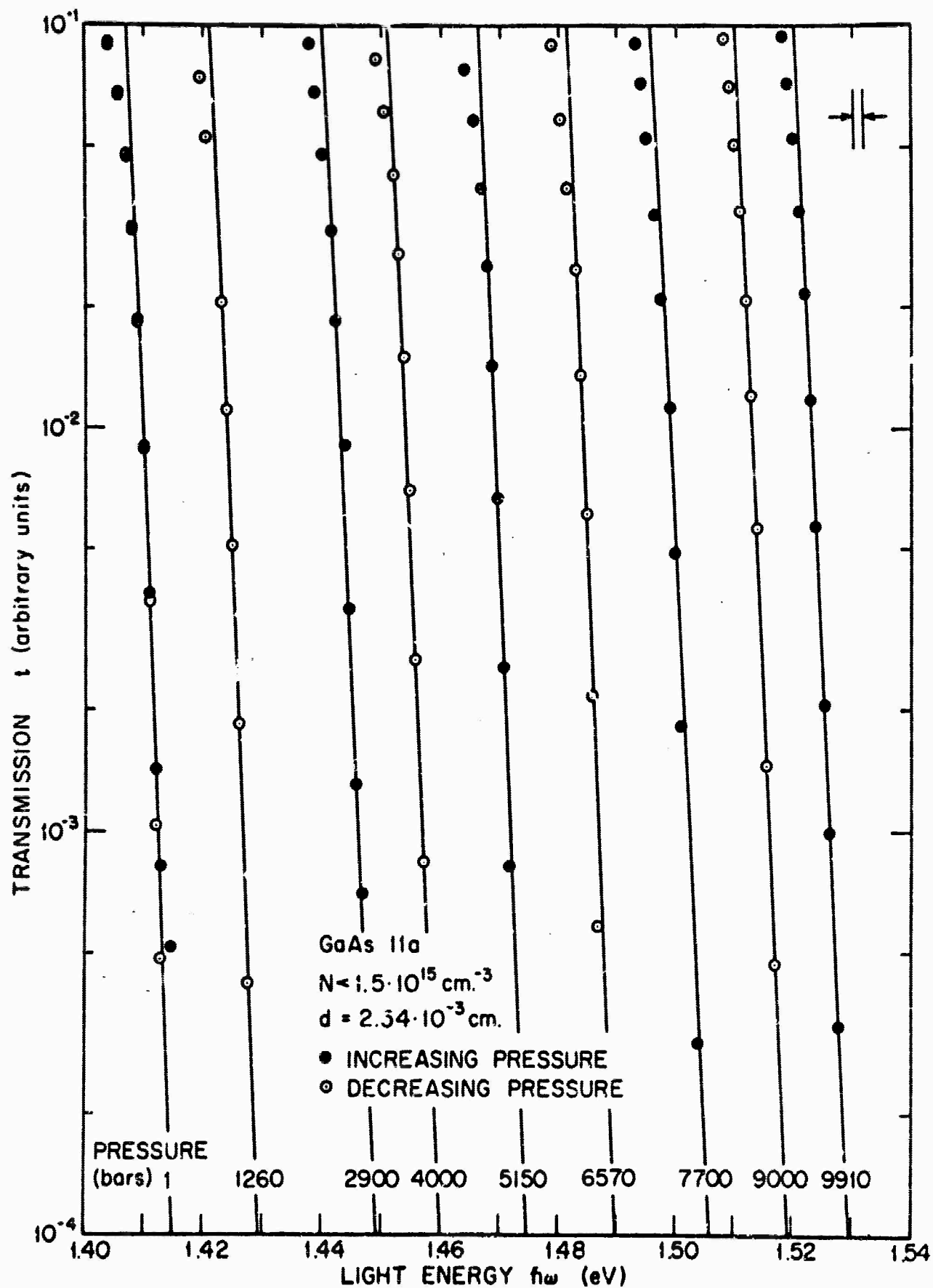


FIG. 3-3 EFFECT OF PRESSURE ON THE OPTICAL TRANSMISSION OF GoAs 11a.

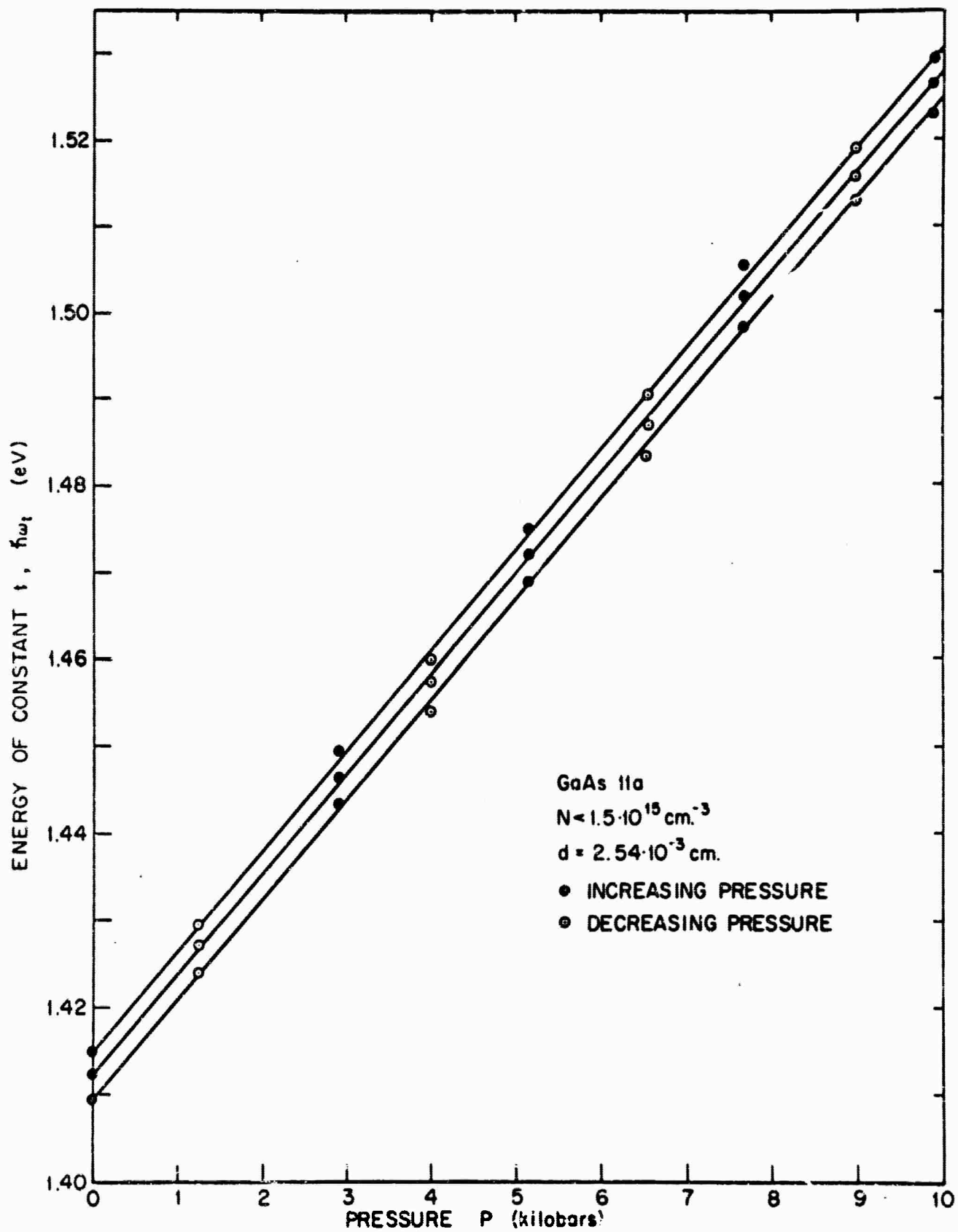


FIG. 3-4 ENERGY OF CONSTANT TRANSMISSION VERSUS PRESSURE FOR GaAs 11a

Within experimental error, there are no trends in the pressure shift of energy of constant transmission presented in Figs. 3-2 and 3-4. An average gives

$$\frac{d(\hbar\omega_t)}{dP} = (1.17 \pm .03) \cdot 10^{-5} \text{ eV/bar} , \quad (3-6)$$

$$\frac{d(\ln \hbar\omega_t)}{dP} = (8.27 \pm .21) \cdot 10^{-6} \text{ 1/bar} . \quad (3-7)$$

The connection between this pressure coefficient of isotransmission near the optical energy gap and the pressure dependence of various energy gaps will be discussed in Chapter 4. However, it can be noted that Eq. (3-6) agrees moderately well with a pressure coefficient of isotransmission, measured at constant $t > .1$, of $1.22 \cdot 10^{-5}$ eV/bar reported by Warschauer and Paul [3-5]. Equation (3-6) is also in agreement with the proposal of Paul [3-7], based on isotransmission measurements, that the pressure dependence of the energy of the $|\Gamma_{15V} - \Gamma_{1C}|$ or $|\Gamma_{25'V} - \Gamma_{2'C}|$ transition in group III-V or IV semiconductors is about $1.3 \cdot 10^{-5}$ eV/bar independent of material.

A more precise measurement near the optical energy gap is that of Feinleib et al. [3-8] which reported $(1.07 \pm .03) \cdot 10^{-5}$ eV/bar for the pressure shift of spontaneous emission in GaAs diodes at 300°K, in fair agreement with Eq. (3-6). A speculation concerning the relation between this result and Eq. (3-6) will be made in Chapter 4.

C. REFRACTIVE INDEX OF GaAs

For sufficient resolution, a measurement of transmission under the conditions given by Eqs. (3-3) and (3-4) will display oscillations or fringes as a function of wavelengths with maximum and minimum transmissions at wavelength given by

$$\text{maxima: } 2nd = \ell\lambda \quad \ell = 1, 2, 3, \dots \quad (3-8)$$

$$\text{minima: } 2nd = (\ell + \frac{1}{2})\lambda \quad \ell = 0, 1, 2, \dots \quad (3-9)$$

Determinations of these maximum and minimum positions were used in this investigation to measure (1) n as a function of $\hbar\omega$ from .3 to 1.2 eV at 2 temperatures T , 298°K and 96°K, and (2) n as a function of $\hbar\omega$ from .3 to 1.4 eV and as a function of pressure to 8 kilobars at 298°K.

The experimental system has been described by Prakash [2-2]. Detectors and prisms for various wavelength ranges were specified in Chapter 2. All measurements were performed on sample GaAs 11. A variation in sample thickness of about 1μ prevented fringes being observed until the sample was masked to present an area of 10^{-2} cm^2 . For suitable resolution, the transmission then displayed fringes whose amplitude was about 10 to 30% of the total transmission. Maximum and minimum positions were estimated visually and differed by $< .1\%$ from positions determined by normalizing transmission and plotting half-width points. The order ℓ was determined unambiguously by assuming n does not change significantly at long wavelengths

between successive extrema of the same kind at wavelengths λ_1 and λ_2 . This assumption holds to .1% for GaAs at 4μ for d about 15μ [3-9], and using Eq. (3-8)

$$\ell = \frac{\lambda_2}{\lambda_2 - \lambda_1} \quad (3-10)$$

which for GaAs 11 ranged from $\ell = 25$ near .3 eV to $\ell = 120$ at 1.4 eV. Equation (3-10) also defines the minimum resolution needed to resolve two successive extrema for given ℓ .

Equations (3-8) and (3-9) define uniquely only the quantity nd . For both samples GaAs 11 and GaAs 11a, values of n near .3 eV were taken from the literature [3-9] and used with Eqs. (3-8), (3-9), and (3-10), to determine d . This value of d was then used to determine values of n at other energies. The experimental error in deriving d was $\pm .5\%$ and this is also taken as the experimental error in n . However, it can be noted that the functional dependence of n on λ is more accurate than the absolute value since the normalization was done at only 1 point.

Figure 3-5 displays n determined in the above way as a function of light energy at 298°K, and, for comparison, values of n determined uniquely by the prism method by Hambleton et al. [3-9] and Marple [3-10].[†] There is excellent agreement with Hambleton et al. between .3 eV and .7 eV, and with Marple between 1.2 and 1.4 eV. The agreement with

[†] The author is grateful to Dr. D. T. F. Marple for supplying a graph of unpublished measurements of n versus λ for several temperatures.

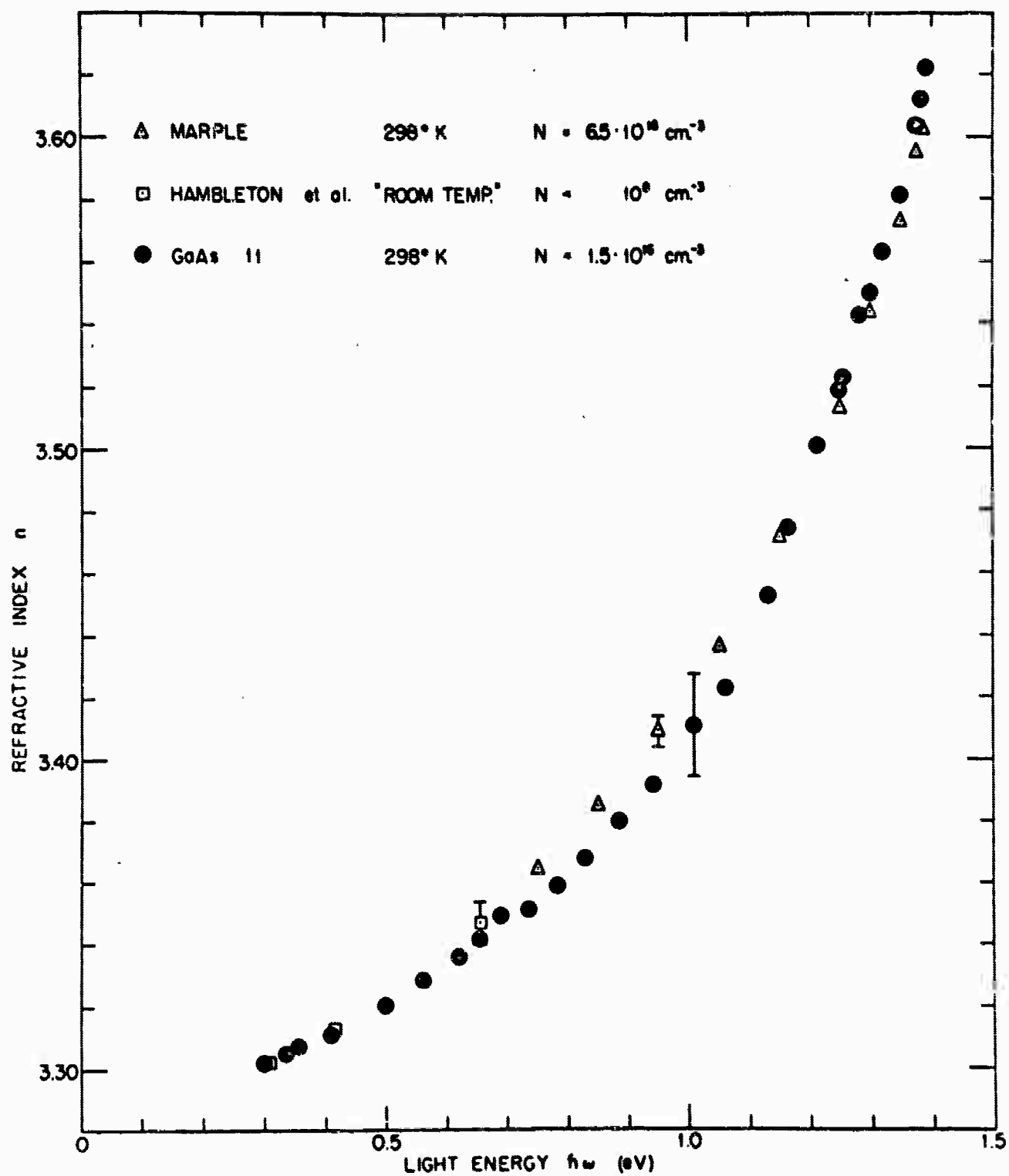


FIG. 3-5 REFRACTIVE INDEX OF GaAs VERSUS LIGHT ENERGY

Marple between .7 and 1.2 eV is slightly poorer but still nearly within experimental error. This slight deviation could possibly be explained by strains and defects built into the sample by mechanical polishing damage. An alternative explanation could be that in Marple's less pure sample transitions from impurity levels slightly increased the refractive index in the energy region 0.7 to 1.3 eV.

From plots similar to Fig. 3-5 at various temperatures and pressures (after correcting d for thermal expansion [3-11] and for compression [3-12]) it is possible to obtain the change in n at constant energy versus temperature or pressure. A representative graph of n versus T at constant energy is shown in Fig. 3-6a and compared with Marple's results [3-10]. The estimated error in measuring dn/dT in GaAs is $\pm 20\%$. It can be seen that the two determinations agree within experimental error but that the more complete and more accurate data of Marple [3-10] must be regarded as the best measure of dn/dT .

A representative graph of n versus P at constant energy is shown in Fig. 3-6b. The experimental error in dn/dP is estimated as $\pm 5\%$.

Figure 3-7a shows the variation of $d \ln n/dT$ at constant energy versus light energy for results reported by Marple [3-10], Cardona [3-13], and this investigation. The agreement is good within experimental error.

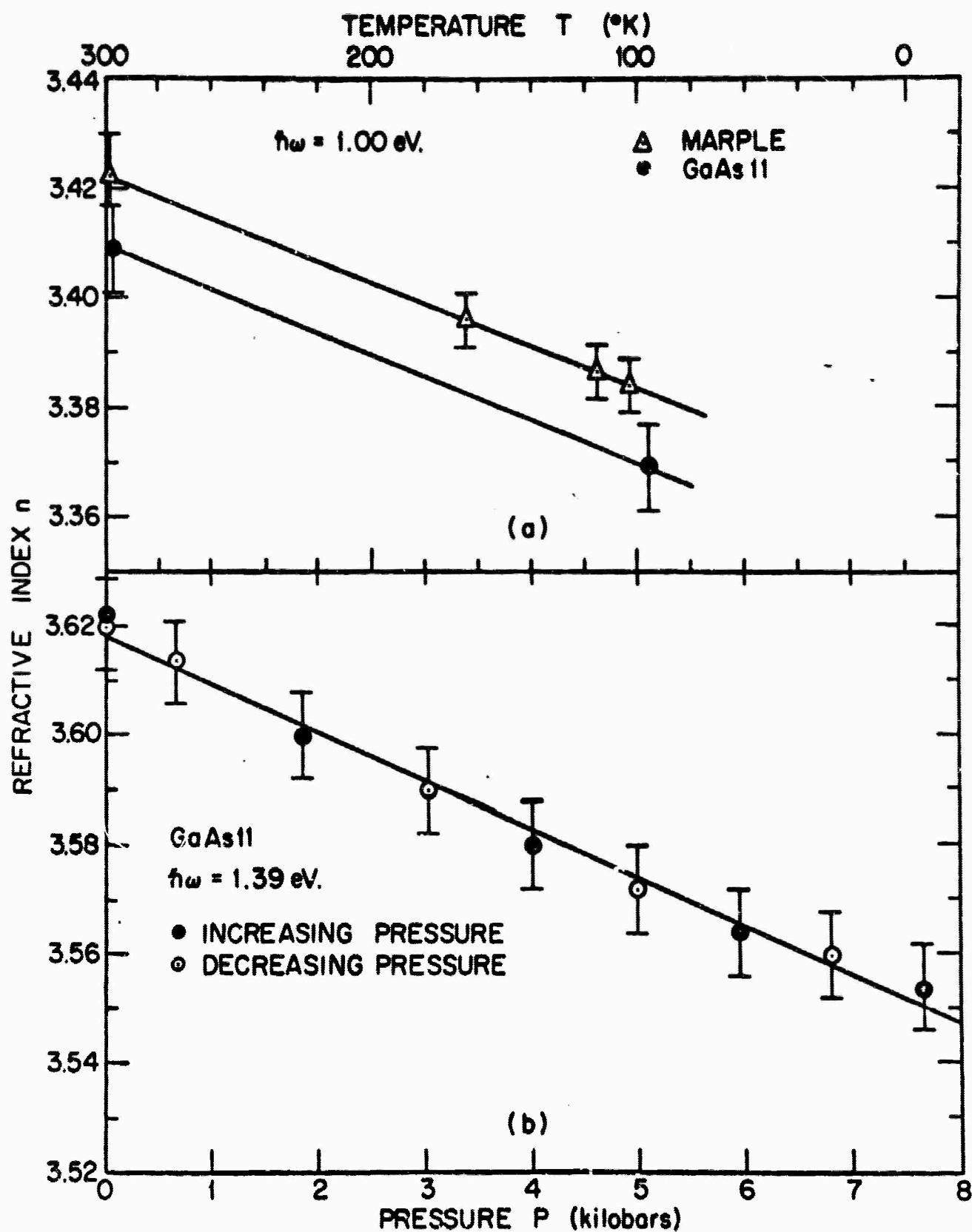


FIG. 3-6 (a) REFRACTIVE INDEX OF GaAs AT 1.00 eV VERSUS TEMPERATURE.
(b) REFRACTIVE INDEX OF GaAs AT 1.39 eV VERSUS PRESSURE.

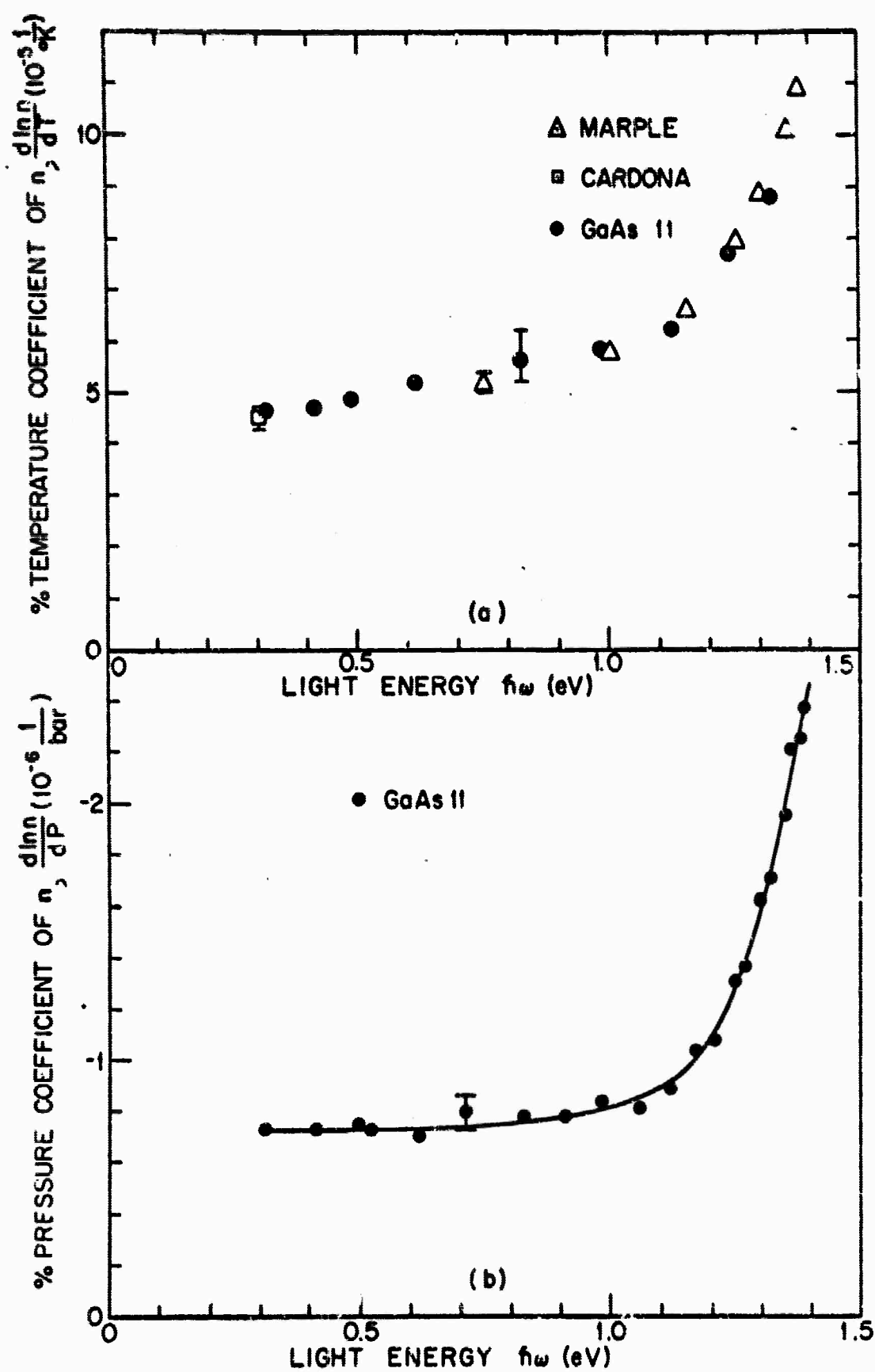


FIG. 3-7 (a) % TEMPERATURE COEFFICIENT OF n VERSUS LIGHT ENERGY.
 (b) % PRESSURE COEFFICIENT OF n VERSUS LIGHT ENERGY.

The variation of d in n/dP at constant energy versus light energy is shown in Fig. 3-7b. It can be noted that results of Fig. 3-7b, assumed constant as a function of temperature and extrapolated to appropriate energies, were used by Feinleib et al. [3-8] and Stern [3-14] to explain the pressure coefficient of stimulated emission of GaAs diodes at 77°K.

D. FARADAY ROTATION MEASUREMENTS IN GaAs

a. Experimental Method

The experimental system has been described in Chapter 2 and is illustrated in Fig. 2-1. The method used in this investigation to measure Faraday rotation was a null-balance technique based on a system first developed by Pidgeon [3-15]. In both the original method and the modification used here, the measurement of angle of rotation at a fixed wavelength was converted into an intensity measurement by assuming the Law of Malus [3-16] which asserts that the intensity transmitted through two polarizers varies as the square of the cosine of the angle between their principal axes of polarization. More simply, the intensity is governed by an equation similar to Eq. 2-1 and looks like Fig. 2-2 when one polarizer is rotated. If the polarizers are fixed at some angle $\omega_A = \text{constant}$ relative to each other and the Faraday rotation induced in a sample between them is considered only to add to or subtract from this constant angle, it is clear that measurements of intensity yield directly the angle of Faraday rotation.

In particular, the arrangement adopted in this investigation is shown schematically in Fig. 3-8. The situation for zero magnetic field is displayed in Fig. 3-8a. Light of intensity I_0 was incident on the polarizer which divided it into a completely linearly polarized portion I_1^P with a vertical polarization mode, and a completely unpolarized mode I_1^U . This light then passed through the sample becoming in the polarized mode I_2^P and in the unpolarized part I_2^U . The analyzer, set with its principal polarization axis at an angle θ relative to the polarization direction of I_2^P , passed intensity $I_3^P \cos^2(\theta) + I_3^U$ to the detector where I_3^U and $I_3^P + I_3^U$ were the minimum and maximum transmitted intensities of the system.

In Fig. 3-8b when the magnetic field was non-zero, the light incident on the analyzer $I_{2H}^P + I_{2H}^U$ had had its polarization mode changed from its former direction by the angle $\pm\theta_F$ of Faraday rotation.[†] After passing through the analyzer the intensity detected was $I_{3H}^P \cos^2(\theta \pm \theta_F) + I_{3H}^U$.

The above description may be considered perfectly general except for two assumptions: (1) that, for $H \neq 0$, the linear polarization direction was changed in the sample only by Faraday rotation of transmitted light; that is, the reflectivities are the same for the oppositely circularly polarized components of the linearly polarized light; and (2) the mirror (not shown in Fig. 3-8) focusing radiation on the detector has the same reflectance for all light polarizations.

[†] θ_F is positive when clockwise for radiation propagating along the magnetic field toward the observer.

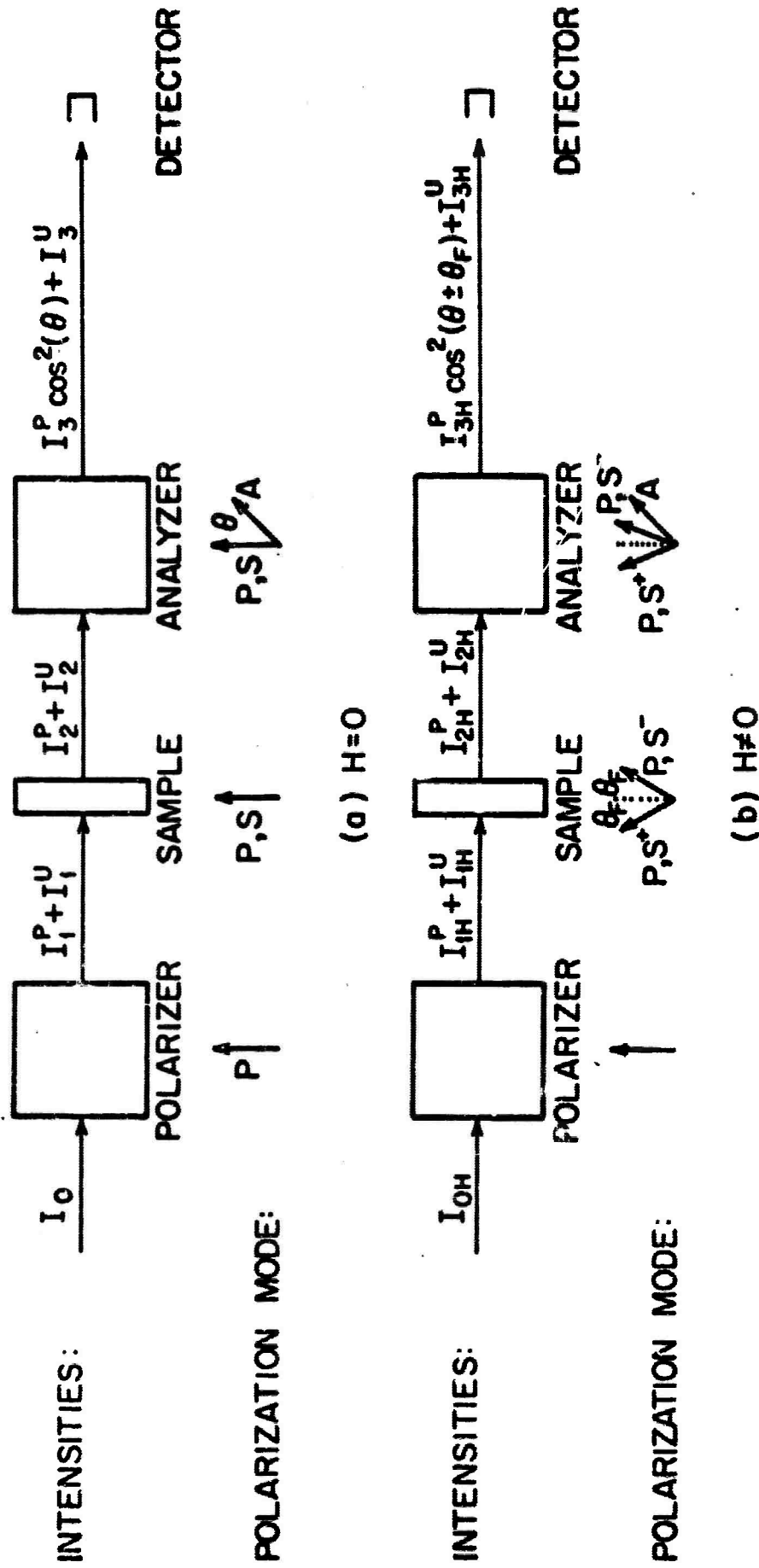


FIG. 3-8 SCHEMATIC DIAGRAM OF FARADAY ROTATION MEASUREMENT.

The failure of either assumption implies that the magnitude of one component of polarization is enhanced with respect to the other. This in turn implies a change in ellipticity and a consequent change in degree of polarization. As seen below, no such change was observed and hence the assumptions hold. The validity of assumption (1) confirms a theoretical conclusion of Donovan and Medcalf (3-17) for infra-red light.

To make use of the final experimentally detected intensities in Figs. 3-8a and 3-8b, the further assumption was made that

$$I_{3H}^P = I_3^P \equiv I^P ; \quad I_{3H}^U = I_3^U \equiv I^U , \quad (3-11)$$

which to be true in general required, for magnetic field on and off:

- (1) the incident light intensity to be constant, $I_o = I_{oH}$, which was found true to .4% for the period of a Faraday rotation measurement (about 15 minutes)
- (2) the degree of polarization of the system to be unchanged, which was found to hold < .3% ;
- (3) the total transmission to be constant, except for the variation due to the Law of Malus, which was found true to < .3% ;
- (4) and the detector sensitivity to be constant, which was found to hold to < .1%.

Using Eq. (3-11), the system of Fig. 3-8 yielded three experimentally measurable intensities

$$H = 0 \quad I = I^P \cos^2(\theta) + I^U \quad (3-12)$$

$$H^+ \neq 0 \quad I^+ = I^P \cos^2(\theta - \theta_F) + I^U \quad (3-13)$$

$$H^- \neq 0 \quad I^- = I^P \cos^2(\theta + \theta_F) + I^U \quad (3-14)$$

Define

$$\begin{aligned} \Delta I &= I^+ - I^- = I^P [\cos^2(\theta - \theta_F) - \cos^2(\theta + \theta_F)] \\ &= I^P \sin(2\theta_F) \sin(2\theta) \end{aligned} \quad (3-15)$$

For maximum sensitivity, $\theta = 45^\circ + \delta$ where δ was a small error in setting the analyzer relative to the linear polarization direction. Equations (3-12) and (3-15) became respectively

$$I = I^P \cos^2(45^\circ + \delta) + I^U = \frac{1}{2} I^P [1 - \sin(2\delta)] + I^U \quad (3-16)$$

$$\Delta I = I^P \sin(2\theta_F) \sin[2(45^\circ + \delta)] = I^P \sin(2\theta_F) \cos(2\delta) \quad (3-17)$$

Dividing Eq. (3-17) by Eq. (3-16)

$$\frac{\Delta I}{I} = \frac{2I^P \sin(2\theta_F) \cos(2\delta)}{I^P [1 - \sin(2\delta)] + 2I^U} \quad (3-18)$$

and assuming terms of order δ^2 may be neglected compared to 1

$$\sin(2\theta_F) = \frac{\Delta I}{2I} \frac{I^P (1 - 2\delta) + 2I^U}{I^P} \quad (3-19)$$

If $\delta < .005$ radians = .29 degrees, 2δ may be neglected compared to 1 with an error < 1%.

Finally, the depolarization factor was defined as

$$D \equiv \frac{I^P + 2I^U}{I^P} \quad (3-20)$$

Thus the angle of Faraday rotation was determined by measuring three experimental quantities, D , I , and ΔI :

$$\sin(2\theta_F) = \frac{D \cdot \Delta I}{2I} . \quad (3-21)$$

b. Experimental Procedure

The method of section 3.D.a. tacitly assumed axial symmetry and perfect alignment of axes of polarizers with the light axis. Deviations produced irregularities in transmission as the analyzer rotated which invalidated Eqs. (3-12), (3-13), and (3-14). Thus, the first step in procedure was to align the system of Fig. 3-8. The f number of the light beam varied from 6 to 10. When the polarizers were properly aligned, there were no transmission irregularities due to non-normal incidence of some light rays.

The second step involved making the tests described in the discussion on page 3-19 of the assumption of Eq. (3-11).

Third, Eq. (3-12) was ascertained to hold and D determined to be constant as a function of wavelength and hence constant throughout the experiment. The analyzer next was set, using Eq. (3-12), to an accuracy of $< .5\%$ which implied $\delta < .2$ degrees and satisfied the assumption following Eq. (3-19).

Lastly, the actual experimental measurement of ΔI and I was performed. A typical recorder trace at constant wavelength is shown in Fig. 3-9. At a certain gain setting A , a deflection D_1 ,

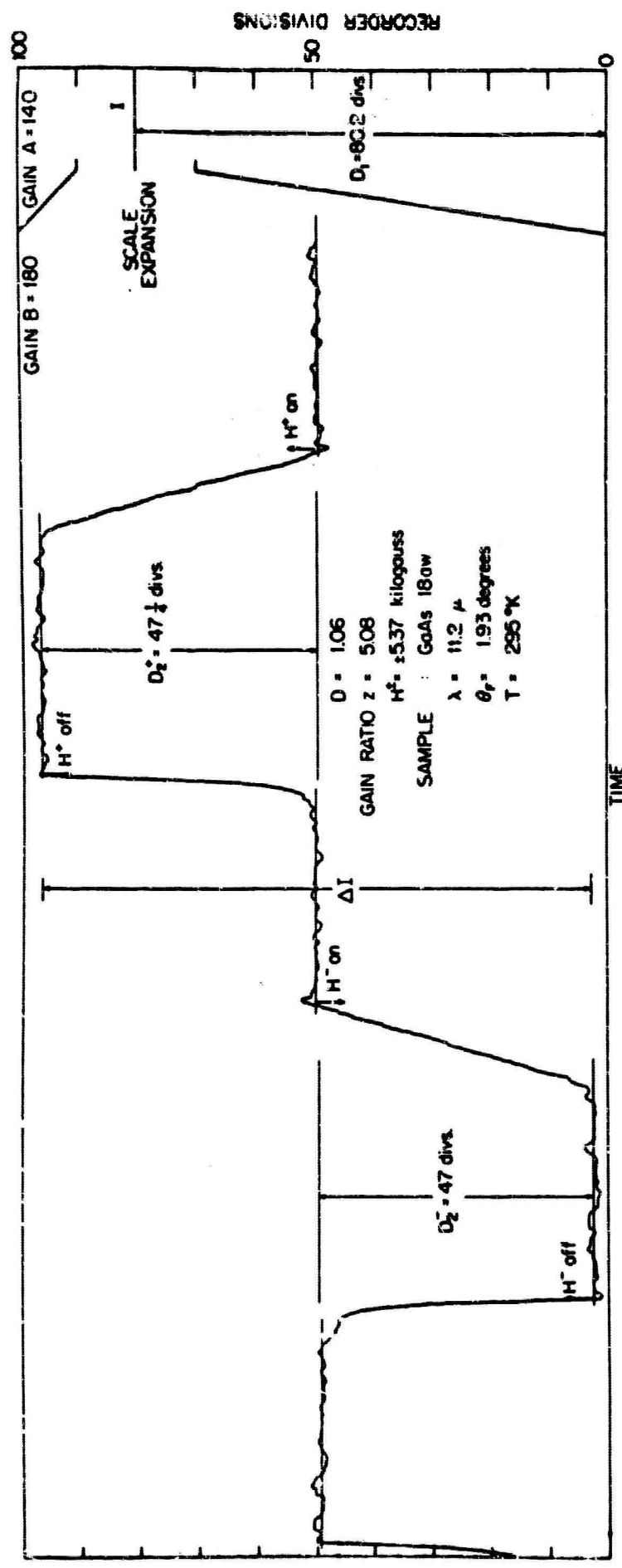


FIG 3-9 RECORDER TRACE SHOWING MEASUREMENT OF ANGLE OF FARADAY ROTATION (START IS ON RIGHT)

proportional to I was measured. A scale expansion of a factor of 5 to 10 was then made by increasing the gain and subtracting 90% of I with an electronic signal at the detector. The field was turned on for two directions and the quantity ΔI proportional to the deflection $D_2^+ - D_2^-$ at gain setting B was measured by averaging over the noise visually. The ratio $\Delta I/I$ was then given by

$$\frac{\Delta I}{I} = \frac{(D_2^+ + D_2^-)}{zD_1} \quad (3-22)$$

where z was the gain ratio between gains B and A. Equation (3-21) then gives

$$\sin(2\theta_F) = \frac{D(D_2^+ + D_2^-)}{2zD_1} \quad (3-23)$$

As D , z , and D_1 could be measured to $< 1\%$ the principal error in θ_F arises from error in $(D_2^+ + D_2^-)$ which was typically about 2% as shown in Fig. 3-9. The main source of this error was the .4% instability in I_0 over the measurement period. The original method [3-13] avoided this difficulty by using two spectrometers and subtracting from I for scale expansion by source light of opposite phase, thus avoiding stability problems and giving an error in θ_F of only 1%.

A typical test demonstrating direct proportionality between magnetic field and θ_F is shown in Fig. 3-10.

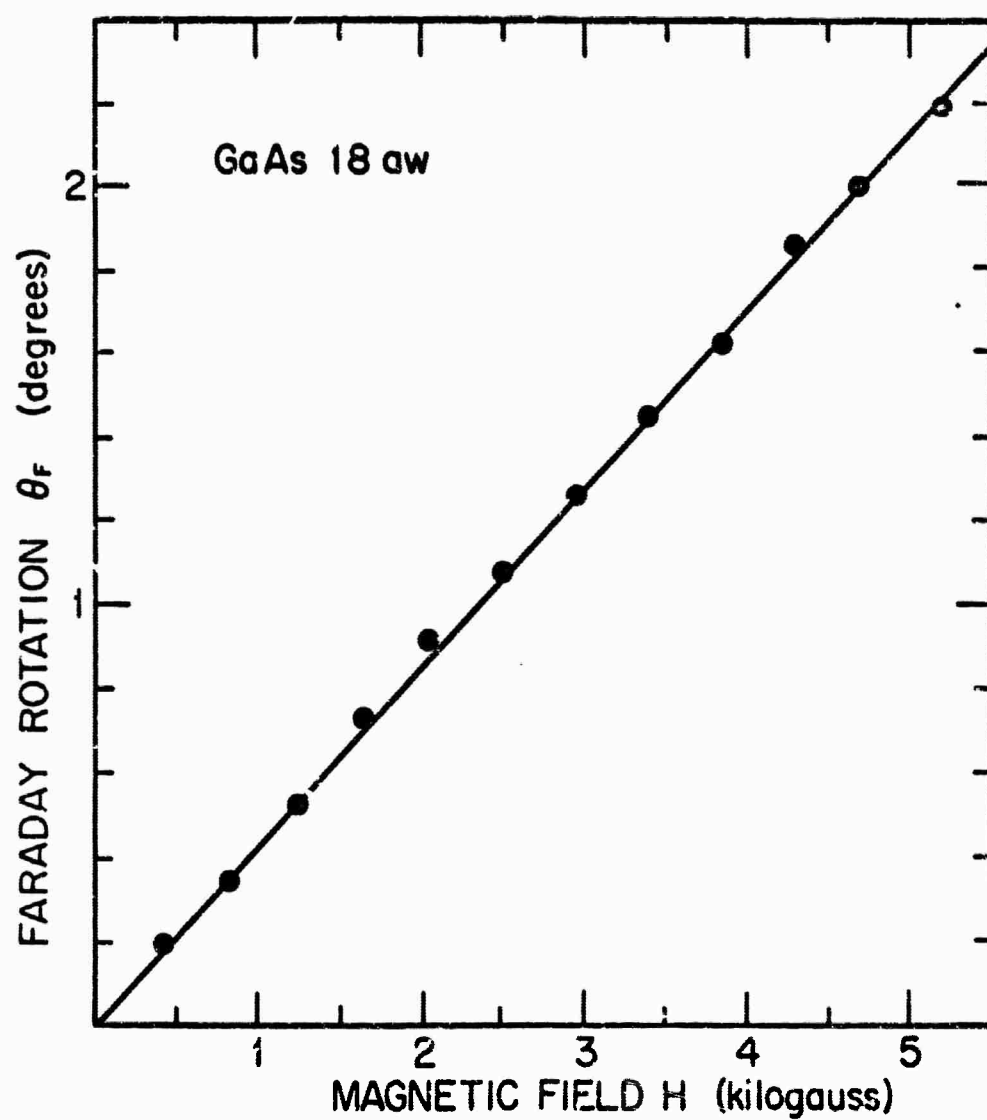


FIG. 3-10 MAGNETIC FIELD DEPENDENCE OF FARADAY ROTATION.

c. Experimental Difficulties

The theoretical expressions for θ_F given in Chapter 1 assume monochromatic incident light. The experiment demands a certain spectral slit width in the monochromator to insure sufficient light energy for detection. The first difficulty to arise, then, was slit width dependence of θ_F . In Eq. (3-22) ΔI was the essential variable of θ_F and was proportional to λ^2 . However, the magnitude of I was also wavelength dependent. For illustration let $\Delta\lambda = A\lambda^2$, $I = B/\lambda$, then

$$\theta_F(\lambda) = \frac{DA\Delta I}{2I} = \frac{DA}{2B} \lambda^3. \quad (3-24)$$

Integrating near λ_0 for spectral slit width $\Delta\lambda$ gives

$$\theta_F(\lambda_0) = \frac{DA}{2B} \lambda_0^3 \left[1 + \frac{1}{4} \left(\frac{\Delta\lambda}{\lambda_0} \right)^2 \right] \quad (3-25)$$

where $\frac{1}{4}(\Delta\lambda/\lambda_0)^2$ is the error in θ_F due to finite slit width. In general, the λ dependence of I was not as simple as $1/\lambda$ and the situation must be regarded as a possible source of error. For all Faraday rotation measurements reported in this investigation checks were made on possible slit width dependence of θ_F and spectral slits reduced until the dependence disappeared.

Scattered light of different λ than λ_0 will also contribute to error in $\theta_F(\lambda_0)$. In the Perkin-Elmer 12c monochromator, scattered light, mainly of low wavelength, can be as much as 15% of the total

light beam at 15μ . In this report, all measurements were made with long wavelength band pass filters which, by blocking short wavelength light, reduced the scattered light in the beam to $< 1\%$.

Aside from the general "black body" wavelength dependence of I due to the source, atmospheric absorption bands presented drastically varying I at certain wavelengths in the infra-red. Figure 3-11 shows measurements of θ_F in a GaAs sample near the 4.25μ CO_2 absorption band. The straight line gives λ^2 dependence of θ_F expected both from theory and from extrapolation of other measured points. However, the experimental points indicate an anomaly in θ_F which, since it is resolution dependent, is due to the rapidly changing I near the absorption band. In general, to avoid misleading results, it is well not to take measurements in absorption band regions and this policy was adopted in this investigation.

With the above sources of error in mind, Faraday rotation measurements were made on parallel-sided samples of GaAs. Typical results are presented in Fig. 3-12 which shows Verdet coefficient as a function of λ^2 . The Verdet coefficient is defined as

$$V = \frac{\theta_F(\text{radians})}{dH} \quad (3-26)$$

The raw experimental points in Fig. 3-12 do not go to zero as λ^2 goes to zero. The λ^2 dependence is not simply proportional ($V = A\lambda^2$) as predicted by theory in Chapter 1, but, rather, proportional with

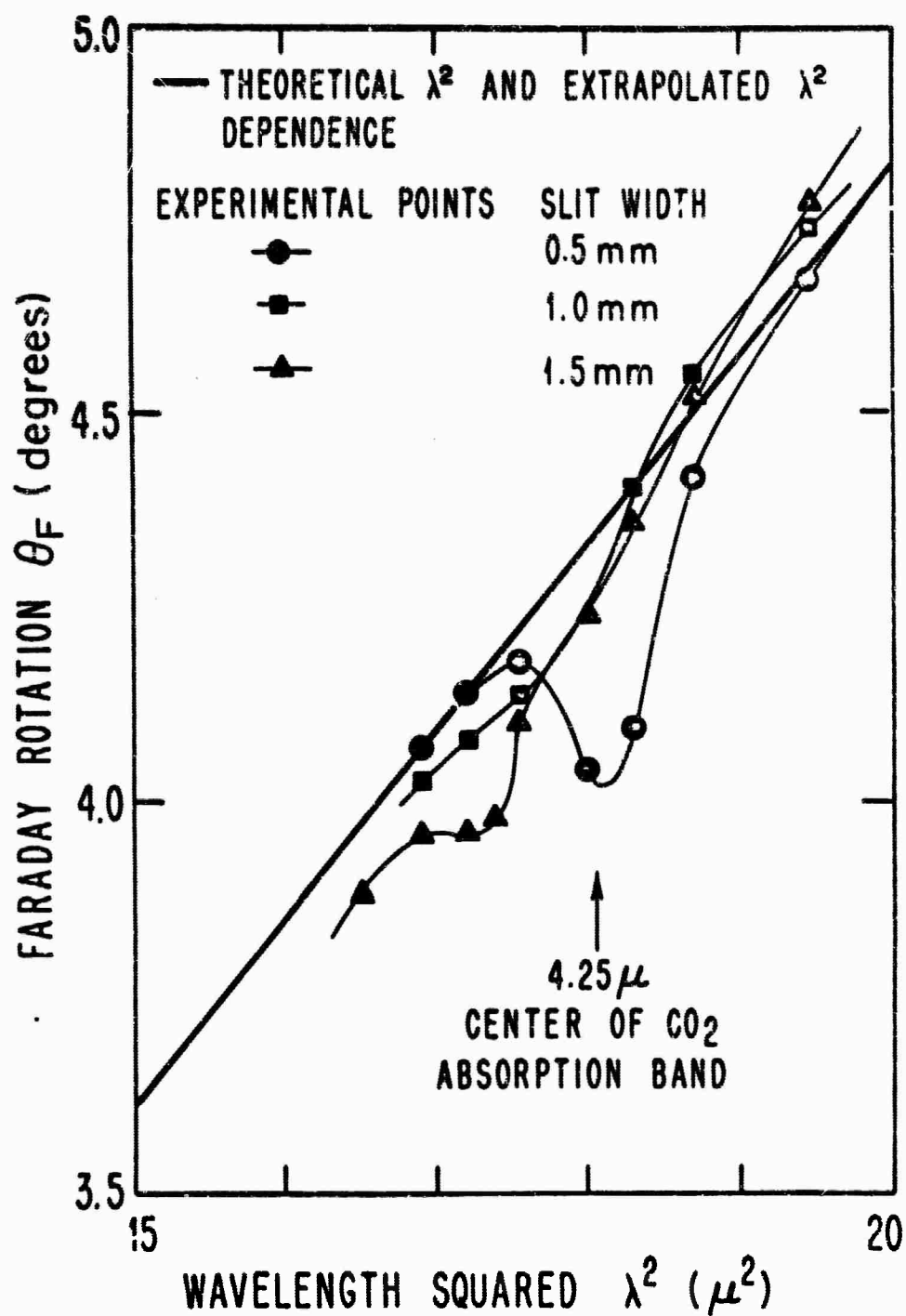


FIG. 3-11 ANOMALOUS ROTATION IN GaAs NEAR THE $4.25 \mu \text{CO}_2$ ABSORPTION BAND.

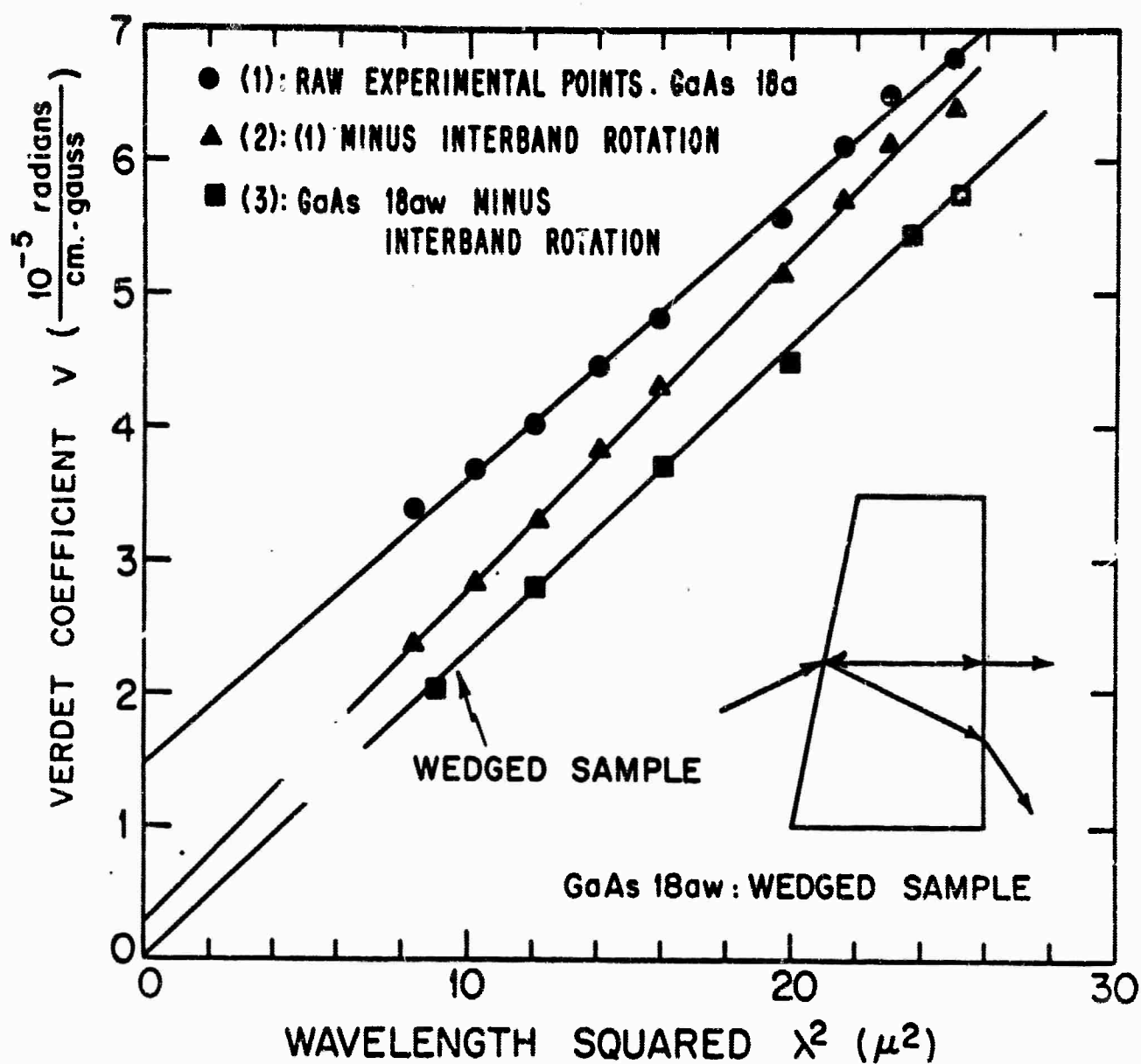


FIG. 3-12 THE EFFECT OF INTERBAND ROTATION AND MULTIPLE REFLECTION ON FREE CARRIER VERDET COEFFICIENT.

an additive constant ($V = B\lambda^2 + C$). The same phenomenon has been reported without explanation by Ukhanov [3-18], Cardona [3-19], and Piller [3-20]. Subtraction of the interband rotation does not completely remove the anomaly as shown in Fig. 3-12.

Extension of the measurements to longer λ did produce experimental points which, as a function of λ^2 , gave a straight line which extrapolated to $V = 0 = \lambda^2$. The increase in free carrier absorption at long wavelengths suggested that multiple reflections allowed by low absorption at short λ in the parallel-sided sample were affecting V as measured in Fig. 3-12.

Consequently measurements were made on a GaAs sample which was wedged 1° (see Fig. 3-12) to reject multiple reflected rays. Experimental points measured for such a configuration and corrected for interband rotation are also shown in Fig. 3-12 and it can be seen that the λ^2 dependence extrapolates to $V = 0 = \lambda^2$.

In retrospect it is clear that multiple reflections would naturally affect V since light reflected twice within a sample has passed through an equivalent length of sample that is three times longer than the path of the basic transmitted beam, and hence will have a linear polarization direction that has been rotated three times farther. Further, the reflected polarization direction will now have a phase difference of 2π and c with the transmitted polarization and may add or subtract from the basic V depending on the

sign of $\exp[2i\omega d/c]$. Finally, the magnitude of the twice-reflected V varies with respect to the basic V as $\exp[-2\alpha d]$ where α is λ dependent. Thus, in general, Faraday rotation results are suspect unless provision has been made to reject multiple reflected beams by wedging or unless the absorption is sufficient to eliminate multiple passes.

In this investigation, measurements were made on plane parallel samples at wavelengths long enough to insure that internally doubly-reflected light was $< 1\%$ and higher reflections even less. As mentioned, these measurements gave straight lines of V versus λ^2 that passed accurately through $V = 0 = \lambda^2$. The samples were then wedged 1° which was calculated to be a sufficient angle to reject **amply** from the main beam all multiple reflections. Rotation measurements were extended to low wavelengths and still gave straight lines through $V = 0 = \lambda^2$. Because of wedging there was an uncertainty in d in all but the two thickest samples, GaAs 11 bw and 24 aw, thus giving a corresponding uncertainty in the absolute V . This fact is unimportant for the pressure and temperature measurements since only relative changes with these parameters are of interest. However, for consistency, all room condition results are presented normalized to the long wavelength measurements.

The last experimental difficulty concerned the sapphire windows used in the optical bomb for pressure measurements. When used

as grown, the cylinder axis of the $\frac{1}{2}$ inch diameter by $\frac{1}{2}$ inch long windows was at an angle of 60° to the c axis. The birefringence resulting from this configuration degraded the linear polarization of the experimental system by introducing ellipticity which seriously reduced the sensitivity. It was found necessary to obtain sapphires whose c axis was aligned to the cylinder axis to within 1° . With care, the polarization then obtained was 88%.

d. Infra-red Faraday Rotation Results

The dependence of free carrier Verdet coefficient (V_F) on wavelength squared (λ^2) for 4 n-type samples of GaAs under room conditions[†] is shown in Figs. 3-13 and 3-14. Included in Fig. 3-14 is the long wavelength interband Verdet coefficient of a near-intrinsic sample of GaAs which agrees within experimental error with a measurement by Smith [3-21] on a crystal of semi-insulating GaAs. This agreement confirms the theoretical result of Chapter 1 that the slight variation of the long wavelength interband rotation with carrier concentration may be neglected and thus the interband rotation for a near-intrinsic sample may be subtracted from the experimental results on doped samples to obtain the free-carrier contribution (V_F).

[†] Room conditions are defined for this investigation as measurements in air at atmospheric pressure at a controlled temperature of 295°K .

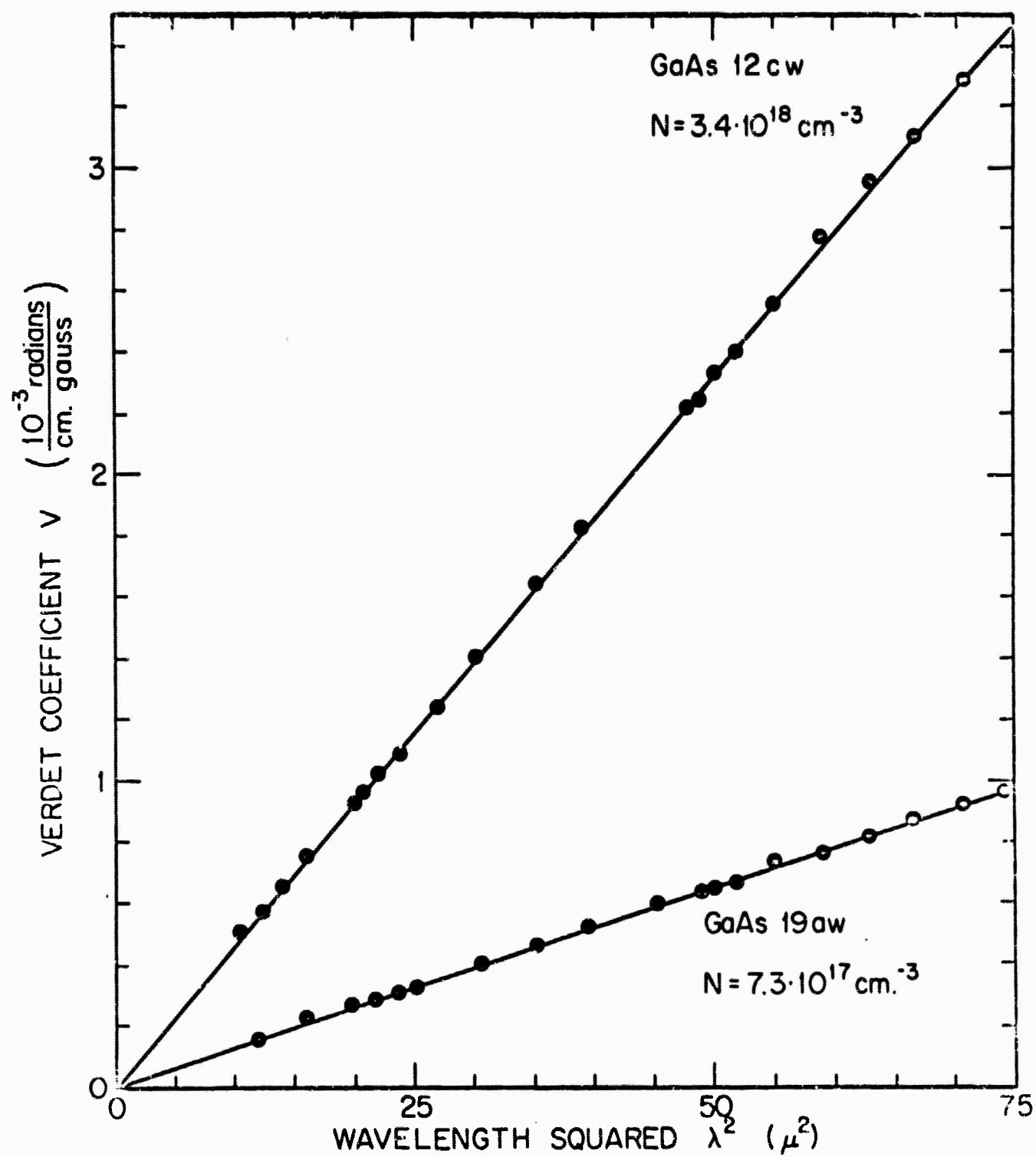


FIG. 3-13 V FOR GaAs 12 cw AND 19 aw AS A FUNCTION OF λ^2 FOR ROOM CONDITIONS.

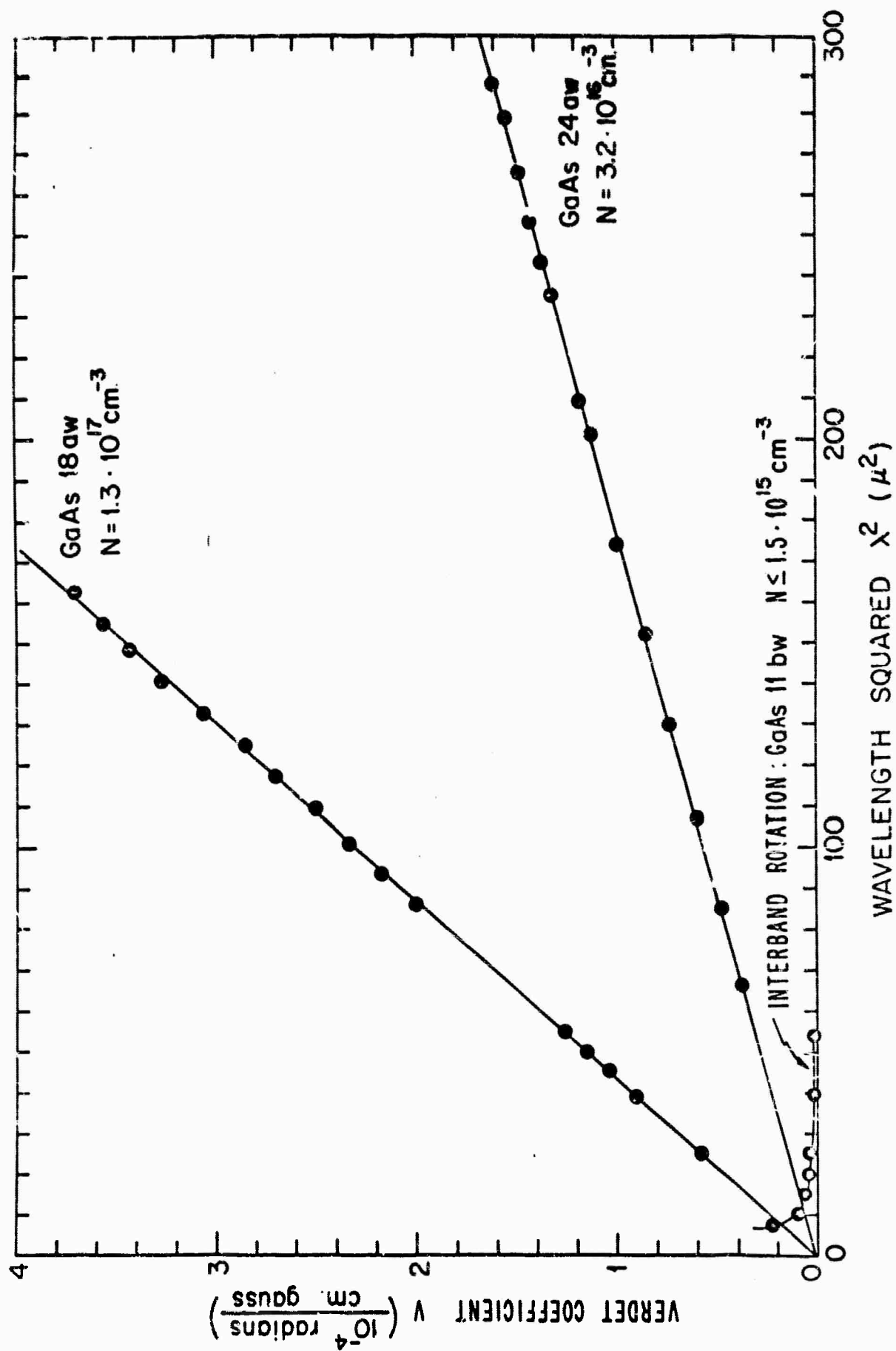


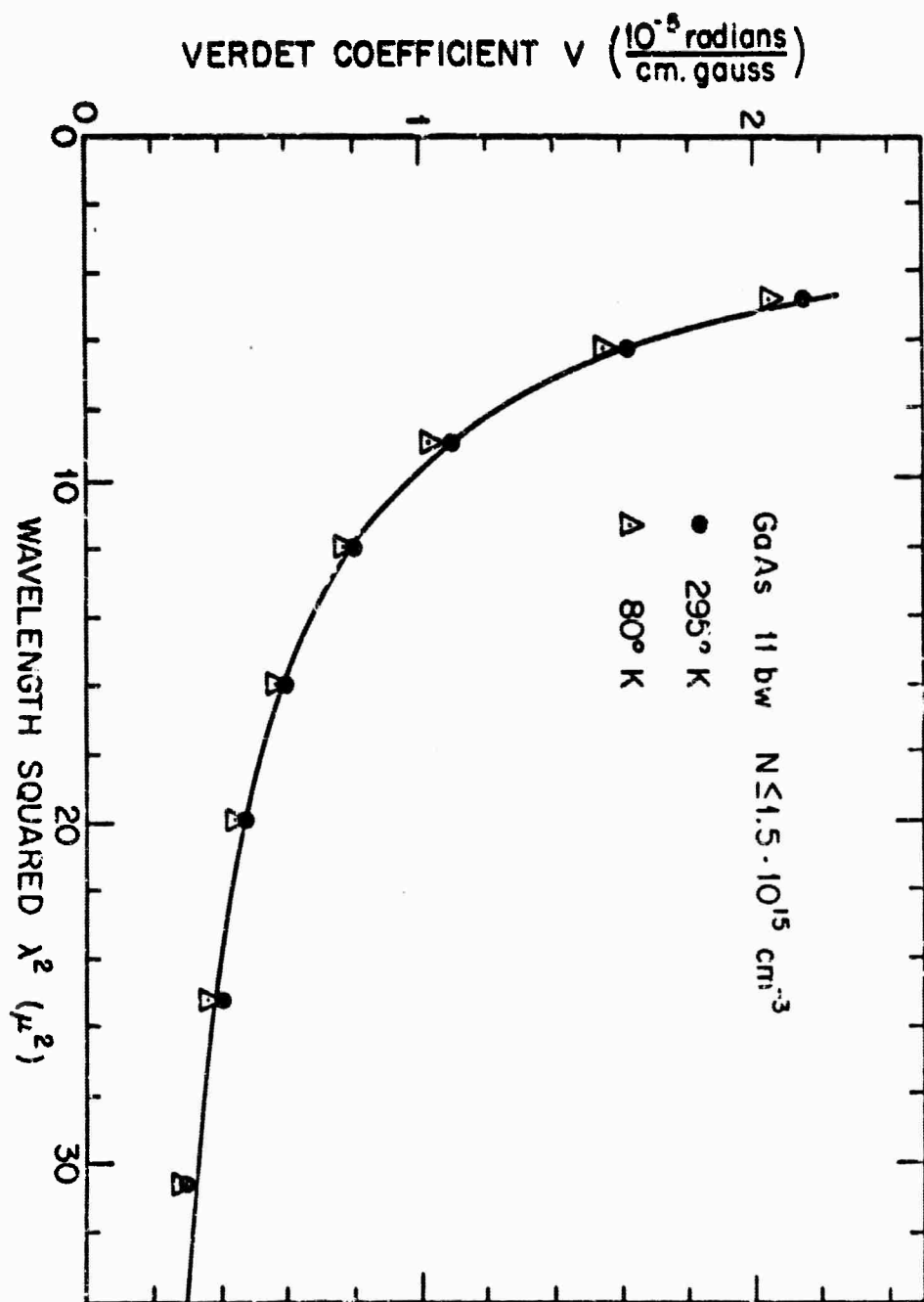
FIG. 3-14 V FOR GaAs 18aw, 24aw, AND 11bw AS A FUNCTION OF λ^2 FOR ROOM CONDITIONS

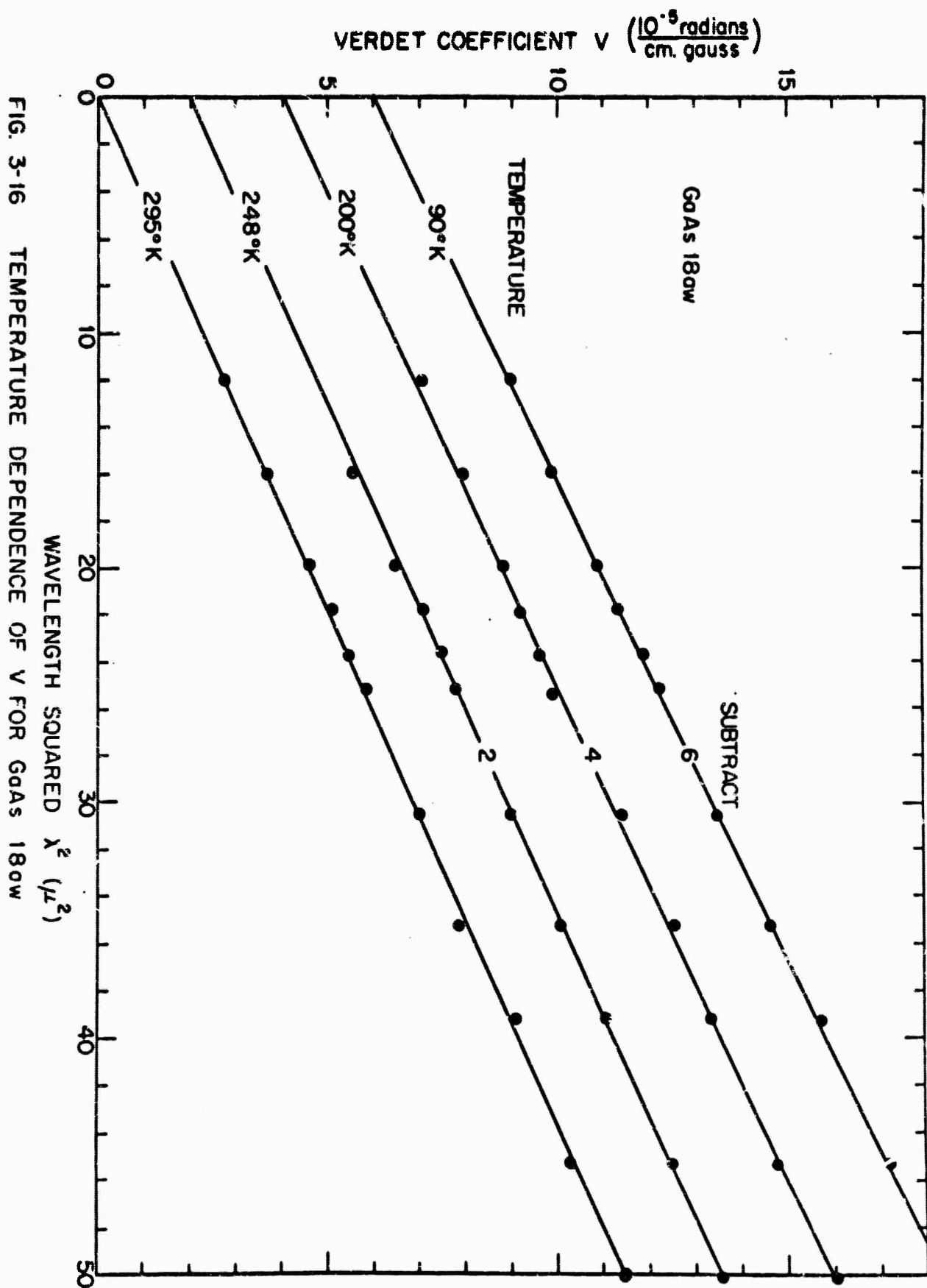
It can also be seen in Figs. 3-13 and 3-14 that there are no deviations in the region 3 to 5μ (9 to $25\mu^2$) of V_F from λ^2 straight line dependence which confirms the theoretical conclusion of Chapter 1 that the additional absorption in this region reported by Spitzer and Whelan [3-22] does not contribute significantly to Faraday Rotation.

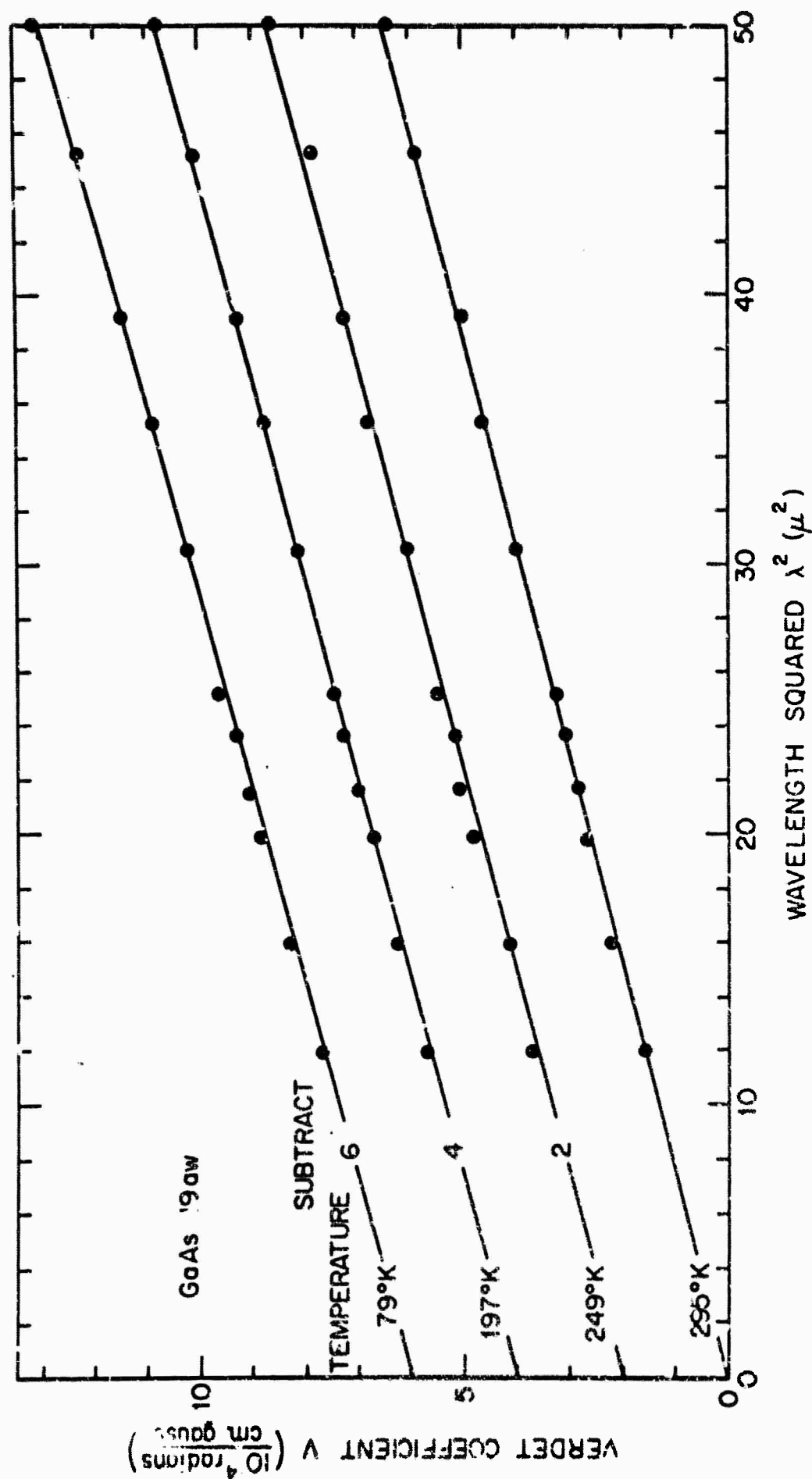
In Chapter 4 the effective mass of GaAs for room conditions is derived from Figs. 3-13 and 3-14 and compared with the literature.

The dependence of interband V on λ^2 as a function of temperature between 80°K and 300°K is shown in Fig. 3-15. The dependence of V_F on λ^2 as a function of temperature between 80°K and 300°K for three n-type samples of GaAs is shown in Figs. 3-16, 3-17, and 3-18. Points at each temperature are displaced a constant amount for clarity. The percentage change of effective mass in GaAs with temperature is derived in Chapter 4 and compared with changes in various energy gaps.

Figure 3-19 shows the pressure dependence of interband V versus λ^2 for 1 bar and 10 kilobars. Figures 3-20, 3-21, and 3-22 show the pressure dependence of V_F versus λ^2 from 1 bar to 10 kilobars for three n-type samples of GaAs. Points at each pressure are displaced a constant amount for clarity. The percentage change of effective mass in GaAs with pressure is derived in Chapter 4 and related to changes in various energy gaps.

FIG. 3-15 TEMPERATURE DEPENDENCE OF INTERBAND V .



FIG. 3-17 TEMPERATURE DEPENDENCE OF V FOR GaAs 19aw.

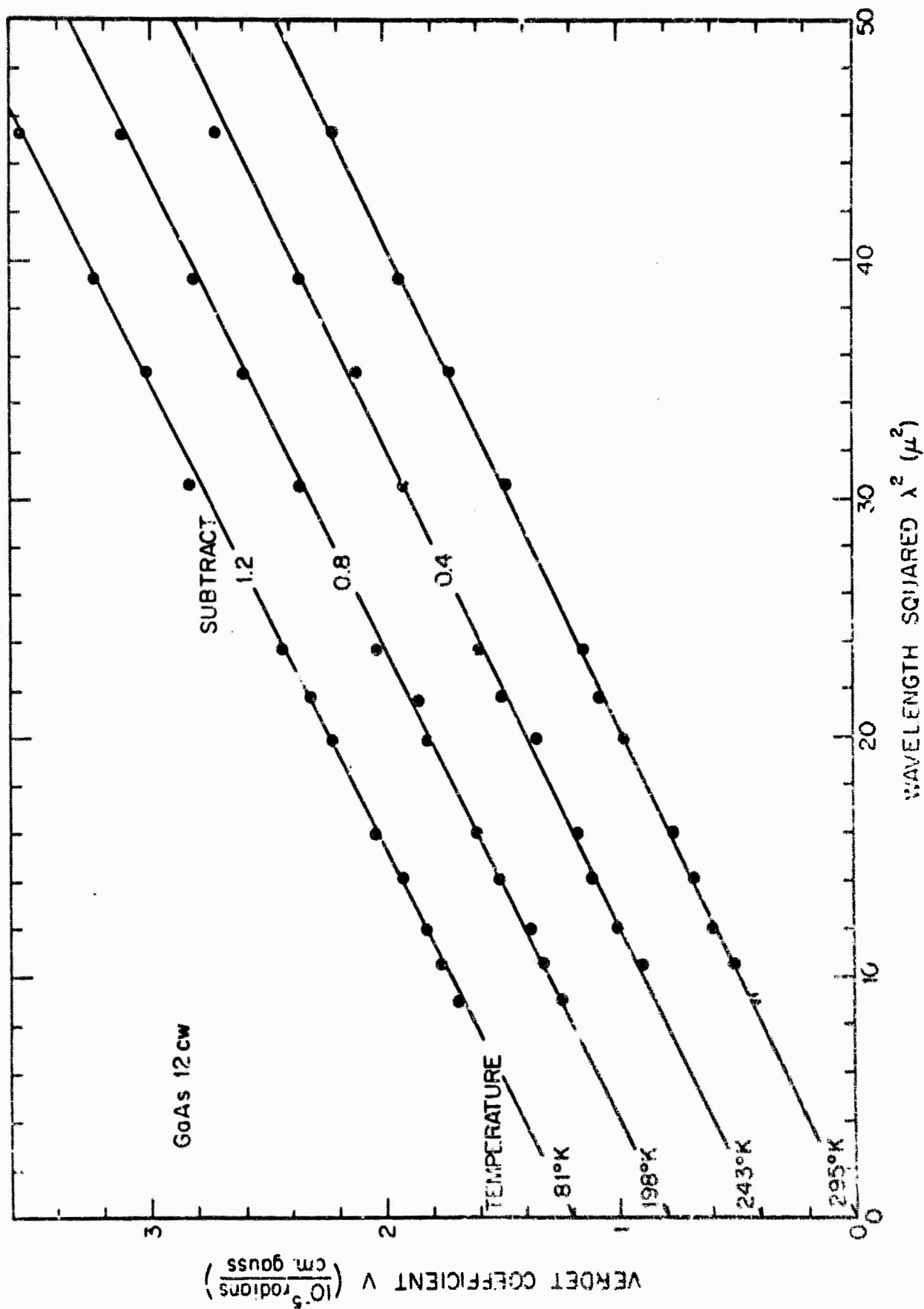


FIG 3-18 TEMPERATURE DEPENDENCE OF V FOR GaAs 12 CW

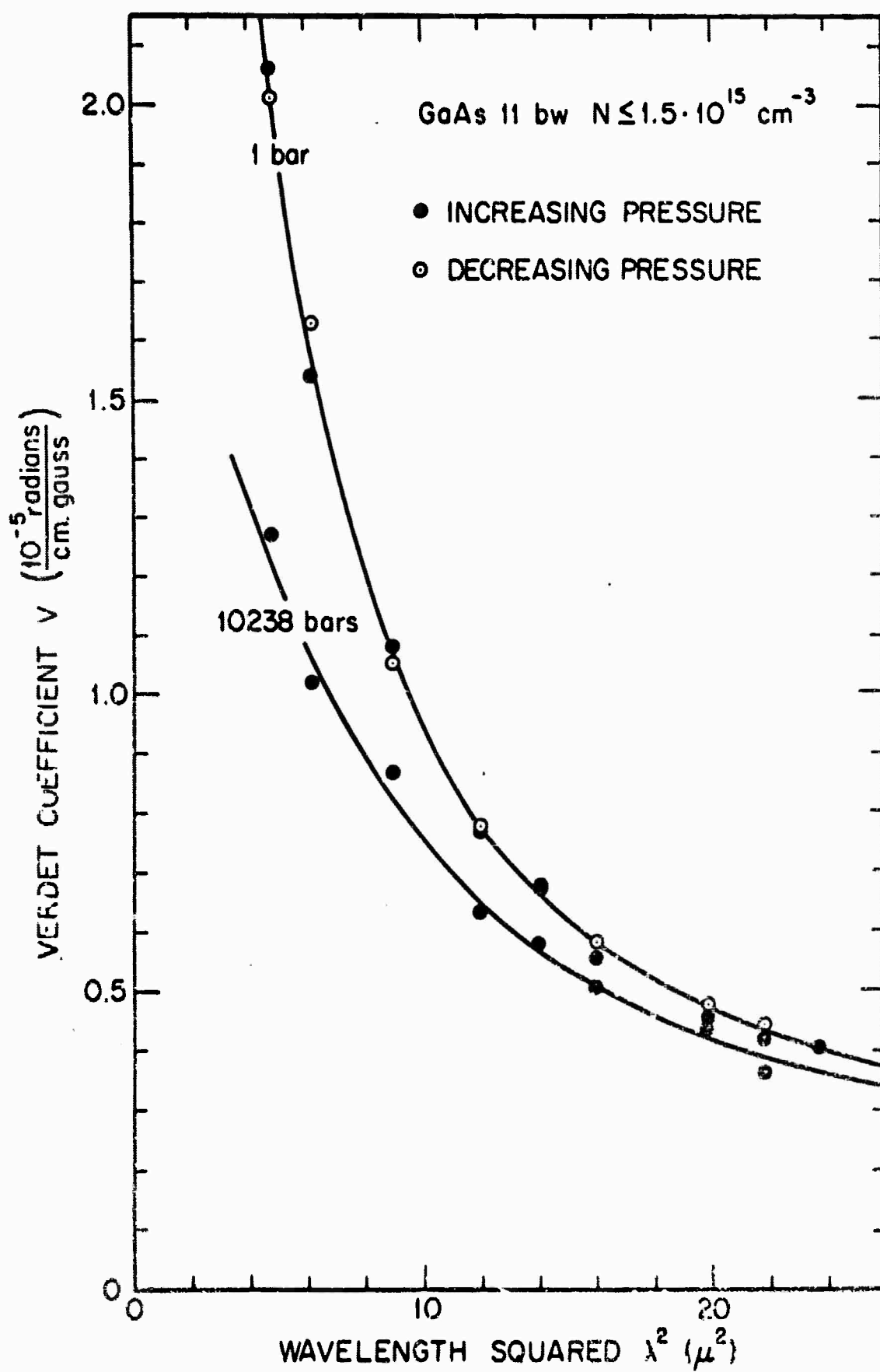


FIG. 3-19 PRESSURE DEPENDENCE OF INTERBAND V.

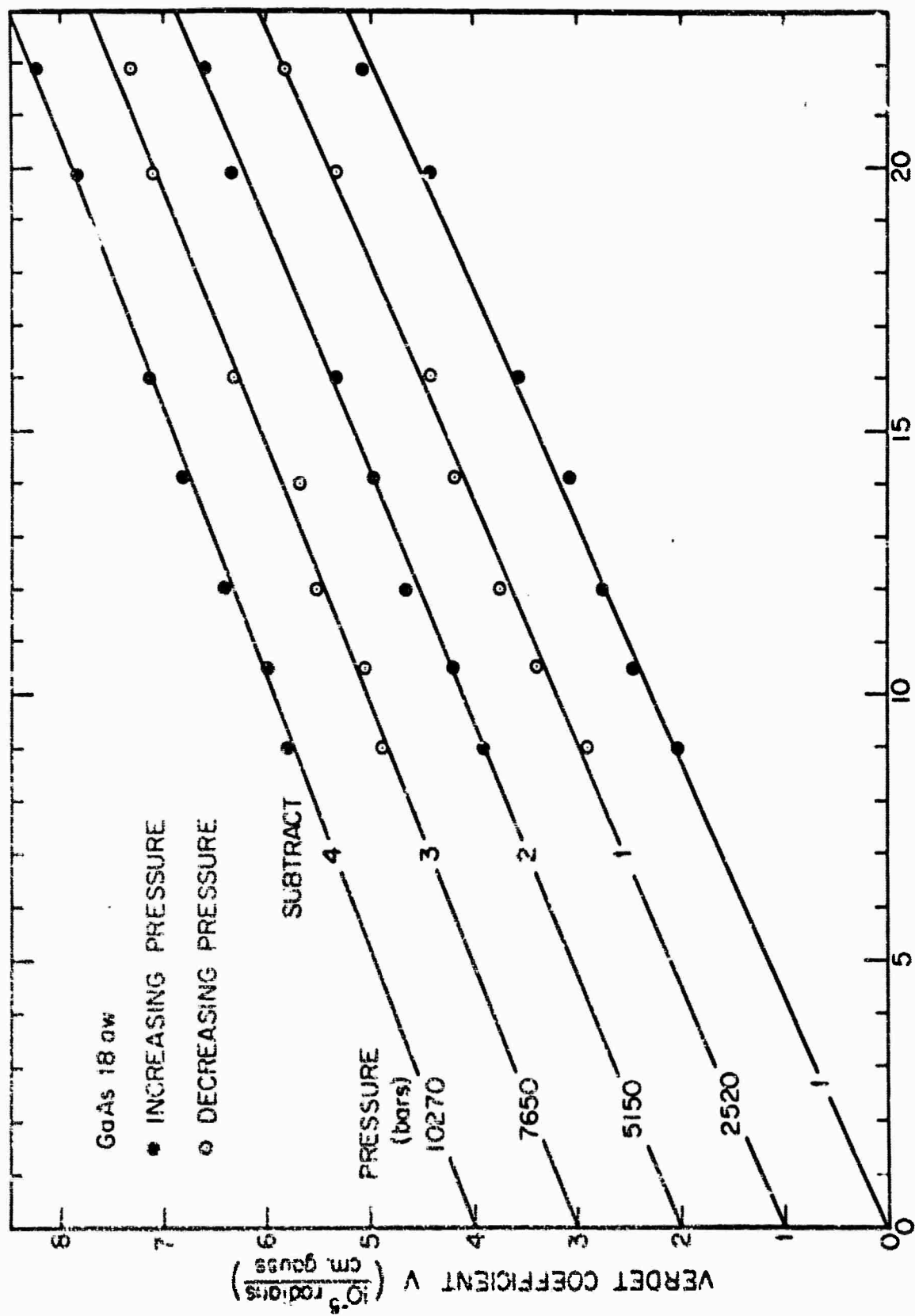
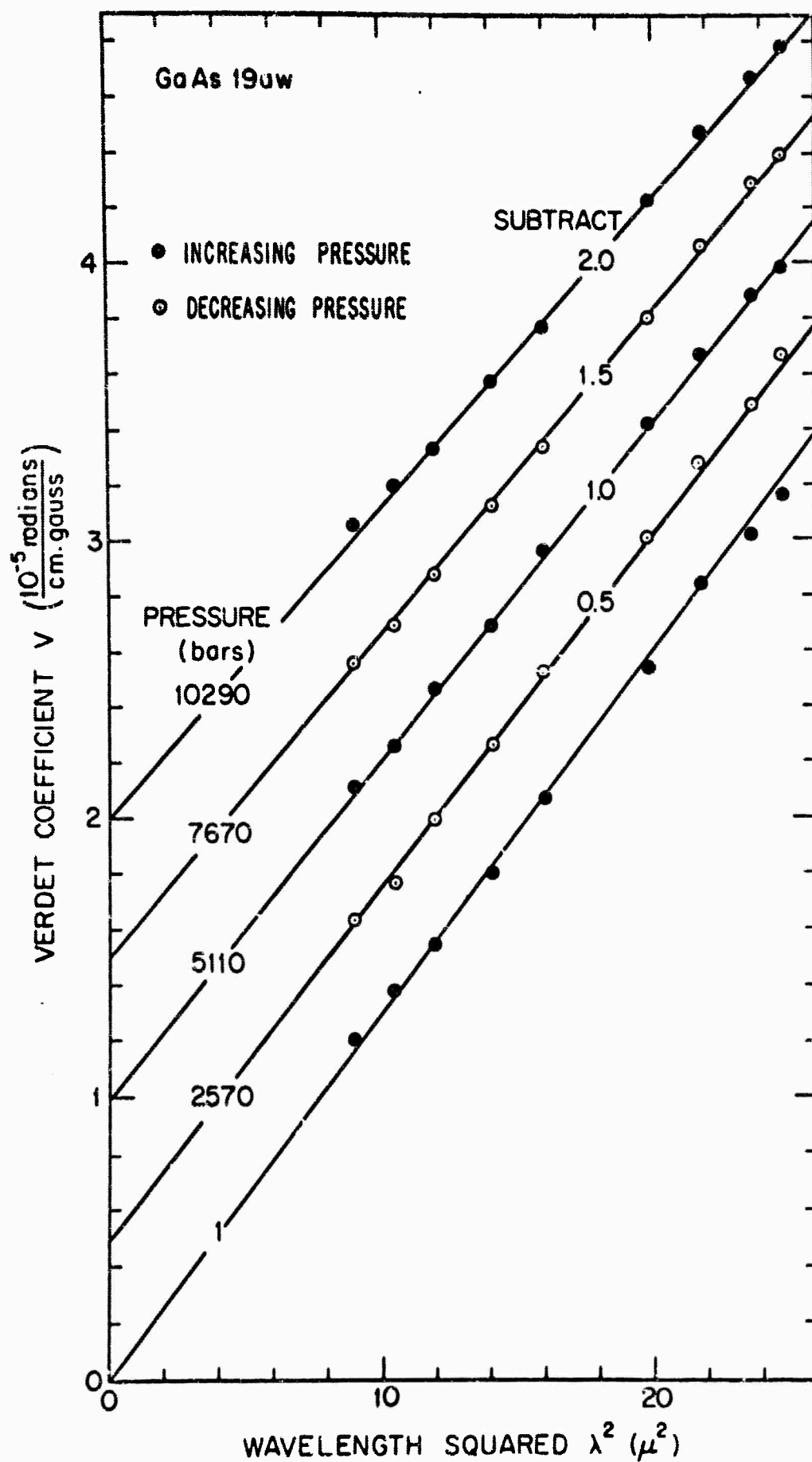


FIG 3-20 PRESSURE DEPENDENCE OF V FOR GoAs 18 aw.

FIG. 3-21 PRESSURE DEPENDENCE OF V FOR GaAs 19uw

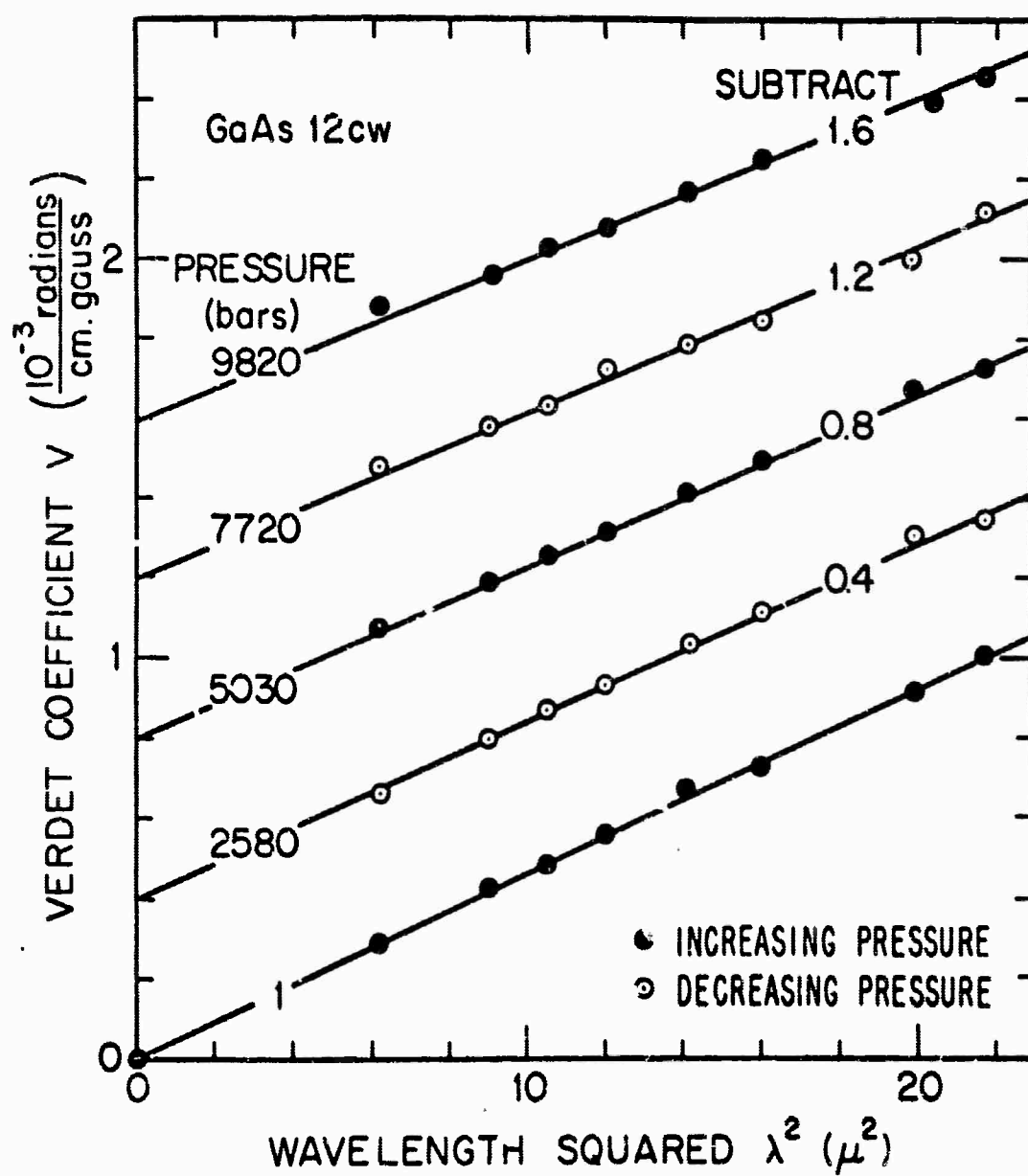


FIG. 3-22 PRESSURE DEPENDENCE OF V FOR GaAs 12cw

BLANK PAGE

CHAPTER 3 -- BIBLIOGRAPHY

- [3-1] I. Isenberg, B. R. Russell, and R. F. Green, Rev. Sci. Instr., 19, p. 685, 1948.
- [3-2] H. Ehrenreich, Phys. Rev., 120, p. 1951, 1960.
- [3-3] See reference [2-1], but p. 2-13.
- [3-4] M. Czerny, Z. Phys., 65, p. 600, 1930.
- [3-5] A. Kahan and H. G. Lipscom, AFCRL-63-325, Air Force Cambridge Research Laboratories, Hanscom Field, Massachusetts, 1963 (unpublished).
- [3-6] D. M. Warschauer and W. Paul, unpublished measurements, ref. (45) of W. Paul, J. Appl. Phys., 30 supp., p. 2082, 1961.
- [3-7] W. Paul, J. Appl. Phys., 30 supp., p. 2082, 1961
- [3-8] J. Feinleib, S. Groves, W. Paul, and R. Zallen, Phys. Rev., 131, p. 2070, 1963.
- [3-9] K. G. Hambleton, C. Hilsum, and B. R. Holeman, Proc. Phys. Soc., 77, p. 1197, 1961. V. F. Oswald and R. Schade, Z. Natur., 9A, pl 611, 1954.
- [3-10] D. T. F. Marple, G. E. Laboratories, Schenectady, New York, private communication, 1963. D. T. F. Marple, J. Appl. Phys., 35, p. 1241, 1964.
- [3-11] S. I. Novikova, Sov. Phys. Sol. State, 3, p. 129, 1961.
- [3-12] C. W. Garland and K. C. Park, J. Appl. Phys., 33, p. 759, 1962.
- [3-13] M. Cardona, Proceedings of the International Conference on Semiconductor Physics, Prague, 1960, p. 588, Czechoslovak Academy of Sciences, Prague, 1961.
- [3-14] F. Fern, Phys. Rev., 133, p. A1653, 1964.
- [3-15] C. R. Pidgeon, Infrared Magneto-Optical Phenomena in Semiconductors, thesis, University of Reading, England, 1962 (unpublished).

- [3-16] E. Malus, Mém. Soc. Accueil, 1, p. 113, 1808.
- [3-17] B. Donovan and T. Medcalf, Phys. Rev. Letters, 7, p. 304, 1963.
- [3-18] Y. I. Ukhonov, Sov. Phys. Sol. State, 5, p. 75, 1963.
- [3-19] M. Cardona, Phys. Rev., 121, p. 752, 1961.
- [3-20] H. Piller, Physics of Semiconductors, Proceedings of the 7th International Conference, Paris, 1964, p. 297, Dunod, Paris, 1964.
- [3-21] S. D. Smith, University of Reading, England, private communications, 1964.
- [3-22] W. G. Spitzer and J. M. Whelan, Phys. Rev., 114, p. 59, 1959.
- [3-23] C. Hilsum and A.C. Rose Innes Semiconducting III-V Compounds p. 77, Pergamon Press, New York, 1961.
O. Madelung, Physics of III-V Compounds, p. 223, John Wiley and Sons, Inc., New York, 1964.
- [3-24] R. F. Broom, K. Barrie, and I.M. Ross, Halbleiter und Phosphor, p. 453, Friedr. Vieweg und Sohn, Braunschweig, 1958.

CHAPTER 4

CONCLUSIONS

A. FORBIDDEN ENERGY GAP IN GaAs

a. Pressure Dependence

The experimental results presented in Eqs. (3-7) and (3-8) of section 3.B are obtained from isotransmission measurements on the exponential absorption edge of GaAs at energies slightly below the optical energy gap. Zallen [4-1] has shown that constant transmission measurements are equivalent to constant absorption measurements. Since the results of Eqs. (3-7) and (3-8) show no variation of isotransmission pressure coefficient over 2 decades of transmission variation, it is assumed that no change of shape of absorption edge with pressure occurred. The isotransmission pressure change can then be interpreted as a change in energy of the states determining the absorption.

Sturge [4-2] has shown experimentally that the exponential absorption edge below the true optical energy gap in GaAs is caused by exciton absorption. There exists no explicit relation for exciton states in GaAs. However, Elliott [4-3] has developed expressions for the case of a semiconductor with two simple bands which may be considered an approximation to the actual situation in GaAs.

According to Elliott [4-3], transmission below the optical energy gap between two simple parabolic bands will be governed

by the absorption arising from direct allowed exciton transitions at energies $\hbar\omega_x$ given by

$$\hbar\omega_x = F_g(T) - E_x. \quad (4-1)$$

The energy gap determining the exciton effect has been written as a free energy gap $F_g(T)$ to conform to the theory of section 1.B which suggests that optical energy gaps are really free energy gaps. E_x is the exciton binding energy given by

$$E_x = \frac{m_e m_h}{(m_e + m_h) l^2} - \frac{e^4}{2 \hbar^2 \epsilon^2}, \quad l = 1, 2, 3 \dots, \quad (4-2)$$

where $\epsilon (= n^2)$ is the dielectric constant and m_e and m_h are the effective electron and hole masses respectively.

Using Eq. (1-22) the pressure dependence of $F_g(T)$ may be found to be

$$\frac{dF_g(T)}{dP} = \frac{dE_{gT}}{dP} + \frac{d\Delta F_g(T)}{dP} \approx \frac{dE_{gT}}{dP} \quad (4-3)$$

where E_g in Eq. (1-22) has been replaced by E_{gT} (the implicitly temperature dependent energy gap corrected for lattice expansion and defined in Eq. (4-19)), and where $d[\Delta F_g(T)]/dP$, the pressure change of the electron-phonon interaction per electron, has been neglected. This has been done because it seems reasonable that the 1/4% change in GaAs lattice constant for a pressure change of 10 kilobars will have negligible effect on the electron-phonon interaction.

The pressure dependence of $\hbar\omega_x$ is then

$$\frac{d \hbar\omega_x}{dP} = \frac{d F_g(T)}{dP} - \frac{dE_x}{dP} = \frac{dE_{gT}}{dP} - \frac{dE_x}{dP}, \quad (4-4)$$

and the pressure dependence of E_x is

$$\frac{dE_x}{dP} = E_x \left[\frac{m_h}{m_e(m_e + m_h)} \frac{dm_e}{dP} + \frac{m_e}{m_h(m_e + m_h)} \frac{dm_h}{dP} - \frac{4}{n} \frac{dn}{dP} \right]. \quad (4-5)$$

For 2 simple parabolic bands

$$\frac{1}{m_e} \frac{dm_e}{dP} = \frac{1}{m_h} \frac{dm_h}{dP} = \frac{1}{E_{gT}} \frac{dE_{gT}}{dP}, \quad (4-6)$$

Equation (4-5) becomes

$$\frac{dE_x}{dP} = E_x \left[\frac{1}{E_{gT}} \frac{dE_{gT}}{dP} - \frac{4}{n} \frac{dn}{dP} \right], \quad (4-7)$$

and Eq. (4-4) becomes

$$\frac{d \hbar\omega_x}{dP} = \frac{dE_{gT}}{dP} \left[1 - \frac{E_x}{E_{gT}} \right] + \frac{4E_x}{n} \frac{dn}{dP}. \quad (4-8)$$

Sturge [4-2] calculates $E_x \approx 4 \cdot 10^{-3}$ eV and, since $E_{gT} \approx 1.5$ eV, E_x/E_{gT} is negligible compared to 1. Also, from Fig. (3-7b), $(1/n)(dn/dP)$ can be seen to be of the order of $2.5 \cdot 10^{-6}$ (bar) $^{-1}$ near the optical energy gap. This implies that the last term in Eq. (4-8) is of order $4 \cdot 10^{-8}$ eV/bar which may be neglected compared to the experimentally determined dE_g/dP of order $1.2 \cdot 10^{-5}$ eV/bar.

Thus Eq. (4-8) becomes

$$\frac{d \hbar\omega_x}{dP} \approx \frac{dE_{gT}}{dP} \quad (4-9)$$

The individual exciton lines at energies $\hbar\omega_x$ are broadened so that experimentally measured absorption below the optical energy gap has an exponential dependence on energy. However, Eq. (4-9) shows that the pressure dependences of all exciton lines are nearly identical and hence the results of Eq. (3-7) for isotransmission measurements on the exponential edge may be identified with Eq. (4-9) to give

$$\frac{d \hbar\omega_T}{dP} = \frac{d \hbar\omega_x}{dP} = \frac{dE_{gT}}{dP} = (1.17 \pm .03) \cdot 10^{-5} \frac{\text{eV}}{\text{bar}} \quad (4-10)$$

Equation (4-10) and the diode pressure coefficient of Feinleib et al. [3-8] of $(1.07 \pm .03) \cdot 10^{-5}$ eV/bar disagree by a margin exceeding experimental error. This can be most simply explained by associating the energy of diode spontaneous emission with non-band-to-band transitions such as those between non-hydrogenic impurity levels (near the conduction band) and valence band. Indeed, Feinleib et al. tentatively found transitions from a degenerate conduction band unlikely since they saw no pressure change of line-width of the spontaneous emission line for constant current.

However, it is possible to reconcile and indeed explain the temperature dependent pressure results of Feinleib et al. with

the Pankove [4-4] model of diode emission by photon-assisted tunneling between degenerate conduction and valence bands. It will be shown in section 4.B that the conduction band effective mass m_0^* increases about 6% in 10 kilobars. From Eq. (1-32) m_0^* enters to the $3/2$ power in determination of Fermi level. If the Pankove [4-4] model is assumed to hold, it is thus necessary to assume an increase in injected carriers of about 10% in 10 kilobars to maintain the Fermi level at a constant distance from the conduction band edge. In this case no significant pressure change would be expected in a linewidth determined by a degenerate conduction band distribution.

Such an increase of carriers was possible in the constant current experiments of Feinleib et al. but a detailed analysis of the actual current-voltage relations for the diodes used and a knowledge of pressure changes of such quantities as mobility and recombination time would be necessary in order to establish the exact magnitude of any carrier density change.

Granted that the increase took place, the pressure coefficient discrepancy could then be explained by attributing the energy of the spontaneous emission line to a free energy separation $F_S(T)$ between degenerate conduction and valence bands written as

$$F_S(T) = E_{gT} + E_F + \Delta F_g(T) \quad (4-11)$$

where E_{gT} is again the forbidden energy gap corrected for lattice expansion, E_F is the pressure independent energy contribution from the electron distribution, and $\Delta F_g(T)$ is the electron-phonon interaction per electron. The quantity $\Delta F_g(T)$ essentially arises from the distortion of the lattice from perfect periodicity at 0°K to thermally distorted positions at a temperature T. It is perhaps not unreasonable to assume that the presence of quasi-free electrons in the conduction band will also further distort the lattice of ion cores by coulombic interaction. Thus it can be expected that a free energy gap or separation may depend on carrier concentration. Indeed, several reports [4-5] have noted the dependence of optical absorption in GaAs on carrier density. If the optical gap should be interpreted as a free energy gap, the reports indicate that increased carrier concentration lowers the free energy or increases the negative electron-phonon interaction. Since a pressure dependent carrier density has been postulated for the diode results of Feinleib et al., the above argument leads to a pressure dependent $\Delta F_g(T)$. As the simplest assumption, it will be stipulated that $\Delta F_g(T)$ increases linearly with percentage increase of carriers.

The pressure change of $F_g(T)$ would then be given as

$$\frac{dF_g(T)}{dP} = \frac{dE_{gT}}{dP} + \frac{d[\Delta F_g(T)]}{dP} \approx \frac{dE_{gT}}{dP} + \Delta F_g(T) \frac{1}{n_i} \frac{dn_i}{dP}. \quad (4-14)$$

The quantity $\Delta F_g(T)$ is found from Fig. (4-1) by subtracting $E_{gT}(T)$. Assuming dE_g/dP does not change with temperature, Eq. (4-14) yields for two temperatures

$$\begin{aligned} 300^\circ\text{K}; \quad \frac{d F_S(T)}{dP} &\approx (1.17 \pm .03) \cdot 10^{-5} \frac{\text{eV}}{\text{bar}} + (-.08)\text{eV} \cdot 10^{-5} \frac{1}{\text{bar}} \\ &= (1.09 \pm .03) \cdot 10^{-5} \frac{\text{eV}}{\text{bar}} ; \end{aligned} \quad (4-15)$$

$$\begin{aligned} 77^\circ\text{K}; \quad \frac{d F_S(T)}{dP} &\approx (1.17 \pm .03) \cdot 10^{-5} \frac{\text{eV}}{\text{bar}} + (-.01)\text{eV} \cdot 10^{-5} \frac{1}{\text{bar}} \\ &= (1.16 \pm .03) \cdot 10^{-5} \frac{\text{eV}}{\text{bar}} . \end{aligned} \quad (4-16)$$

Equations (4-15) and (4-16) agree within experimental error with the diode line pressure coefficients of Feinleib et al. [3-8]:

$$300^\circ\text{K}; \quad \frac{d \hbar\omega}{dP} = (1.07 \pm .03) \cdot 10^{-5} \frac{\text{eV}}{\text{bar}} ; \quad (4-17)$$

$$77^\circ\text{K}; \quad \frac{d \hbar\omega}{dP} = (1.13 \pm .03) \cdot 10^{-5} \frac{\text{eV}}{\text{bar}} . \quad (4-18)$$

If a free energy separation is indeed the correct energy to assign to the diode spontaneous emission line, the fact would lend support to the suggestion of James [1-4] that changes in optical energy gaps with temperature should be interpreted in terms of changes in electron-phonon interaction rather than as changes in thermal energy gaps.

b. Temperature Dependence

While no independent determinations of the temperature dependence of GaAs energy gaps were performed in this investigation, the available experimental data from the literature are presented in Fig. (4-1).

The forbidden energy gap E_g was defined in Chapter 1 for constant volume. Consequently the temperature dependent E_{gT} presented in Fig. (4-1) arises from lattice expansion and is derived as

$$E_{gT} = E_g + \frac{dE_g}{dP} \int_0^T \frac{\alpha(T)}{\beta(T)} dT \quad (4-19)$$

where dE_{gT}/dP is assumed independent of temperature ($dE_{gT}/dP = dE_g/dP$), E_g is taken from extrapolation to 0°K of the optical results of Sturge [4-2], $\alpha(T) = (1/V)(dV/dT)$ is the temperature dependent volume thermal expansion, and $\beta(T) = (1/V)(dV/dP)$ is the temperature dependent volume compressibility. The integration was performed graphically.

Finally, the free energy gap, $F_g(T)$ defined in Chapter 1, was taken as determined by the optical energy gap derived by Sturge [4-2] from analysis of exciton absorption.

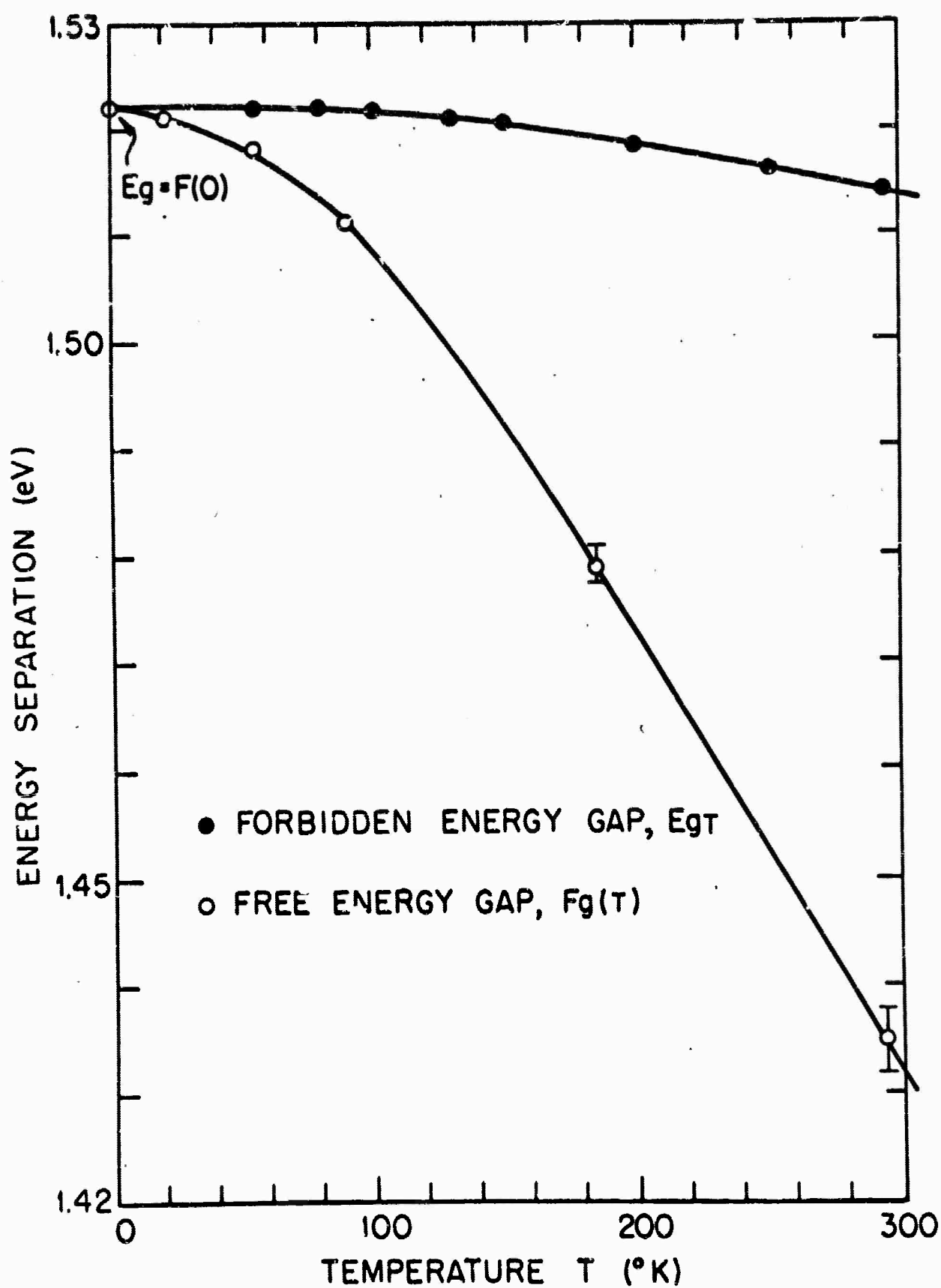


FIG. 4-1 ENERGY SEPARATIONS IN GaAs VERSUS TEMPERATURE

B. EFFECTIVE MASS IN GaAs

a. Room Conditions

The quantity m_{op}^* is defined experimentally in Eq. (1-31) and is obtained from slopes of free carrier Verdet coefficient V_F versus λ^2 for long wavelengths as

$$m_{op}^* = \left[\frac{e^3 N d H \lambda^2}{2\pi n_c c^4 \theta_F} \right]^{1/2} = \left[\frac{e^3 N \lambda^2}{2\pi n_c c^4 V_F} \right]^{1/2} \quad (4-20)$$

It is assumed that carrier concentration N is constant with wavelength, since the incident photon flux was about 10^{17} photons/sec. for the experimental conditions. Assuming 100% quantum efficiency and lifetimes $\approx 10^{-5}$ sec. [4-6] would lead to a change in carrier density of 10^{12} cm.⁻³, which is negligible. The refractive index n_c was corrected for free carrier susceptibility χ_c using

$$n_c^2 = n^2 - \chi_c = n^2 - \frac{Ne^2}{\omega^2 m_{op}^*} \quad (4-21)$$

where n is the refractive index determined in Chapter 3 and m_{op}^* could be roughly estimated since the correction is quite small for the measurements reported in section 3.D.d.

The m_{op}^* derived from the experimental results of Figs. (3-13) and (3-14) for 4 n-type GaAs samples are presented in Fig. (4-2) as a function of carrier concentration.

The theoretical lines shown in Fig. (4-2) are calculated from Eq. (1-5) using for E_g the forbidden energy gap at 295°K, $E_{gT} = 1.51$ eV,

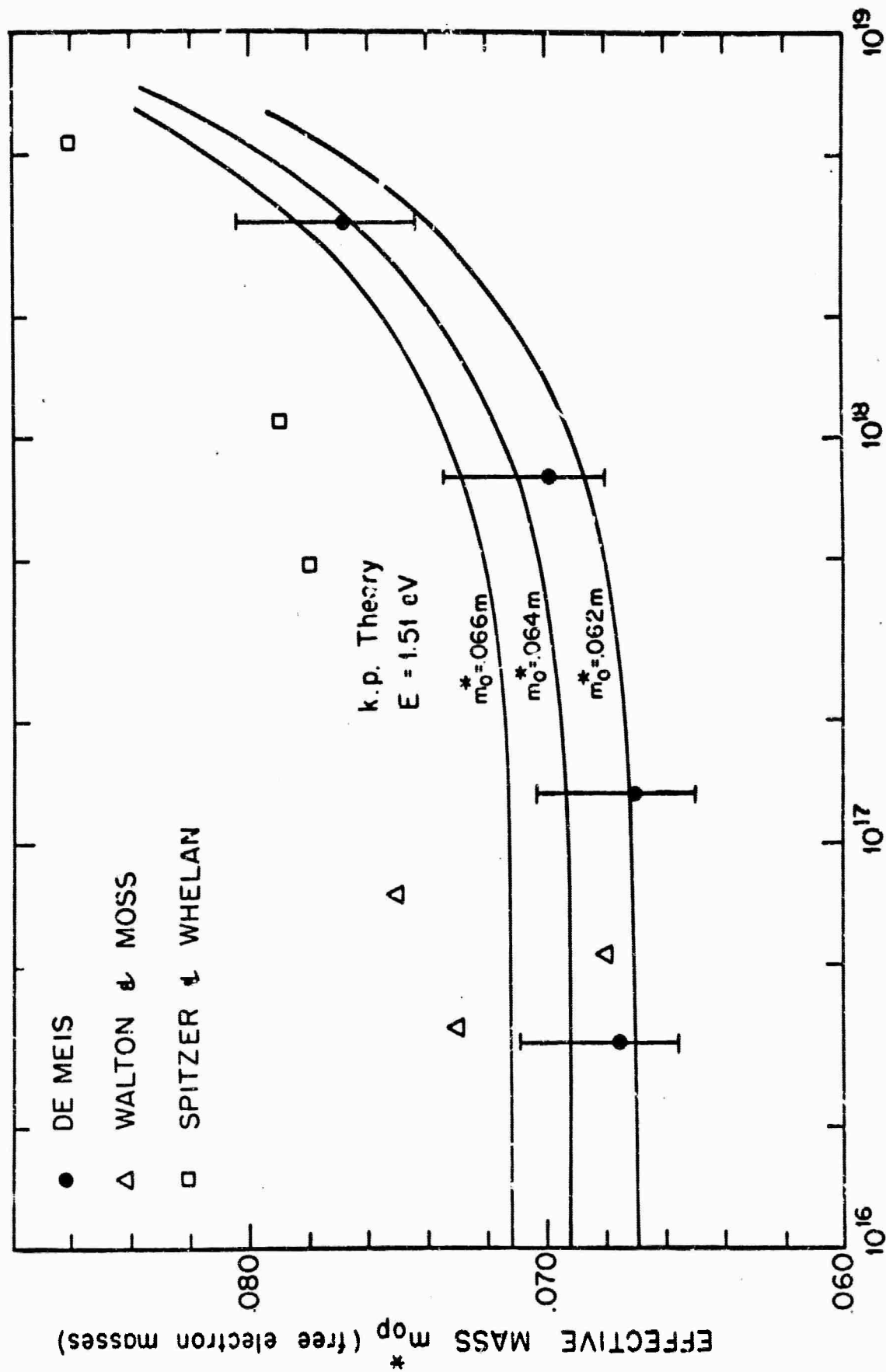


FIG. 4-2 EFFECTIVE MASS OF N-TYPE GaAs AS A FUNCTION OF CARRIER CONCENTRATION

taken from Fig. (4-1). The spin-orbit splitting was taken to be $\Delta = .35$ eV [4-2]. Several curves are shown for a variety of choices of m_0^* , and $m_0^* = .064$ m seems the best fit. The theoretically calculated lines in Fig. (4-2) are not sensitive to choice of energy gap, varying by less than 1% for a change of E_{gT} from 1.51 eV to 1.44 eV. Thus while the $k \cdot p$ theory can adequately describe the variation of m^* with carrier concentration for room conditions, it does not distinguish between types of energy gaps.

In comparing results of this report with the literature, previous determinations of effective mass by Faraday rotation which do not extrapolate through $V = 0 = \lambda^2$ have been ignored. Polarization results determined by varying magnetic field at a fixed wavelength have also been ignored since there can be no assurance that the experimental difficulties shown to exist in section 3.D.d. were avoided.

The Faraday results of Moss and Walton [4-7], which do go through zero, are presented in Fig. (4-2). However, their samples were such that multiple reflections were possible even at the longest wavelengths. The free carrier reflectivity results of Spitzer and Whelan [1-12] are also shown in Fig. (4-2) and do not agree with the present results. It should be noted that the discrepancy between the results of Moss and Walton, Spitzer and Whelan, and the present investigation exists even though all three determined

carrier concentration from Hall effect by using $R = 1/(Nec)$. The discrepancy exists independent of a knowledge of the Hall coefficient scattering dependence.

Finally, the infrared cyclotron absorption result of $m_{\text{op}}^* = .071 m$ by Palik, Stevenson, and Wallis [4-8] cannot be reconciled with the results of this investigation.

b. Pressure Dependence

The experimental pressure change of m_{op}^* was found from the slopes of V_F versus λ^2 at various pressures given in Figs. (3-20), (3-21), and (3-22). The pressure change of the interband correction was small and is shown in Fig. (3-19). The percent pressure changes in m_{op}^* for three n-type samples of GaAs are shown in Fig. (4-3) after correcting for the small pressure change in thickness d [3-12] and refractive index n [measured at long wavelengths in Fig. (3-7)]. N was assumed constant.

In Fig. (4-3) two theoretical calculations of m_{op}^* pressure dependence were obtained by using Eqs. (1-5), (1-6), and (1-32). For each sample the dashed line represents calculations using $F_g(T)$, the optical or free energy gap, for E_g , the energy separation determining the effective mass. Similarly, the solid line represents calculations for each sample using for E_g the forbidden energy gap corrected for lattice expansion E_{gT} . The calculations assumed P

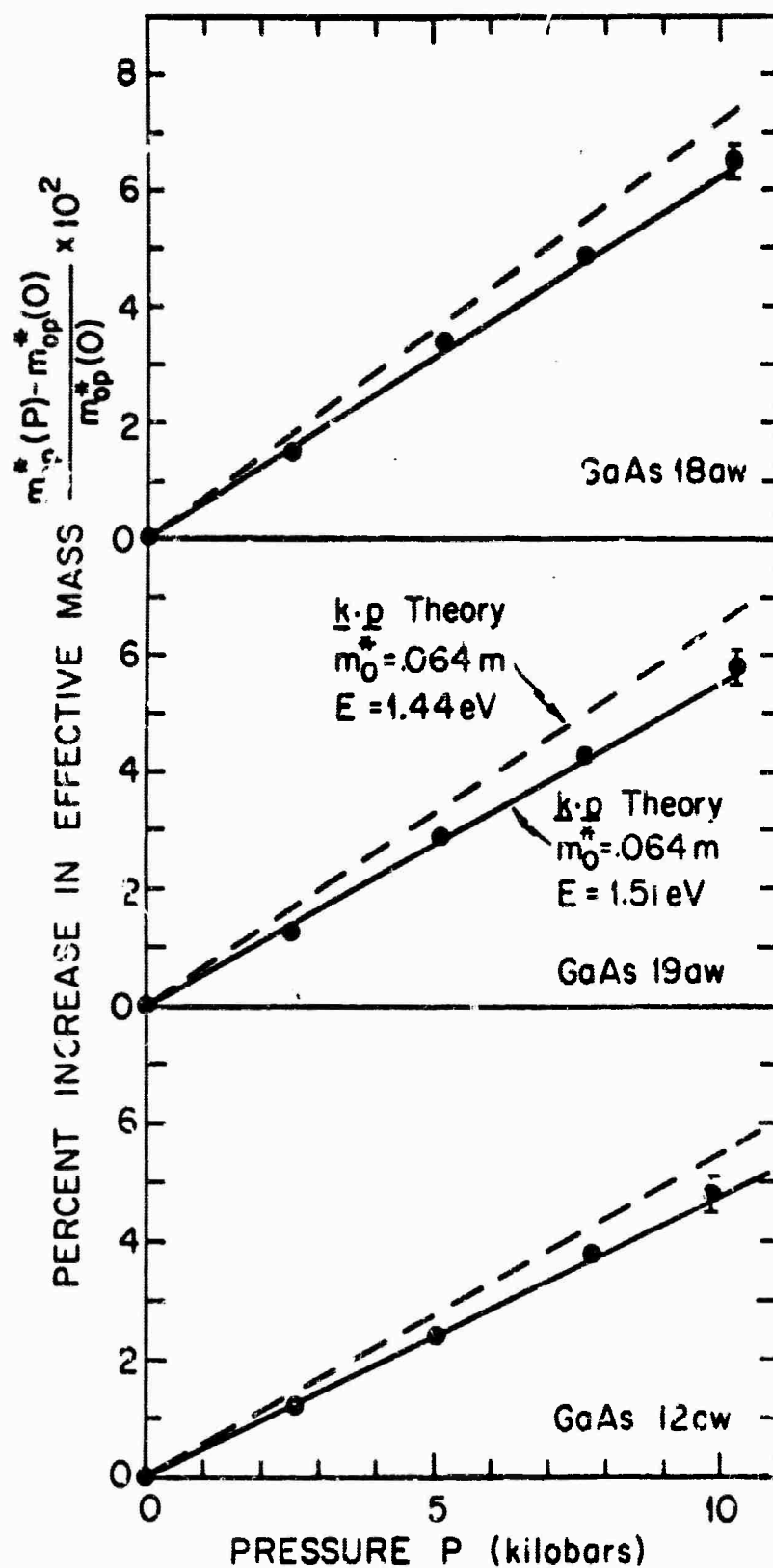


FIG. 4-3 PERCENT INCREASE OF m_0^* VERSUS PRESSURE FOR 3 N-TYPE GaAs SAMPLES

and Δ constant with pressure. This assumption for Δ is supported by the experimental results of Paul and Warschauer [4-9] on infrared absorption in p-type Ge and of Kosicki and Paul [4-10] on infrared absorption in p-type GaSb. For both calculations m_0^* at 1 bar was assumed to be .064 m, but the results were not sensitive to choice of m_0^* since the calculations varied $< 1\%$ by changing m_0^* from .064 m to .072 m. It is clear that the data are fitted best by using the $k \cdot p$ theory with the forbidden energy gap corrected for lattice expansion as the energy separation.

c. Temperature Dependence

The experimental temperature change of m_{op}^* was found from the slopes of V_F versus λ^2 at various temperatures given in Figs. (3-16) (3-17), and (3-18). The temperature change of the interband correction was small as is seen in Fig. (3-15). The percent temperature changes in m_{op}^* for three n-type samples of GaAs are shown in Fig. (4-4) after correcting for the small temperature change in thickness d [3-11] and refractive index n [measured at long wavelengths in Fig. (3-7a)]. N was assumed constant.

Two theoretical calculations of m_{op}^* temperature dependence obtained by using Eqs. (1-5), (1-6), and (1-32), assuming P and Δ constant with temperature, and recalculating the Fermi levels at each temperature, are shown in Fig. (4-4). In Fig. (4-4), the

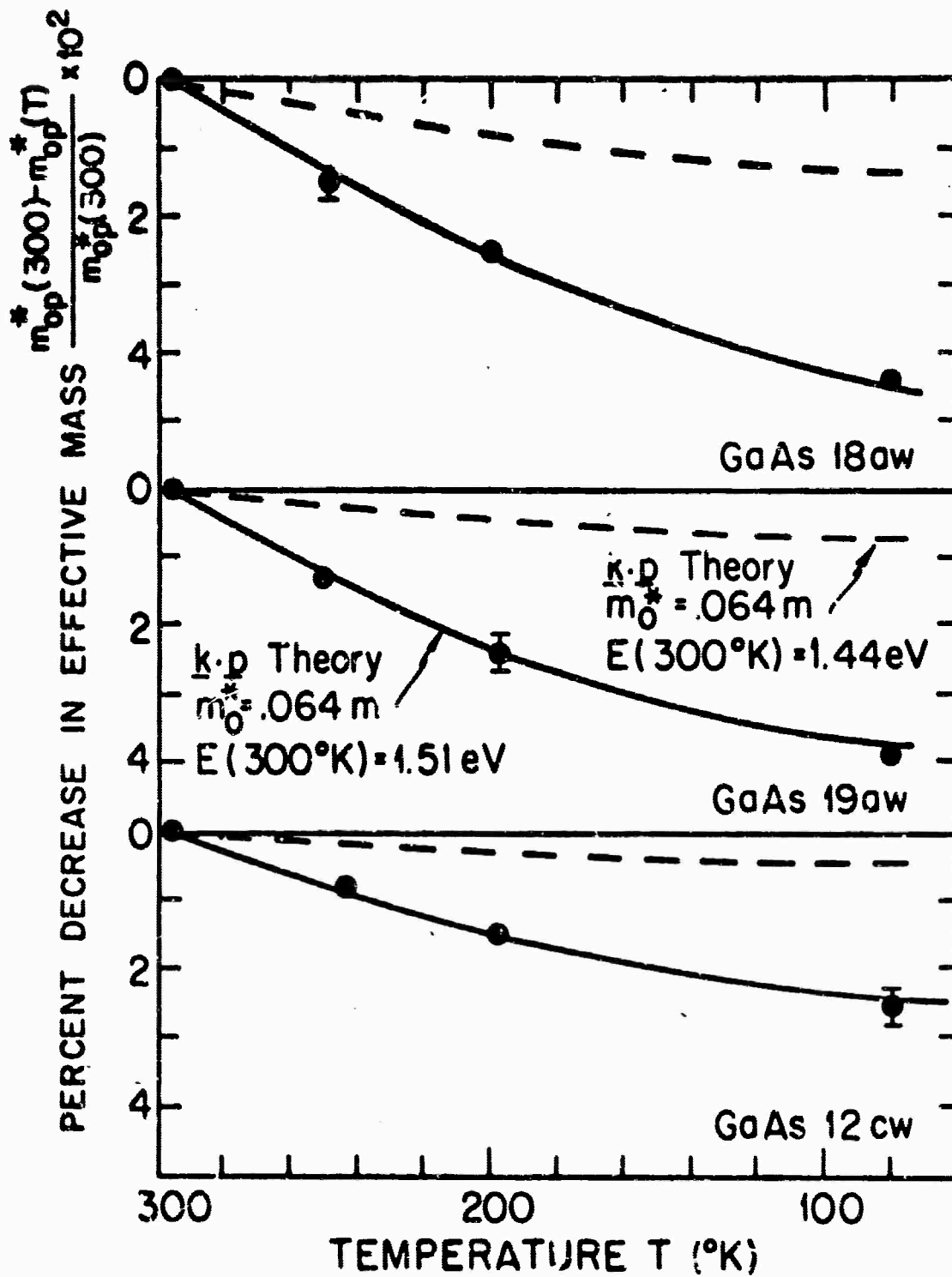


FIG. 4-4 PERCENT DECREASE OF m_{op}^* VERSUS TEMPERATURE FOR 3 N-TYPE GaAs SAMPLES

dashed line represents calculations with $E_g = F_g(T)$, the optical or free energy gap, while the solid line was calculated using $E_g = E_{gT}$, the forbidden energy gap corrected for lattice expansion. For both calculations m_0^* at 295°K was assumed to be .064 m, but the results were not sensitive to choice of m_0^* since the calculations varied by < 1% by changing m_0^* from .064 m to .072 m. It is evident that the data can be fitted best by using the $k \cdot p$ theory with the forbidden energy gap corrected for lattice expansion as the energy separation.

C. SUMMARY

Three "cataloging" measurements have been performed in this investigation as necessary adjuncts to the careful measurement of effective mass. They were : (1) determination of GaAs refractive index as a function of temperature; (2) determination of GaAs refractive index as a function of pressure; and (3) determination of the pressure coefficient of the forbidden energy gap in GaAs to be $(1.17 \pm .03) \cdot 10^{-5}$ eV/bar.

A side effect of this investigation has been to point out some possible errors that can arise in determining effective mass by means of Faraday rotation. Careful considerations of such errors in the room condition results of this report indicate that the effective mass at the bottom of the Γ_{1c} minimum in GaAs is certainly lower than the generally accepted value of .072 m, and may be as low as $(.064 \pm .002)$ m.

This investigation has also shown that the "finite temperature" pressure and temperature dependences of effective mass in GaAs can be explained by using semiconductor "zero-temperature" $k \cdot p$ theory with an energy separation appropriate to the forbidden energy gap corrected for lattice expansion rather than the optical or free energy gap. In practice, the forbidden energy gap at any temperature is determined by taking a measured energy gap at zero temperature and correcting to a finite temperature using lattice expansion only. It can be noted that Ehrenreich [4-11] used much the same point of view in a paper investigating scattering in InSb, and he also drew distinctions between the thermal and optical gaps and the "effective mass band-gap", termed here the forbidden energy gap.

A number of other investigations have noted that the forbidden energy gap corrected for lattice expansion is the more appropriate energy separation to use when fitting the temperature dependence of effective mass to the Kane $k \cdot p$ theory. Smith, Pidgeon, and Prosser [4-12] found this true for InSb, as did Palik et al. [4-13]. Cardona [3-19] also demonstrated it for InAs.

The relevant energy gap, then, in determining effective mass is the energy separation between quantized states, rather than, for example, the experimental optical gap. If the suggestion of James is correct, the optical energy gap may be equated to the forbidden energy gap plus the energy of electron-phonon interaction. The results of this investigation, together with the other reports

above, tend to indicate that, within the quoted experimental errors of the measurements, and given the necessary assumptions of Chapter 1, semiconductors for which the Kane $k \cdot p$ theory is applicable have effective masses very little affected, if at all, by electron-phonon interactions. This indication is of course proved only for GaAs, InSb, and InAs, the materials for which the temperature dependence of effective mass has actually been measured.

Finally, the results of this investigation which distinguish between the forbidden energy gap and the optical energy gap tend to support the suggestion of James [1-4] that optical energy gaps are in reality free energy gaps. In this connection, additional support is lent to the suggestion by the fact that interpretation of spontaneous emission as a free energy can explain previously unexplained temperature dependent pressure coefficients of diode emission lines.

CHAPTER 4 BIBLIOGRAPHY

- [4-1] See reference [2-1], but p. 4-2.
- [4-2] M. D. Sturge, Phys. Rev., 127, p. 768, 1962.
- [4-3] R. J. Elliott, Phys. Rev., 108, p. 1384, 1957.
- [4-4] J. I. Pankove, Phys. Rev. Letters, 9, p. 283, 1962.
- [4-5] R. Braunstein, J. I. Pankove, and H. Nelson, Applied Phys. Letters, 3, p. 31, 1963. D. E. Hill, Phys. Rev., 133, A866, 1964.
- [4-6] C. Hilsum and B. Holeman, Proceedings of the International Conference on Semiconductor Physics, Prague, 1960, p. 962, Czechoslovak Academy of Sciences, Prague, 1961.
- [4-7] T. S. Moss and A. K. Walton, Proc. Phys. Soc., 74, p. 131, 1959.
- [4-8] E. D. Palik, J. R. Stevenson, and R. F. Wallis, Phys. Rev., 124, p. 701, 1961.
- [4-9] W. Paul and D. M. Warschauer, Harvard University, (unpublished measurements).
- [4-10] B. B. Kosicki and W. Paul, Harvard University, (unpublished measurements).
- [4-11] H. Ehrenreich, J. Phys. Chem. Solids, 2, p. 131, 1957.
- [4-12] S. D. Smith, C. R. Pidgeon, and V. Prosser, Proceedings of the International Conference on the Physics of Semiconductors, Exeter, 1962, p. 301, The Institute of Physics and the Physical Society, London, 1962.
- [4-13] E. D. Palik, G. S. Picos, S. Teitler, and R. F. Wallis, Phys. Rev., 122, p. 475, 1961.

DOCUMENT CONTROL DATA - R&D

(Security classification of title, body of abstract and indexing annotation must be entered when the overall report is classified)

1. ORIGINATING ACTIVITY (Corporate author) Division of Engineering and Applied Physics Harvard University Cambridge, Massachusetts		2a. REPORT SECURITY CLASSIFICATION Unclassified	
		2b. GROUP	
3. REPORT TITLE THE EFFECT OF PRESSURE AND TEMPERATURE ON THE EFFECTIVE MASS AND ENERGY GAP OF GaAs			
4. DESCRIPTIVE NOTES (Type of report and inclusive dates) Interim technical report			
5. AUTHOR(S) (Last name, first name, initial) De Meis, Walter M.			
6. REPORT DATE August 1965		7a. TOTAL NO. OF PAGES 180	7b. NO. OF REFS 66
8a. CONTRACT OR GRANT NO. Nonr-1866(10) b. PROJECT NO. NR-017-308 c. ARPA SD-88 d.		9a. ORIGINATOR'S REPORT NUMBER(S) Technical Report No. HP-15 9b. OTHER REPORT NO(S) (Any other numbers that may be assigned this report) ARPA Report No. 16	
10. AVAILABILITY/LIMITATION NOTICES Qualified requesters may obtain copies of this report from DDC. All other persons or organizations should apply to the Clearinghouse for Federal and Scientific Information, 5285 Port Royal Road, Springfield, Virginia 22151			
11. SUPPLEMENTARY NOTES Supported in part by the Division of Engineering and Appl. Phys., Harvard University, Cambridge, Massachusetts		12. SPONSORING MILITARY ACTIVITY Office of Naval Research and Advanced Research Projects Agency Washington, D. C.	
13. ABSTRACT This report describes the results of an investigation of the effect of pressure and temperature on the energy gap and electron effective mass of GaAs. For this material, the applicability of the zero temperature Kane $k \cdot p$ theory at finite temperature was quantitatively tested by measuring the Faraday rotation as a function of pressure and temperature. The quantitative comparison of experimentally determined masses with theory required three subsidiary measurements: (1) the pressure change of energy gap of GaAs was found to be $dE_g/dP = (1.17 + .03) \cdot 10^{-5}$ eV/bar; (2) the long wavelength pressure change of refractive index of GaAs was found to be $(1/n)(dn/dP) = -(7.0 + 0.5) \cdot 10^{-7}$ (1/bar); and (3) the long wavelength temperature change of refractive index of GaAs was confirmed to be $(1/n)(dn/dT) = (4.5 + 0.5) \cdot 10^{-5}$ (1°/K). In the process of determining effective mass, a number of possible experimental errors in measuring Faraday rotation were delineated. Careful consideration of these errors led to an effective mass at the bottom of the GaAs Γ_{1c} conduction band of $m_0^* = (.064 \pm .002)m$ for room temperature and atmospheric pressure. The results of measurements on three n-type samples of GaAs as a function of temperature and pressure show that the data were fitted best by using the Kane $k \cdot p$ theory at finite temperature with an energy gap corrected from 0°K by accounting only for lattice expansion, rather than the experimentally determined optical energy gap which may be considered to have an implicit temperature dependence due to lattice expansion and an explicit temperature dependence.			

Unclassified
Security Classification

14. Key Words

Link A
Role Wt

Link B
Role Wt

Link C
Role Wt

Semiconductors
Gallium arsenide
Faraday rotation
Pressure effects

ABSTRACT (Continued)

If a suggestion by James is correct, the optical energy gap should be considered a free energy gap composed of the forbidden energy gap and an explicitly temperature dependent electron-phonon interaction. In this context, this investigation demonstrated that the most appropriate GaAs energy gap for the Kane $k \cdot p$ theory is the forbidden energy gap corrected for lattice expansion, and that effective mass in GaAs is very little affected, if at all, by electron-phonon interaction.